UNIVERSITY OF ALBERTA

Mechanisms of Chromium Containment in Tricalcium Silicate

by

Oladipo Emmanuel Omotoso

A thesis submitted to the Faculty of Graduate Studies and Research in partial fulfillment of the requirements for the degree of **Doctor of Philosophy**

in

Metallurgical Engineering

Department of Mining, Metallurgical and Petroleum Engineering

Edmonton, Alberta

Spring 1996

National Library
of Canada

Acquisitions and
Bibliographic Services Branch

395 Wellington Street
Ottawa, Ontario
K1A 0N4

Bibliothèque nationale
du Canada

Direction des acquisitions et
des services bibliographiques

395, rue Wellington
Ottawa (Ontario)
K1A 0N4

Your file Votre référence

Our file Notre référence

The author has granted an irrevocable non-exclusive licence allowing the National Library of Canada to reproduce, loan, distribute or sell copies of his/her thesis by any means and in any form or format, making this thesis available to interested persons.

L'auteur a accordé une licence irrévocable et non exclusive permettant à la Bibliothèque nationale du Canada de reproduire, prêter, distribuer ou vendre des copies de sa thèse de quelque manière et sous quelque forme que ce soit pour mettre des exemplaires de cette thèse à la disposition des personnes intéressées.

The author retains ownership of the copyright in his/her thesis. Neither the thesis nor substantial extracts from it may be printed or otherwise reproduced without his/her permission.

L'auteur conserve la propriété du droit d'auteur qui protège sa thèse. Ni la thèse ni des extraits substantiels de celle-ci ne doivent être imprimés ou autrement reproduits sans son autorisation.

ISBN 0-612-10621-7

Canada

UNIVERSITY OF ALBERTA

LIBRARY RELEASE FORM

NAME OF AUTHOR: **Oladipo Emmanuel Omotoso**

TITLE OF THESIS: **Mechanisms of Chromium Containment in Tricalcium Silicate**

DEGREE: **Doctor of Philosophy**

YEAR THIS DEGREE GRANTED: **1996**

Permission is hereby granted to the University of Alberta Library to reproduce single copies of this thesis and to lend or sell such copies for private, scholarly, or scientific research purposes only.

The author reserves all other publication and other rights in association with the copyright of the thesis, and except as hereinbefore provided, neither the thesis nor any substantial portion thereof may be printed or otherwise reproduced in any material form whatever without the author's prior written permission.

c/o. Mrs G.T. Ajayi
No. 53 Temitope Street
Ilasamaja, Lagos
Nigeria.

DATE: February 5, 1996

UNIVERSITY OF ALBERTA

FACULTY OF GRADUATE STUDIES AND RESEARCH

The undersigned certify that they have read, and recommend to the Faculty of Graduate Studies and Research for acceptance, a thesis entitled **MECHANISMS OF CHROMIUM CONTAINMENT IN TRICALCIUM SILICATE** by **OLADIPO EMMANUEL OMOTOSO** in partial fulfillment of the requirements for the degree of **DOCTOR OF PHILOSOPHY** in **METALLURGICAL ENGINEERING.**

Dr. D. G. Ivey
Supervisor

Dr. M. L. Wayman

Dr. R. Mikula

Dr. S. Wanke

Dr. R. L. Eadie

Dr. J. Luo

Dr. F. K. Cartledge

DATE: Jan. 29/96

Oladipo Omotoso
Department of Mining, Metallurgical
& Petroleum Engineering,
University of Alberta, Edmonton. AB.
T6G 2G6.

December 21, 1995

Applied Science Publishers
Ripple Road, Barking,
Essex,
United Kingdom.

Dear Sir/Ma'am:

REQUEST FOR COPYRIGHT PERMISSION

I am a Ph.D. student in the department of Metallurgical Engineering, University of Alberta, Edmonton, Canada. It is my intention to use some materials printed in one of your publications, in the Literature Review Chapter of my doctoral thesis;

Structure and Performance of Cement (1983),
ed. P. Barnes
Jawed, I., Skanly, J. and Young J.F., Hydration of Portland Cement.

- **Fig. 1 Schematic representation of changes taking place in the C_3S - water system (p 240)**
- **Equation 1 $2C_3S + 7H \rightarrow C_3S_2 + 3CH$, $\Delta H = -1114kJ/mol$ (p 239)**

I am attaching the pages as it would appear in my thesis.

The thesis is strictly for academic circulation.

Chapman & Hall

Royalty Department
International Thomson Publishing Services Ltd
Cheriton House, North Way, Andover, HANTS, SP10 5BE
Tel: 01264 342756 Fax: 01264 342792

Dear Sir/Madam

Permission is granted for use of the attached material, subject to the following conditions.

1. The material to be quoted/produced was published without credit to another source. If another source is acknowledged, please apply directly to that source for permission clearance.

2. The material is to be used only as described in your letter. Permission is non-exclusive and for one-time use only. Any further use (including storage, transmission or reproduction by electronic means) shall be the subject of a separate application for permission.

3. Full acknowledgement must be given to the original source, with full details of figure/page numbers, title, author (s), publisher and year of publication.

Yours faithfully

Annemieke Dolfing - Permissions Department
Please call direct on: 01264-342781

Dated 16/1/96

Chapman & Hall Ltd Scientific, Technical & Medical Publishers REG No 13655
Also incorporating E & FN Spon, Van Nostrand Reinhold (International), Blueprint, H K Lewis, BMMR, Blackie A & P
Distribution Centre: Cheriton House, North Way, Andover, Hampshire, England SP10 5BE Telephone Andover (0264) 332424
Cables APT Andover Telex 47214 Answerback ITT AND G Fax GP 2/3 (0264) 364418

permsubc.doc

Department of Mining, Metallurgical
& Petroleum Engineering,
University of Alberta, Edmonton. AB.
T6G 2G6.

December 21, 1995

Applied Science Publishers
Ripple Road, Barking,
Essex,
United Kingdom.

Dear Sir/Ma'am:

REQUEST FOR COPYRIGHT PERMISSION

I am a Ph.D. student in the department of Metallurgical Engineering, University of Alberta, Edmonton, Canada. It is my intention to use some materials printed in one of your publications, in the Literature Review Chapter of my doctoral thesis;

Structure and Performance of Cement (1983),
ed. P. Barnes
Jawed, I., Skanly, J. and Young J.F., Hydration of Portland Cement.

- **Fig. 1 Schematic representation of changes taking place in the C_3S - water system (p 240)**
- **Equation 1 $2C_3S + 7H \rightarrow C_3S_2 + 3CH$, $\Delta H = -1114kJ/mol$ (p 239)**

I am attaching the pages as it would appear in my thesis.

The thesis is strictly for academic circulation.

Chapman & Hall

Royalty Department
International Thomson Publishing Services Ltd
Cheriton House, North Way, Andover, HANTS, SP10 5BE
Tel: 01264 342756 Fax: 01264 342792

Dear Sir/Madam

Permission is granted for use of the attached material, subject to the following conditions.

1. The material to be quoted/produced was published without credit to another source. If another source is acknowledged, please apply directly to that source for permission clearance.

2. The material is to be used only as described in your letter. Permission is non-exclusive and for one-time use only. Any further use (including storage, transmission or reproduction by electronic means) shall be the subject of a separate application for permission.

3. Full acknowledgement must be given to the original source, with full details of figure/page numbers, title, author (s), publisher and year of publication.

Yours faithfully

Annemieke Dolfing - Permissions Department
Please call direct on: 01264-342781

Dated 16/1/96

Chapman & Hall Ltd Scientific, Technical & Medical Publishers REG No 13655
Also incorporating E & FN Spon, Van Nostrand Reinhold (International), Blueprint, H K Lewis, BMMR, Blackie A & P
Distribution Centre: Cheriton House, North Way, Andover, Hampshire, England SP10 5BE Telephone Andover (0264) 332424
Cables APT Andover Telex 47214 Answerback ITT AND G Fax GP 2/3 (0264) 364418

permsubc doc

Oladipo Omotoso
Department of Mining, Metallurgical
& Petroleum Engineering,
University of Alberta, Edmonton. AB.
T6G 2G6.

December 21, 1995

RECEIVED
18 JAN 1996

Academic Press
24 - 28 Oval Road,
London, NW1 7DX
United Kingdom.

Dear Sir/Ma'am:

REQUEST FOR COPYRIGHT PERMISSION

I am a Ph.D. student in the department of Metallurgical Engineering, University of Alberta, Edmonton, Canada. It is my intention to use a diagram printed in one of your publications, in the Literature Review Chapter of my doctoral thesis;

Cement Chemistry (1990),
H.F.W. Taylor
Fig. 6.4a, page 179 (Crystal Structure of Ettringite)

I am attaching the page as it would appear in my thesis.

The thesis is strictly for academic circulation.

I will deeply appreciate it if you can grant me the necessary permission to use this Figure.

Sincerely,

Oladipo Omotoso

Enclosures: [1]

PERMISSION GRANTED
provided:
The material to be used has appeared in our
publication without credit or acknowledgement
to another source
Proper credit to the other publication
Date 22/1/96 By
Rights and Permissions
ACADEMIC PRESS LTD
London, England

Oladipo Omotoso
Department of Mining, Metallurgical
& Petroleum Engineering,
University of Alberta, Edmonton. AB.
T6G 2G6.

02 JAN. 1996

December 21, 1995

Annales de Chimie,
Masson Periodiques,
Villa Laromiguiere
F 75005, Paris
France.

Dear Sir/Ma'am:

REQUEST FOR COPYRIGHT PERMISSION

I am a Ph.D. student in the department of Metallurgical Engineering, University of Alberta, Edmonton, Canada. It is my intention to use a Figure printed in one of your publications, in the Literature Review Chapter of my doctoral thesis;

Annales de Chimie (Fr) 4(1979),.
IR and Raman spectroscopy studies of tricalcium silicate structures (p 145)

- **Fig. 2 Jeffery's structure of Ca_3SiO_5** ac projection **(p 148).**

I am attaching the page as it would appear in my thesis.

The thesis is strictly for academic circulation.

I will deeply appreciate it if you can grant me the necessary permission to use this material.

Sincerely,

Oladipo Omotoso

Enclosures: [*1*]

MASSON S.A.
Date: 2.1.96
Signature:

Permission granted subject to :
- ~~permission~~ from the author(s)
- ~~and to~~ full acknowledgement of the original source of publication

To my mother, ***Funso*** *whose perseverance has been an inspiration.*

ABSTRACT

The containment of chromium wastes in tricalcium silicate (C_3S) has been investigated. Tricalcium silicate is the main constituent of Portland cement responsible for the strength and stability of hardened Portland cement paste. Hexavalent and trivalent chromium compounds, added as dopants to C_3S, simulate chromium waste forms that might be stabilized in a cement matrix. Scanning electron microscopy (SEM) and transmission electron microscopy (TEM), were used to identify the microstructural changes accompanying the addition of Cr(III) and Cr(VI) solutions to C_3S. Energy dispersive spectroscopy (EDS) was used to probe the distribution of chromium in the phases within the hazardous waste forms. Elucidation of the molecular structure of the reaction products and their concentrations were accomplished with x-ray diffraction (XRD), infrared (FTIR) and nuclear magnetic resonance (NMR) spectroscopies.

In monolithic waste forms containing hexavalent chromium, $CaCrO_4.2H_2O$ was found to form within a few minutes of the hydration reaction. With increasing concentration of Ca^{2+} in the pore solution, $Ca_2CrO_5.3H_2O$ became the stable species. The chromium in this phase was found to be very mobile in a standard acetic acid leaching test. Small quantities of Cr(VI) were found to be chemically incorporated in the stable calcium silicate hydrate (C-S-H) phase. When added in the trivalent form, chromium has been found to be primarily contained in C_3S pastes as calcium chromium hydroxide complexes. The nature of the complex formed depended on the ambient conditions within the reaction chamber. The concentration of the chromium complex was also found to increase with both age and the chromium concentration in the initial chromium/C_3S mixture. Some chromium was also found to be chemically incorporated in the C-S-H phase, independent of the prevailing conditions of hydration and, to a lesser extent, the initial chromium concentration in the mixture. Trivalent chromium has been found to be totally stabilized in C_3S paste and immobile in the standard acetic acid leaching test.

Mechanistic models describing the containment of Cr(III) and Cr(VI) in C_3S throughout the hydration period have been proposed. These are based on direct evidence from the various microstructural, microchemical and molecular characterization techniques employed.

ACKNOWLEDGMENTS

My profound gratitude goes to my supervisor, Dr. D.G Ivey for giving me the opportunity and the guidance to work in an exciting research area. My co-supervisor, Dr. Randy Mikula provided invaluable advice towards the realization of my research goals.

I will like to express my appreciation to the Natural Resources Canada (CANMET) and the Natural Sciences and Engineering Research Council (NSERC) for funding the research.

I am indebted to Ms. Tina Barker, Mr. Shiraz Merali and Mr. Bob Konzuk for providing adequate technical assistance in my laboratory work.

I am also grateful to Dr. Kim Kaperski, Dr. Alfred Saffa and Dr. Kelly Akers of CANMET Western Research Centre, Devon for the assistance they provided in calorimetry and vibrational spectroscopy.

And to my friends and colleagues, especially my fiancee, Moremi, you made my stay at the University of Alberta worthwhile. Thank you.

TABLE OF CONTENTS

Chapter 1 Introduction 1

Chapter 2 Literature Review 3

2.1 Composition of Ordinary Portland Cement 3

2.2 Hydration of Tricalcium Silicate 5

2.2.1 Mechanisms of Hydration Reactions 5

2.2.1.1 Early Stages of Hydration 6

2.2.1.2 Middle and Late Stages of Hydration 7

2.2.1.3 Hydration of Aluminate and Ferrite Phases 8

2.2.2 Influence of Admixtures on the Hydration of Tricalcium Silicate 9

2.2.3 Methods of Analysis 10

2.2.3.1 Composition and Speciation of C_3S/OPC Pastes 10

2.2.3.2 Structure of Hydration Products 12

2.3 Stabilization/Solidification of Heavy Metal Ions in Cement Matrices. 17

2.3.1 Analytical Techniques Employed in Studying the Mechanisms of Waste Containment in Cement Matrices 17

2.3.2 Overview of Stabilization/Solidification Mechanisms in Cement 19

2.3.3 Solution Chemistry of Chromium 23

2.3.3.1 Hydrolysis of Cr(VI) (CrO_3) 23

2.3.3.2 Hydrolysis of Cr(III) 23

Chapter 3 Experimental Techniques 30

3.1 Production of Tricalcium Silicate 30

3.1.1 Determination of Particle Size 30

3.1.2 Determination of Free Lime (CaO) 30

3.2 Preparation of Chromium Doped Samples 31

3.3 X-ray Diffraction 32

3.3.1 Routine Identification of Samples 32

3.3.2 Quantitative X-ray Diffraction Analysis 32
3.3.2.1 Preparation of Standards 32
3.3.2.2 Data Collection and Analysis 34
3.4 Electron Microscopy 35
3.4.1 Scanning Electron Microscopy 35
3.4.2 Transmission Electron Microscopy 36
3.5 Molecular Spectroscopy 35
3.5.1 Fourier Transform Infrared (FTIR) 37
3.5.2 Nuclear Magnetic Resonance 38
3.6 Leaching Studies 39
Chapter 4 Results and Discussions 40
4.1 X-ray Powder Diffraction 40
4.1.1 Trivalent Chromium Doped C_3S Pastes 40
4.1.2 Effects of Varying Cr(III) Concentrations on Hydration Reactions 44
4.1.3 Hexavalent Chromium Doped C_3S Pastes. 46
4.1.4 Effect of Varying Cr(VI) Concentrations on Hydration 49
4.2 Microstructure and Composition of Undoped and Chromium Doped C_3S Pastes 49
4.2.1 Microstructure of Undoped C_3S Pastes 49
4.2.2 Microstructure and Composition of Cr(III) Doped Paste 51
4.2.3 Microstructure and Composition of Cr(VI) Pastes 56
4.3 FTIR Spectroscopy 58
4.3.1 Chromium (III) Pastes 60
4.3.1.1 Rate of Formation of Calcium Chromium Complexes in 2M Cr(III) Pastes 63
4.3.1.2 Effects of Cr(III) Concentrations on the C_3S Hydration 64
4.3.2 Chromium (VI) Pastes 67
4.3.2.1 Effect of Cr(VI) Ion on Hydration of C_3S 68

4.3.2.2 Effect of Cr(VI) Concentrations on C_3S Hydration 69

4.4 Nuclear Magnetic Resonance Spectroscopy 73

4.4.1 C-S-H Anion Structure of the Blank, 2M Cr(III) and Cr(VI) Pastes. 73

4.5.2 Rate of Formation of Dimeric and Polymeric C-S-H 74

4.5 Leaching Studies 77

Chapter 5 Proposed Reaction Mechanisms 132

5.1 Containment Mechanism of Cr(III) in C_3S Pastes 133

5.2 Containment Mechanism of Cr(VI) in C_3S Pastes 134

Chapter 6 Conclusions and Recommendations 136

6.1 Conclusions 136

6.2 Recommendations 137

References 138

LIST OF TABLES

Table 2.1	Actvities of dissolved species at the triple point; [CaO] = 2.80×10^{-2}M, $[SiO_2] = 2.00 \times 10^{-5}$M	6
Table 2.2	FTIR spectra assignments of Tricalcium Silicate	13
Table 2.3	Vibrational frequencies of some hydroxyl groups	14
Table 2.4	Guidelines for Canadian drinking water quality	17
Table 3.1	Hydration experiments detailing concentrations of chromium solutions and hydration times	31
Table 4.1.1	X-ray powder diffraction data of early calcium - chromium complex (Ca: Cr = 3)	43
Table 4.1.2	X-ray powder diffraction data of late calcium - chromium complex (Ca: Cr = 2)	44
Table 4.1.3	QXRD of 2M Cr(III) pastes hydrated for varying times	44
Table 4.1.4	QXRD analyses of partially hydrated 0.1M and 1M chromium pastes	46
Table 4.1.5	X-ray powder diffraction data of $Ca_2CrO_5.3H_2O$	48
Table 4.1.6	QXRD of 2M Cr(VI) pastes hydrated for varying times	49
Table 4.2.1	Average Ca/Si ratios in hydrated blank and chromium - doped pastes	51
Table 4.2.2	Average Ca/Cr ratios in chromium - doped pastes	53
Table 4.3.1	FTIR spectra assignments of C_3S and fully hydrated blank and 2M Cr(III) doped pastes	59
Table 4.3.2	FTIR spectra assignments of early calcium chromium complex	61
Table 4.3.3	FTIR spectra assignments of 24 hour old Cr(III) pastes	65
Table 4.3.4	FTIR spectra assignments of 60 hour old Cr(III) pastes	66
Table 4.3.5	FTIR spectra assignments of $CaCrO_4.2H_2O$ and $Ca_2CrO_5.3H_2O$	69
Table 4.3.6	FTIR spectra assignments of 2M Cr(VI) pastes	70
Table 4.3.7	FTIR spectra assignments of 24 hour old Cr(VI) pastes	71

Table 4.3.8	FTIR spectra assignments of 60 day old Cr(VI) pastes	72
Table 4.4.1	^{29}Si chemical shift data of partially and fully hydrated chromium doped tricalcium silicate	75
Table 4.5.2	Integrated intensity ratios (Q_2/Q_1) of partially and fully hydrated chromium doped tricalcium silicate	76
Table 4.5.1	AAS leachate analyses of standard and Cr - doped pastes subjected to TCLP leaching	78

LIST OF FIGURES

Fig. 2.1	Jeffery's C_3S structure showing the ac projection	26
Fig. 2.2	Scanning electron micrograph of anhydrous C_3S	26
Fig. 2.3	Schematic representation of changes taking place in the C_3S - water system	27
Fig. 2.4	Crystal structure of ettringite.	28
Fig. 2.5	^{29}Si chemical shift ranges in aluminosilicates	29
Fig. 4.1.1	XRD patterns of anhydrous C_3S and 14 month old blank paste	79
Fig. 4.1.2	XRD patterns of 2M Cr(III) pastes	80
Fig. 4.1.3	XRD patterns of 15 day old 2M Cr(III) pastes	81
Fig. 4.1.4	XRD pattern of early Ca - Cr complex	82
Fig. 4.1.5	Rate of reaction of C_3S and formation of early Ca - Cr complex	83
Fig. 4.1.6	XRD patterns of 24 hour old Cr(III) pastes	84
Fig. 4.1.7	XRD patterns of 60 day old blank and Cr(III) pastes	85
Fig. 4.1.8	QXRD analysis of 14 month old 2.75M Cr(III) paste	86
Fig. 4.1.9	XRD patterns of 2M Cr(VI) pastes hydrated for varying times	87
Fig. 4.1.10	Rate of reaction of C_3S and formation of $Ca_2CrO_5.3H_2O$	88
Fig. 4.1.11	XRD patterns of 24 hour old Cr(VI) pastes	89
Fig. 4.1.12	XRD patterns of 60 day old Cr(VI) pastes	90
Fig. 4.2.1	SEM micrographs of a blank paste hydrated for 24 hours	91
Fig. 4.2.2	Backscattered electron micrographs of a 24 hour old blank paste	92
Fig. 4.2.3	SEM micrograph of a blank paste hydrated for 60 days	93
Fig. 4.2.4	TEM micrograph of a blank paste hydrated for 60 days	93
Fig. 4.2.5	SEM micrograph of a polished blank paste hydrated for 14 months	94
Fig. 4.2.6	X-ray microanalysis of fully hydrated blank (C_3S) pastes	95
Fig. 4.2.7.	SEM micrograph and EDS spectra of 0.1M Cr(III) chloride hydrated for 24 hours	96
Fig. 4.2.8	SEM micrograph of 24 hour old 0.1M chromium nitrate	97
Fig. 4.2.9	SEM micrograph of a 60 day old 0.1M chromium nitrate	98
Fig. 4.2.10	SEM micrograph of a 60 day old 0.1M chromium chloride paste	98
Fig. 4.2.11	SEM micrograph and EDS spectra of a fractured 24 hour old 1M Cr(III) nitrate paste	99
Fig. 4.2.12	TEM micrograph and SAD pattern of 1M Cr(III) nitrate hydrated for 24 hours	100
Fig. 4.2.13	SEM micrograph and EDS spectra of 60 day old 1M Cr(III) nitrate	

	paste	101
Fig. 4.2.14	SEM micrograph and EDS spectra of a fractured 60 day old 1M Cr(III) chloride paste	102
Fig. 4.2.15	X-ray map of a polished 1M Cr(III) nitrate paste hydrated for 60 days	103
Fig. 4.2.16	TEM micrograph of a 60 day old 1M chromium nitrate paste	103
Fig. 4.2.17	TEM micrograph of a 5 minute old 2M chromium nitrate paste	104
Fig. 4.2.18	Variation of Ca and Si with Cr in a 5 minute old 2M Cr(III) paste	104
Fig. 4.2.19	SEM micrograph of a 24 hour old 2M chromium nitrate paste	105
Fig. 4.2.20	TEM micrographs of a 24 hour old 2M chromium nitrate paste	106
Fig. 4.2.20c	Variation of Ca and Si with Cr in a 24 hour old 2M Cr(III) paste (EDS of CH and C_3S excluded)	107
Fig. 4.2.21	TEM micrographs of a 60 day old 2M chromium nitrate paste	108
Fig. 4.2.22	TEM micrograph of a 60 day old 2M chromium nitrate paste showing Ca - Cr complex rods	109
Fig. 4.2.23	Relationship between Cr concentrations and Ca and Si concentrations in the products of hydration of a 60 day old 2M Cr(III) paste	109
Fig. 4.2.24	TEM micrograph and EDS spectra of a 14 month old 2.75M Cr(III) paste	110
Fig. 4.2.25	TEM micrograph of a 14 month old 2.75M chromium nitrate paste showing late Ca - Cr complex rods (Ca: Cr ratio = 2)	111
Fig. 4.2.26	Variation of Ca and Si with Cr in a 14 month old exposed 2.75M Cr(III) paste	111
Fig. 4.2.27	Low magnification SEM micrograph of a polished 14 month old 2.75M Cr(III) paste	112
Fig. 4.2.28	X-ray line scan of a polished 14 month old 2.75M Cr(III) paste	112
Fig. 4.2.29	SEM/EDS analysis plot of Cr/Ca mole ratio against Si/Ca mole ratios in a typical 14 month old 2.75M Cr(III) paste	113
Fig. 4.2.30	TEM micrograph and SAD pattern of early Ca - Cr complex powder examined on a carbon coated grid. (Ca/Cr ratio = 3)	114
Fig. 4.2.31	SEM micrograph and EDS spectra of a typical 0.1M Cr(VI) paste hydrated for 24 hours. The analyzed regions are mainly CH and C-S-H	115
Fig. 4.2.32	SEM micrograph of 0.1M Cr(VI) paste hydrated for 60 days	116
Fig. 4.2.33	SEM micrograph of 1M Cr(VI) paste hydrated for 60 days	116
Fig. 4.2.34	X-ray maps of a polished 1M Cr(VI) paste hydrated for 60 days	117

Fig. 4.2.35	SEM micrograph and EDS spectrum of a 5 minute old 2M Cr(VI) paste	118
Fig. 4.2.36	TEM micrograph of a typical $CaCrO_4.2H_2O$ rod in a 5 minute old 2M Cr(VI) paste	119
Fig. 4.2.37	TEM/x-ray microanalysis of typical phases in a 5 minute old 2M Cr(VI) paste	119
Fig. 4.2.38	SEM micrograph of 2M Cr(VI) paste hydrated for 24 hours	120
Fig. 4.2.39	TEM micrograph of 2M Cr(VI) paste hydrated for 24 hours	120
Fig. 4.3.1	FTIR spectra of C_3S and fully hydrated pastes	121
Fig. 4.3.2	FTIR spectra of early calcium chromium complex formed from $Ca(OD)_2$ /$Cr(NO_3)_3.9H_2O$ in D_2O and $Ca(OH)_2$/$Cr(NO_3)_3.9H_2O$ in H_2O	122
Fig. 4.3.3	FTIR spectra of exposed 2M Cr(III) pastes	123
Fig. 4.3.4	FTIR spectra of varying Cr(III) concentrations in C_3S paste hydrated for 24 hours	124
Fig. 4.3.5	FTIR spectra of 60 day old samples	125
Fig. 4.3.6	FTIR spectra of calcium chromates formed during hydration of Cr(VI) doped C_3S	126
Fig. 4.3.7	FTIR spectra of exposed 2M Cr(VI) pastes	127
Fig. 4.3.8	FTIR spectra of 24 hour old Cr(VI) pastes	128
Fig. 4.3.9	FTIR spectra of 60 day old Cr(VI) pastes	129
Fig. 4.4.1	^{29}Si MAS NMR spectra obtained at 59.6 MHz of partially and fully hydrated chromium doped tricalcium silicate pastes	130
Fig. 4.5.1	XRD patterns of leached pastes	131

SYMBOLS

Generic symbols in Chapters 1 and 2 are listed separately from symbols adopted in other chapters.

Symbols in Chapters 1 and 2

Conventional Cement Notations

CaO: C

SiO_2: S

Al_2O_3: A

Fe_2O_3: F

SO_3: $\bar{S}$

H_2O: H

$CaSO_4$: $C\bar{S}$

Aft (Ettringite): $C_3A.3C\bar{S}.H_{32}$

Calcium Hydroxide: CH

Calcium Silicate Hydrate: C-S-H

Tricalcium Silicate: C_3S

Dicalcium Silicate: C_2S

Tricalcium Aluminate: C_3A

Calcium alumino-ferrite: C_4AF

OPC: Ordinary Portland Cement

pfa: Pulverized fly-ash

w/s: water to solid ratio or solution to solid ratio

Other Coventional Notations

SEM: Scanning electron microscopy

TEM: Transmission electron microscopy

STEM: Scanning/transmission electron microscopy

EDS: Energy dispersive spectroscopy

XRD: X-ray diffraction

QXRD: Quantitative x-ray diffraction

I(fix): Integrated XRD intensity obtained with a fixed slit

I(var): Integrated XRD intensity obtained with a variable slit

TG: Thermogravimetry

DTA: Differential thermal analysis

BSE:	Backscattered electron image analysis
MAS NMR:	Magic angle spinning nuclear magnetic resonance
FTIR:	Fourier transform infrared spectrometry
GLC:	Gas liquid chromatography
GPC:	Gel permeation chromatography
Q_n:	n - number of Si attached to an orthosilicate unit (Q)
EXAFS:	X-ray absorption fine structure
EXELFS:	Extended energy loss fine structure
XPS:	X-ray photoelectron spectroscopy
EPA-TCLP:	Environmental Protection Agency - Toxicity Characteristic Leaching Procedure

Symbols in other Chapters

Sample Identification

Bl-24H:	24 hour old blank paste
Bl-60D:	60 day old blank paste
0.1MCC3-24H:	24 hour old 0.1M chromium chloride paste
0.1MCN3-24H:	24 hour old 0.1M chromium nitrate paste
0.1MC6-24H:	24 hour old 0.1M chromium (VI) paste
1MCC3-24H:	24 hour old 1M chromium chloride paste
1MCN3-24H:	24 hour old 1M chromium nitrate paste
1MC6-24H:	24 hour old 1M chromium (VI) paste
2MC3-5MIN:	5 minute old 2M chromium nitrate paste
2MC3-6H:	6 hour old 2M chromium nitrate paste
2.75MC3-14M:	14 month old 2.75M chromium nitrate paste

Chapter 1 Introduction

The disposal of hazardous heavy metal liquid wastes in landfills is an age long practice. Unfortunately, after some time, these wastes can be exposed to soil water leaching action and end up as contaminants in ground water. This poses a threat to the environment since the toxicity of these heavy metal ions (as elements or compounds) is not reduced. Among others, activated carbon, clays, and gypsum have been used as sorption media to minimize leaching of toxic metal ions. Also common are; macroencapsulation of a large volume of waste, isolation by jacketing with plastic drums, and sometimes microencapsulation which involves blending waste particulate with melted asphalt or bitumen (Means et al. [1995]). All these techniques are physical processes which do not reduce contaminant leaching potential in the long run.

The use of cements as binding agents is the most successful method for disposing of toxic heavy metal ions in terms of economics and safety regulations. By making use of the resultant properties of cement - water reactions, liquid wastes are mixed with cement (usually ordinary Portland cement - OPC), to develop a high strength, monolithic cement/waste matrix. Depending on the heavy metal ion, stabilization could be through chemisorption, precipitation, chemical incorporation in the hydrated cement components, physical entrapment or simultaneous occurrence of several of these possibilities. Because of the specificity of heavy metal ions' reaction with cement and the complexity of cement chemistry, it has been very difficult to optimize and even understand the mechanisms involved in stabilization and solidification processes.

The heavy metals that pose the greatest threat to the environment (excluding radioactive substances) include; Cd, Cr, Pb, Hg and Zn. To simulate actual landfill conditions, most investigators immobilize reagent grade toxic heavy metal salts in cement and subject the solidified waste to different tests to evaluate the stability and strength of the cement.

The main thrust of this research centres around understanding the mode of chromium containment in tricalcium silicate (C_3S), the component of Portland cement responsible for its strength and stability. Reagent grade Cr(III) and Cr(VI) salts were used to simulate the liquid wastes containing these contaminants. Specific questions addressed are enumerated below:

a. How does chromium affect the hydration reaction of C_3S and the morphology of the normal hydration products?

b. Is chromium incorporated in the leach resistant calcium silicate hydrate phases of hydrated C_3S or as insoluble oxide/hydroxide complexes chemically detached from the normal C_3S hydration products?

c. Why is Cr(III) stabilized in cement and Cr(VI) is not?

By employing various structural, compositional and molecular characterization techniques in addition to leaching studies, most of these questions have been resolved. This will enable development of a stepwise mechanistic model detailing the mode of containment of chromium in C_3S and Portland cement.

In determining the effects of hazardous wastes on the strength and stability of the resultant waste/cement matrix, a comprehensive understanding of the complex cement chemistry is essential.

Chapter 2 Literature Review

2.1 Composition of Ordinary Portland Cement

Ordinary Portland cement (OPC) is manufactured by heating a mixture of calcium carbonate and silica - bearing materials such as limestone and clay at ~ 1450 °C. The partially fused clinker obtained is mixed with some gypsum ($CaSO_4.2H_2O$) and ground. The final product is Portland cement. The clinker has a typical composition of 67% CaO, 22% SiO_2, 5% Al_2O_3, and 3% Fe_2O_3. In addition small quantities of MgO, CaO (free lime) and alkali sulphates are often present (Kerton and Murray [1983], Taylor [1990]). The phases constituting OPC are alite (50 - 70%), belite (20 - 30%), calcium aluminate (5 - 22%) and calcium alumino-ferrite (5 - 12%).

Alite is the most important constituent of Portland cement. It controls the normal setting and early strength development of young cement paste and it is also responsible for the ultimate high compressive strength of matured cement paste. Alite is primarily tricalcium silicate (Ca_3SiO_5 or C_3S) whose structure has been modified by the incorporation of foreign ions such as Al^{3+}, Fe^{3+} and Mg^{2+} (Taylor [1990]). Similarly, belite is impure β-C_2S (Ca_2SiO_4) containing foreign ions in solid solution. Both C_3S and β-C_2S form the same product on hydration, but β-C_2S reacts at a much slower rate. In an attempt to simplify the complex cement system, C_3S is usually used to model the hydration of Portland cement. The calcium aluminate phase ($Ca_3Al_2O_6$ or C_3A) may contain many foreign ions such as Si^{4+}, Fe^{3+}, Na^+ and K^+ in solid solution. Its very rapid reactivity is the reason gypsum is added to the clinker. The ferrite phase has a composition $Ca_4(Al_xFe_{1-x})_2O_7$, where $0 < x < 0.7$, approximating to C_4AF.

Pure C_3S is triclinic (T_1) at room temperature (Jeffery [1952]). It undergoes a series of reversible phase transformations at high temperatures exhibiting three polymorphs; triclinic, monoclinic and trigonal. Alite is monoclinic at room temperature. The incorporation of foreign ions in alite stabilizes the high temperature polymorph of pure C_3S. The structure proposed by Jeffery for C_3S comprises independent SiO_4^{4-} tetrahedra (Jeffery [1952]). The Ca ions link the tetrahedra and are octahedrally coordinated to three oxygen ions which are not linked to Si^{4+}.

The crystal structure shows nine unique silicate anion environments in the unit cell as shown in Fig. 2.1 (Golovastikov et al. [1976]). Handke and Jurkiewicz [1979], found from infrared and Raman spectroscopic studies of C_3S that the triclinic structure appears laminar with the symmetry inside the layer close to the R3m symmetry proposed by

Jeffery. The Si-O bond is partially covalent and partially ionic with some d_π-p_π bonding between silicon and oxygen. The bond angle is about 140° (Boehm [1966]).

To act as a hydraulic cement, a substance must react with water to a sufficient extent and at a sufficient rate. Moreover, reaction products must have very low solubility and possess a microstructure that has the requisite mechanical strength and volume stability (Taylor [1990]). C_3S, alite, β-C_2S, belite and Portland cement all meet these criteria making them good hydraulic cements. The reactivity of oxygen atoms towards attack by protons depends on their basicities, which are directly dependent on the electronegativity of the atoms associated with oxygen. The SiO_4^{4-} tetrahedra have a relatively low basicity; therefore, C_3S which contains some oxygen atoms linked only to Ca is more reactive than β-C_2S in which all the oxygen atoms are also linked to Si. Similarly, oxygen atoms within the silicate tetrahedra will be less reactive as the degree of anion condensation with other silicate tetrahedra increases (Taylor [1990]). Other factors controlling the reactivity of C_3S include polymorphism, defects, ionic substitution, crystallite morphology and presence of inclusions (Taylor et al. [1984]). These effects are complex because many variables are involved which are difficult or impossible to control independently. The C_3S surface is most probably protonated and therefore saturated with the silanol group O_3SiOH. Fig. 2.2 shows some interparticle bonding of anhydrous C_3S. It is possible that neutral $\equiv$SiOH groups as well as $\equiv SiO^-$ ionized groups on the surface of the particles condense to form Si-O-Si linkages (Iler [1979]).

Unlike C_3S, pure C_3A is not polymorphic. C_3A has a cubic structure (space group - Pa3) and Z = 24 (number of asymmetric units in the unit cell). The unit cell is built from octahedrally coordinated Ca^{2+} and six AlO_4 tetrahedra (Kerton and Murray [1983], Struble [1986], Taylor [1990]). Lee et al. (1982) found that Al_2O_3 could be replaced by up to 2% SiO_2 or 3 - 4% Fe_2O_3 under equilibrium conditions. C_3A and C_4AF are very reactive owing to the presence of O^{2-} linked only to Ca^{2+}, in addition to those O^{2-} also linked to Al^{3+}. They react faster than C_3S or β-C_2S but do not form good hydraulic cements as their products lack adequate mechanical strength.

2.2 Hydration of Tricalcium Silicate

2.2.1 Mechanisms of Hydration Reactions

Hydration denotes all the changes taking place when an anhydrous cement (or C_3S) is mixed with water (usually with a water/cement ratio of 0.3 to 0.6) to form a paste.

On contact with water, a small amount of heat, commonly attributed to the wetting and initial dissolution of C_3S is liberated (stage 1) - Fig. 2.3a. An induction or dormant period (stage 2) follows which lasts from 30 minutes to 6 hours (Jennings et al. [1981], Rodger et al. [1988]). After the induction period, there is a relatively larger heat evolution which may last for about 10 hours (acceleratory period, stage 3). This is followed by a deceleratory period (stage 4) and subsequent slow hydration over a long time scale (stage 5), which starts after about 24 hours of hydration. Exact periods of stages 1 and 2 depend strongly on the experimental parameters, especially the water/solid ratio, temperature and admixtures present in C_3S (Jawed et al. [1983]). Setting and hardening occur, resulting in the development of the high compressive strength characteristic of cured cement pastes. Typically, about 70% of the C_3S reacts within 28 days and virtually all of it in one year (Taylor [1990]). The overall hydration reaction can be represented by (Jawed et al. [1983]);

$$2C_3S + 7H \rightarrow C_3S_2H_4\,(C\text{-}S\text{-}H) + 3CH \quad \Delta H = -1114\ \text{kJ/mole} \tag{2.1}$$

The reaction does not describe the stoichiometry exactly because C-S-H (calcium silicate hydrate) is amorphous and has a variable composition. The microstructure of a hardened C_3S paste consists primarily of massive $Ca(OH)_2$ and fibrous C-S-H surrounding the anhydrous C_3S grains.

Both C-S-H and CH are easily carbonated when exposed to CO_2. This is especially critical for small laboratory samples and young pastes. The CO_2 content of the paste should be determined to account for the loss of Ca as $CaCO_3$. Most often, polar organic liquids such as methanol, acetone and isopropyl alcohol have been employed to stop hydration reactions in young pastes followed by evacuation (Taylor [1987], Day [1982]). However, these liquids are sometimes very difficult to remove from the hydrating matrix without altering the structure of the C-S-H and CH. It has been claimed that acetone reacts with CH at ordinary temperatures to form calcium methoxide (Beaudoin [1987]).

Table 2.1 Activities of dissolved species at the triple point; [CaO] = 2.80×10^{-2}, [SiO_2] = 2.00×10^{-5} (Gartner and Jennings [1987]).

Dissolved Species	*Computed Activity*
Ca^{2+}	7.9×10^{-3}
$CaOH^{+}$	7.23×10^{-3}
$CaH_3SiO_4^{+}$	1.62×10^{-7}
CaH_2SiO_4	1.61×10^{-5}
OH^{-}	3.78×10^{-2}
H_4SiO_4	7.75×10^{-10}
$H_3SiO_4^{-}$	1.02×10^{-6}
$H_2SiO_4^{2-}$	1.01×10^{-6}
$HSiO_4^{3-}$	3.82×10^{-9}

2.2.1.1 Early Stages of Hydration

During stage 1, the C_3S - water reaction produces a layer of C-S-H (Type E) containing monomeric silicate units. This surrounds the anhydrous C_3S particles and isolates them thermodynamically from the aqueous phase (Jennings [1986]). The presence of an induction period has been a subject of debate for several decades. Taylor (1990) summarized the hypotheses proposed as the cause, initiation and termination of the induction period. These include:

a. Type E-C-S-H forms a protective barrier on the C_3S grain causing the induction period. The induction period ends when the barrier is destroyed or rendered more permeable by aging or phase transformation.

b. Type E-C-S-H forms a semi-permeable membrane enclosing an inner solution. This is destroyed by osmotic bursting.

c. The nucleation and growth of dimeric C-S-H controls the rate of reaction during the induction period. The induction period ends when growth begins.

d. The poisoning of CH nuclei by SiO_2 causes the induction period hindering their growth. This ends when the supersaturation of CH in solution is sufficient to overcome this effect.

When lime or CH was mixed with C_3S prior to hydration, no effect on the length of the induction period was found thereby discounting hypothesis d (Odler and Dorr [1977],

Brown et al. [1984]). On the other hand siliceous materials such as pfa (pulverized fly ash) and silica markedly accelerate hydration (Taylor [1990]). Hypothesis b is suspect because no membrane or inner solution has been identifiable with surface characterization techniques (Menetrier et al. [1979], Sujata and Jennings [1992]). Solution analysis indicates that the $[SiO_2]$ activity falls during the induction period. This might lead to a phase transformation in the type E C-S-H which terminates the induction period. The triple point in the C_3S solubility curve coincides with the end of the induction period at which point the C-S-H is in equilibrium with the solution species in Table 2.1 (Gartner and Jennings [1987]). The accelerating effect that siliceous materials have on C_3S hydration supports the combination of hypotheses a and c.

2.2.1.2 Middle and Late Stages of Hydration

At the end of the induction period, calcium hydroxide (CH) and fibrous C-S-H (Type I) containing dimeric silicate species, start to form. These give rise to the high heat of formation observed during the acceleratory period. Fibrous C-S-H is sometimes referred to as the outer C-S-H. Condensation of monomeric silicates primarily involves the reaction of a $\equiv SiO^-$ ion with a non-ionized silanol group (Iler [1979]).

$$\equiv SiO^- + HOSi\equiv \rightarrow \equiv SiOSi\equiv + OH^- \qquad (2.2)$$

As the pH increases with increasing $[OH^-]$, ionized monomers can also combine to form dimers as described by Ortego et al. (1991) in Equations 2.3a, b and c.

$$SiO_4^{4-} + xH_2O \rightarrow [SiO_3(OH)]^{3-} + [SiO_2(OH)_2]^{2-} + [SiO(OH)_3]^- + yOH^- \qquad (2.3a)$$

$$2[SiO_2(OH)_2]^{2-} \rightarrow [HO(O_2)SiOSiO(O_2)OH]^{4-} + H_2O \qquad (2.3b)$$

$$3[SiO_2(OH)_2]^{2-} \rightarrow [HO(O_2)SiOSi(O_2)OSi(O_2)OH]^{6-} + 2H_2O \qquad (2.3c)$$

The hydrosilicate anion formed depends on the pH of the cement solution. The higher the pH, the more probable the formation of stronger Lewis bases. For example when the pH is between 9.5 and 12, $[SiO(OH)_3]^-$ is formed. At pH > 12, $[SiO_2(OH)_2]^{2-}$ and $[SiO_3(OH)]^{3-}$ are more stable (Heimann [1986]). Due to the high electron affinity of Si^{4+} and the attendant low basicity of the silicate tetrahedra, H^+ bound to a $\equiv SiO^-$ group can be

easily replaced by other positive ions in solution. The formation of $Ca(OH)_2$ is mainly responsible for the high pH (12 - 13) observed in C_3S and OPC pastes. Also, the formation of OH^- in the hydroxylation of SiO_4^{4-} (Equation 2.2), restricts the degree of polymerization resulting in the formation of only short linear polymers (Iler [1979], Ortego et al. [1991]).

During the deceleratory and steady state period, the hydration products grow and densification of the microstructure is observed in the SEM. Further condensation reaction takes place with the formation of polymeric silicate units with a Ca/Si ratio of about 1.7 ± 0.1. This C-S-H is usually referred to as Type II C-S-H or inner C-S-H. Taylor (1990) ascribed the reaction mechanism to the migration of a C-S-H interface into the unreacted C_3S core. Ca^{2+} and some SiO_4^{4-} migrate outwards and H^+ inwards. At the surface, the Ca^{2+} and SiO_4^{4-} enter the solution precipitating as CH and outer C-S-H. The Ca/Si ratio is the standard parameter for describing the composition of amorphous C-S-H.

2.2.1.3 Hydration of Aluminate and Ferrite Phases

Within a few hours of Portland cement hydration, ettringite starts to form from the calcium aluminate and ferrite phases. Its formation reaches a maximum in about 24 hours before decomposing (Kerton and Murray [1983], Taylor [1990]). Ettringite is crystalline and the most important of the Aft phases (Al_2O_3-Fe_2O_3 - tri). The general composition of Aft is $Ca_3(Al,Fe)(OH)_6.12H_2O]_2.X_3.yH_2O$. $y \leq 2$ and X represents one unit of a doubly charged anion or 2 units of a singly charged anion. Aft structures are based on columns in a hexagonal array, running parallel to the c-axis, with the X anions and water molecules in the intervening channels as shown in Fig. 2.4 (Moore and Taylor [1968, 1970], Taylor [1990]). The columns are composed of $(Al,Fe)(OH_6)$ in octahedral coordination. Each calcium atom is coordinated to four water molecules and four OH^- ions. Ettringite, the most important of the Aft compounds, has a chemical formula; $Ca_3(Al,Fe)(OH)_6.12H_2O]_2.(SO_4)_3.2H_2O$. It is also known to occur naturally (Moore and Taylor [1970]). The crystal structure is trigonal with a = 1.123 nm, c = 2.150 nm, Z = 2 and S.G. P31c (Powder File [41-1451]). Analogue compounds exist with Fe^{3+}, Mn^{3+}, Cr^{3+} or Ti^{3+} occupying Al^{3+} sites in the Aft structure (Bensted and Varma [1971]). Other analogues of interest are CrO_4^{2-}, replacing SO_4^{2-} (Bensted and Varma [1972], Poellman et al. [1993]) and thaumasite (Effenberger [1983]) with a formula $Ca_3Si(OH)_6.12H_2O]_2.(SO_4).CO_3$. Si exists in octahedral coordination in the structure. Thaumasite and ettringite are reported to be miscible (Edge and Taylor [1971]).

Afm phases (Al_2O_3-Fe_2O_3 - mono) begin to form as Aft decomposes and remain throughout the course of hydration reactions. The phases are poorly crystalline and have a general formula $Ca_2(Al,Fe)(OH)_6].X.yH_2O$. X and y are as described for Aft phases. The specific composition depends on the initial composition of Portland cement. Analogues containing Cr^{3+}, replacing Al^{3+} or Fe^{3+}, have been reported (Bensted and Varma [1973]).

2.2.2 Influence of Admixtures on the Hydration of Tricalcium Silicate

A lot of work has been done to elucidate the modifying effects of admixtures on the setting and hardening of cement. These studies serve as a reference for understanding the containment mechanisms of hazardous wastes in cement.

Kantro (1975) investigated the hydration of C_3S in the presence of various salts. He observed that most soluble salts act to accelerate the hydration of C_3S, notable exceptions being phosphates, fluorides and salts of Zn, Sn and Pb. His data suggest that both the charge and atomic size of the ions are important. Those with high charge and small size being the most effective accelerators. Approximate order of effectiveness is as follows (Jawed et al. [1983], Thomas [1987]):

$Y^{3+} \sim La^{3+} \sim Ca^{2+} > Ni^{2+} > Mg^{2+} > Sr^{2+} > Ba^{2+} \sim Li^{+} > K^{+} > Rb^{+} \sim Cs^{+} > Na^{+}$; for chlorides,

$CrO_4^{2-} > SO_4^{2-} \sim S_2O_3^{2-} > Cl^{-} \sim Br^{-} > I^{-} > NO_3^{-} \sim NO_2^{-} \sim CNS^{-} > ClO_3^{-} > F^{-}$; for potassium salts.

Kondo et al. (1977) correlated the results of Kantro (1975) with the ionic mobilities and diffusion characteristics of the ions and concluded that acceleration is determined by the rate of ionic diffusion, the added electrolyte providing ions for counter diffusion. Ions that accelerate strongly favour a condensed electrical double layer and low zeta potential which might encourage formation of colloidal C-S-H. A thinner double layer would allow closer approach of solid particles resulting in a denser product with finer pores and hence a C-S-H with a small diffusion coefficient (Jawed et al. [1983]).

Organic compounds with chelating capabilities (presence of β-hydroxy carboxylate) grouping which forms a strong six-membered chelate ring with a metal ion) prolong the induction period by adsorption on the [001] face of CH thereby inhibiting its nucleation (Jawed et al. [1983], Thomas and Double [1983]).

2.2.3 Methods of Analysis

2.2.3.1 Composition and Speciation of C_3S/OPC Pastes

The sequence of hydration reactions has been monitored using various techniques. Kondo and Daimon (1969) highlighted the use of conduction calorimetry for measuring the rate of heat liberation during the reaction. Fig. 2.3a shows a schematic representation of the rate of heat evolution during the hydration of C_3S.

Several investigators have conducted solution phase analysis of partially hydrated cement to monitor the rate at which Ca^{2+}, SiO_4^{4-} and OH^- are released into the pore solution (Fierens and Verhaegen [1976], Young et al. [1977], Brown et al. [1984], Jennings and Parrot [1986], Gartner and Jennings [1987]). Curves for [CaO] and [OH^-] exhibit a sharp rise during the initial reaction and a gentle slope during the induction period. Significant amounts of CH precipitate just before the maximum and grow rapidly during the deceleratory period (Taylor [1990], Nocun-Wczelik [1990]). It was found that the species in solution are in a metastable equilibrium with the hydration products and curves of [CaO] against [SiO_4^{4-}] are independent of the water/solid ratio and the particle sizes of the C_3S used by different investigators (Brown et al. [1984], Jennings [1986], Gartner and Jennings [1987]). The very low concentrations of the species enable the application of the Gibbs-Duhem equation to define the solution thermodynamics and obtain the Ca/Si ratio of the C-S-H. The equation reduces to;

$$(Ca/Si)_{C\text{-}S\text{-}H} = -d\mu_s/d\mu_c \qquad (2.4)$$

μ_s and μ_c are the chemical potentials of SiO_2 and CaO respectively in equilibrium with C-S-H (Gartner and Jennings [1987], Taylor [1990]).

Several methods have been used to determine the composition of C_3S pastes. Methods for determining the amount of CH include: Thermogravimetry (TG), differential thermal analysis (DTA), quantitative x-ray diffraction (QXRD), backscattered electron image analysis (BSE) and solvent extraction. It has been observed, however, that thermal and chemical methods give consistently higher CH values than QXRD (Midgley [1979], Odler and Dorr [1979], Bentur and Berger [1979], Ramanchandra [1979]). This has been attributed to factors ranging from the presence of amorphous CH (Odler and Dorr [1979]) to the adsorption of CH on C-S-H (Bentur and Berger [1979]). Neither scenario has been verified. QXRD and ^{29}Si MAS NMR are the only methods available to determine the amount of unreacted C_3S with a precision of no better than 3% (Taylor [1990]). Generally, a fully hydrated C_3S paste contains about 35% CH, some of which would be carbonated to

$CaCO_3$ depending on the hydrating environment. If the amounts of CH and CO_2 in a fully hydrated paste are known, the Ca/Si ratio in the C-S-H could be determined. For partially hydrated pastes, QXRD and NMR could be used to determine the Ca/Si ratio. The Ca/Si ratio calculated using extraction and thermal methods is 1.7± 0.1 and 1.99 for QXRD (Odler and Dorr [1979]).

Electron microscopy has been extensively used to investigate the structural, morphological and chemical development of the different types of C-S-H (Fig. 2.3c). Among the various electron microscopy techniques, scanning electron microscopy coupled with energy dispersive X-ray analysis (SEM/EDS) has been the most widely used for analyzing fractured and polished surfaces (Williamson [1972], Diamond [1976], Goto et al. [1976], Marchese [1977, 1988]). The SEM has the advantage of great convenience and provides good morphological details of the area exposed by the fracture path. In the secondary electron imaging mode, it suffers from the drawback of not necessarily giving a representative view of the microstructure and failing to give information about relatively dense regions where the fracture surface is flat (Groves [1987]). Backscattered electron imaging in SEM does not have these drawbacks, as it can give compostional variations in relatively dense regions. Backscattered electron imaging has been employed in various investigations of cement hydration (Stucke and Majumdar [1977], Scrivener et al. [1987]). Bulk sections are usually impregnated with a low viscosity epoxy prior to grinding and polishing (Campbell and Ahmed [1979]). The technique which has the greatest potential for high spatial resolution is transmission electron microscopy (Grudemo [1964], Double [1973], Lawrence and Carvalho [1974], Dalgleish and Ibe [1981], Jennings et al. [1981], Groves [1987], Rodger et al. [1987]). Grudemo (1964) and Double (1973) studied cement hydration products in the form of dispersed particles using a high voltage TEM. In this form, cement particles are too thick to allow a significant study of their internal microstructure (Groves [1987]). Also, observation of isolated particles does not give a true representation of the entire nature and orientation of phases. A technique involving dimpling followed by ion milling in a cold stage for about 3-hours could produce 'very large' thin sections suitable for TEM analysis (Ivey and Neuwirth [1989]). However, prolonged ion-milling could amorphize some of the crystalline phases.

X-ray microanalysis of polished surfaces shows the Ca/Si ratio of C-S-H to be dependent on the accelerating voltage. This can range from 1.4 at 6 kV to 2.0 at 25 kV (Taylor and Newbury [1984]). Mean values of 1.72 and 1.78 were obtained when operating at 10 kV with a range between 1.5 and 2.0. X-ray microanalysis in the TEM indicates a wider range of Ca/Si; 1.2 to 2.0 with a mean of 1.4 (Gard et al. [1981], Mohan

and Taylor [1981]), and no significant difference was found in the Ca/Si ratio of inner and outer C-S-H. This problem can be minimized by analyzing the standards and the samples at the same accelerating voltage.

In OPC, containing Afm and Aft phases, the reported mean Ca/Si ratio is 1.7 - 2.0 with a unimodal centroid at 1.75 when the w/s ratio is 0.6 and a bimodal distribution with centroids at 1.75 and 1.95 with a w/s ratio of ~ 0.3 (Rayment and Lachowski [1984]). However, the Ca/(Si + Al) ratio was unimodal.

2.2.3.2 Structure of Hydration Products

Crystallographic studies with x-ray and electron diffraction have been limited to the crystalline components, namely the CH and hydrated calcium aluminate, ferrite and sulphate phases present in OPC. Single crystals of the hydrate calcium aluminate phases can be prepared hydrothermally from stoichiometric compositions (Taylor [1990]). Single crystals of the anhydrous components (C_3S, C_3A and C_4AF) are typically obtained from high temperature melts.

There has been extensive application of infrared and Raman spectroscopies to elucidate the molecular structures of the anhydrous and hydrated phases. The basic principle of infrared spectroscopy involves the absorption of electromagnetic radiation in the infrared region by a substance. This induces transitions within the vibrational and rotational energy levels of molecules. Infrared absorption requires a change in the dipole moment of the vibrating molecule. A Fourier Transform Infrared Spectrometer can be used to measure the intensity and frequency of infrared radiation ($\lambda = 0.9\ \mu m \rightarrow 1$ mm or 14000 $cm^{-1} \rightarrow 10\ cm^{-1}$) which is emitted, reflected or transmitted by the substance. Raman spectroscopy on the other hand entails illuminating a sample with a monochromatic beam of light and observing the light scattered from the sample in the vicinity of the exciting line. The incident beam has an associated electric field which polarizes the molecule. As a result of the interaction, energy is transferred to (or from) the molecule from (or to) the radiation, causing a change in the rotational and vibrational states of the molecule. Unlike infrared spectroscopy, the incident photon is never absorbed by the molecule. Thus, molecules without a net dipole moment could be analyzed. Both Raman and infrared spectroscopies are particularly useful for determining functional groups present in a molecule since many functional groups vibrate at nearly the same frequencies independent of their molecular environment (Marcott [1986]). In an N-atom polyatomic molecule, there are 3N-6 normal vibrational modes. However, only the vibrations permitted by the selection rule

(determined by the symmetry of the molecule) are observed. For a diatomic molecule for example, the vibrating frequency (ν) along the only chemical bond is given by;

$$\nu = \frac{1}{2\pi c}\sqrt{\frac{K}{\mu}} \tag{2.5}$$

K is the force constant, μ the reduced mass and c the velocity of light. Some vibrations that are active in Raman may not be active in infrared and vice versa, making the two techniques complementary. Moreover, unlike x-ray diffraction, amorphous substances with short range order could be characterized although structure determination will be impossible because of the broadness of the peaks. A typical spectra assignment for C_3S is shown in Table 2.2 (Bensted and Varma [1974], Ghosh and Chatterjee [1974], Handke and Jurkiewicz [1979], Hassan and Abdel-Kareem [1989], Bonen et al. [1994], Omotoso et al. [1995]).

The condensation of the silicate and aluminate units could be followed easily using infrared spectroscopy, as well as the presence of hydroxyl groups in CH and hydrated calcium aluminates. Many of the characteristic vibrations are specific, enabling unambiguous assignment to different structural units in a unit cell. Polymerization of the orthosilicate units results in a reduction of the Si-O-Si bond length to ~ 1.60 Å from ~ 1.67 Å (Lazarev [1972], Libeau [1985]). An attendant increase in the force constant ensues and the asymmetric stretching vibration shifts to higher wavenumbers (Matossi [1949], Etchepare [1970], Handke [1986]).

Table 2.2 FTIR spectra assignments of Tricalcium Silicate (C_3S)

Wavenumber (cm^{-1})	*Assignment*
939 (s)	ν_3 - asymmetric stretching of the SiO_4 tetrahedra
873 (s)	
810 (sp)	ν_1 - symmetric stretching of the SiO_4 tetrahedra
525 (s, br)	ν_4 - out-of-plane bending of the SiO_4 tetrahedra
514 (br)	
452 (m, br)	ν_2 - in-plane bending of the SiO_4 tetrahedra

absorbance: s - strong; sp - sharp; m - medium; br - broad

The stretching frequencies of hydroxyl groups (OH^-) with weak proton-donor ability lies within the limit ~ 3550 - 3720 cm^{-1} and those of amphoteric compounds stretch between ~ 2900 to ~ 3660 cm^{-1}. The upper limit corresponds to hydroxyls not involved in hydrogen bonding. They exhibit very sharp absorption bands with the half width ($\Delta\nu_{1/2}$) ~ 11 cm^{-1} (Ryskin [1974]). Amphoteric metal hydroxides have some hydrogen bonding not present in alkali and alkaline earth metal hydroxides. This causes an increase in the degree of covalence of amphoteric M-OH bonds and are thus transformed into bending vibrations. OH bending frequencies of amphoteric hydroxides depend significantly on the energy of the H - bonds linking the OH groups. Table 2.3 shows the vibrational frequencies of some OH groups in Portland cement pastes. The bending vibrations of Fe, Cr and Mn substituted ettringites are very weak (Bensted and Varma [1974]).

Lattice water has a strong H - bond (H-O-H). It exhibits broad stretching vibrations [ν(OH)] between 3750 - 3000 cm^{-1} as in OH^- groups. Lattice water can be distinguished from hydroxyl groups by the presence of the bending vibration [δ(HOH)], which occurs in the 1600 cm^{-1} region. This vibration is absent in hydroxyls. In addition, exchange of water with D_2O can be used to differentiate between the water and hydroxyl groups present in a complex hydroxide hydrate (Ryskin [1974]).

Table 2.3 Vibrational frequencies of some hydroxyl groups

Compound		*Stretching vibration* $\upsilon(OH)$ cm^{-1}	*Bending vibration* $\delta(M\text{-}OH)$ cm^{-1}	*References*
$Ca(OH)_2$		3644 sp	-	Omotoso et al. [1995], Ryskin [1974]
$Ca_3(Al,Fe,Cr,Ti,Mn)(OH)_6.12H_2O]_2.(SO_4)_3.2H_2O$ (Ettringite)	Al	3635 m, 3420 vs	855	Bensted and Varma [1971, 1973]
	Fe	3610 m, 3420 vs	-	Bensted and Varma [1971, 1973]
	Cr	3610 m, 3420 vs	-	Bensted and Varma [1971, 1973]
	Ti	3610 m, 3420 vs	835	Bensted and Varma [1971, 1973]
	Mn	3610 m, 3420 vs	-	Bensted and Varma [1971, 1973]

Trimethylsilylation (TMS) and solid state ^{29}Si MAS NMR (Magic Angle Spinning-Nuclear Magnetic Resonance) have been used to study the silicate structure of the C-S-H in the course of cement hydration (Lippmaa et al. [1980, 1982], Clayden et al. [1984], Barnes et al. [1985], Grimmer and Von Lampe [1986], Hjorth et al. [1988], Rodger et al. [1988], Parry-Jones at al. [1988, 1989], Ishida et al. [1992]). In the TMS method, the silicate is converted into the corresponding silicic acid with the replacement of SiOH with $SiOSi(CH_3)_3$. In this form, the monomer, dimer and individual polysilicate ions can be separated. The resulting derivatives are analyzed using gas liquid chromatography (GLC) or gel permeation chromatography (Taylor [1990]). ^{29}Si MAS NMR complements TMS and does away with the side effects associated with the chemical procedure of TMS. However, it cannot identify individual polysilicate ions, while silylation potentially can (Cartledge [1996]).

NMR spectroscopy entails the absorption of electromagnetic radiation at a precise frequency by a nucleus with nuclear magnetic moments different from zero. Thus in the presence of an external magnetic field, the spin state precesses and absorption of radiation causes a transition from a lower to a higher nuclear spin state. The shielding provided by electrons for the nucleus causes different atoms to absorb at slightly different fields for a fixed frequency. Information from an NMR spectrum is classified into the chemical shifts relative to a standard which is rendered independent of the field (Bennet and Swartzendruber [1986]). The chemical shifts of the resonances of the ^{29}Si nuclei in silicates are dependent on the degree of condensation of the silicate tetrahedra and on the nature of the X group in Si-O-X (where X can be metallic cations present in the cement matrix). Increasing diamagnetic shielding of the ^{29}Si nucleus with increasing condensation leads to higher field chemical shifts. Resonances can therefore be assigned to ^{29}Si nuclei in units of a particular condensation, namely: Orthosilicate, SiO_4^{4-} (Q_o); terminal, $Si(OSi)O_3^{3-}$ (Q_1); internal, $Si(OSi)_2\,O_2^{2-}$ (Q_2); branching, $Si(OSi)_3O^-$ (Q_3) and cross linking units, $Si(OSi)_4$ (Q_4) (Ortego et al. [1991]). The subscripts denote the number of SiO_4^{4-} tetrahedra attached to the main orthosilicate unit. The outer fibrous C-S-H is a dimer (Q_1) while the inner C-S-H that forms late is a polymer with Q_2 units. Since the NMR signal intensity is proportional to the number of nuclei present, the extent of the reaction can easily be followed. The use of magic angle spinning (MAS) NMR with cross polarization (CP) results in a the distinction between silicate tetrahedra bonded to hydrogen and those that are not. This has permitted investigators (Clayden et al. [1984], Rodger et al. [1988]), to distinguish between monomeric C-S-H and unreacted C_3S (both are composed of the orthosilicate anion Q_o).

Stade and Muller (1987) conducted ^{27}Al NMR studies of aluminum doped C-S-H phases, with Ca/Si ratio of 0.8 - 1.5. They found that Al exists in tetrahedral coordination at Ca/Si ratios up to 1.0 and exists in both tetrahedral and octahedral coordination as the Ca/Si ratio increases. Only octahedral Al is present at a Ca/Si ratio of 1.5. The authors postulated that Al may be incorporated in the intermediate layers of silicate and CaO_8 polyhedra. This result is similar to those obtained by Komarneni and Tsuji [1989] and Tsuji et al. [1991]). They conducted a series of ^{27}Al and ^{29}Si MAS NMR experiments on tobermorite [$Ca_5Si_6O_{16}(OH)_2.4H_2O$] substituted with 2 - 45 mol% Al (Ca/Si = 0.83 - 1.5). With up to 15 mol% Al (Ca/Si = 0.98), only tetrahedral Al was present. Above this level, Al in octahedral sites increases with increasing mol% Al. Al was reported to substitute for Si in the Q_2 (1Al) and Q_3 (1Al) sites (-82 ppm and -93 ppm respectively). In unsubstituted tobermorite, Q_2 (0Al) and Q_3 (0Al) are at -85.6 ppm and -96.0 ppm respectively. 0Al or 1Al indicate the absence or presence of one Al in the silicate unit (Fig. 2.5). It is apparent that as the Ca/Si decreases, C-S-H can accommodate increasing amounts of Al in tetrahedral sites. Above 20% Al, XRD shows the formation of an hydrogarnet phase; $Ca_3Al_2SiO_4(OH)_8$. In this phase, Al is octahedrally coordinated while Si is tetrahedrally coordinated. Four hydroxyl ions may replace SiO_4 giving $Ca_3[Al(OH)_6]_2$ and Fe^{3+} can wholly or partially substitute for Al^{3+} (Taylor [1990]). More recently, Richardson and Groves (1993) modeled the incorporation of trivalent metal ions R^{3+} (Al^{3+} and Fe^{3+}) in C-S-H. They found from TEM microanalysis that a linear relationship exists between the R : Ca atom ratio and the Si : Ca ratio as shown in Equation 2.6:

$$Si : Ca = 0.444 + 2.25\ (R:Ca) \qquad (2.6)$$

This is in contrast to results obtained by others whereby R : Ca increases with decreasing Si : Ca ratio (Taylor [1990], Rayment and Lachowski [1984]). Richardson and Groves (1993) proposed the formation of a series of C-S-H phases with a range of Ca : Si ratios in which the same fraction of Si atoms are replaced by Al or Fe in each phase. R : Ca will thus increase as the Ca : Si ratio decreases.

2.3 Stabilization/Solidification of Heavy Metal Ions in Cement Matrices.

Some designated potential hazardous heavy metal contaminants and their maximum allowable concentrations in drinking water are summarized in Table 2.4 (Environmental Protection Series [1990]);

Table 2.4 Guidelines for Canadian Drinking Water Quality

Contaminant	*Maximum Allowable Concentration (ppm)*
Cadmium	0.005
Chromium	0.05
Lead	0.05
Copper	< 1.0
Zinc	< 5.0
Mercury	< 0.001

Immobilization of these hazardous wastes in cement matrices is usually assessed using trial mixes. The solidified product is then subjected to a series of tests to evaluate its permeability, strength, durability and leaching potentials (Poon et al. [1985a]). Presently, mechanisms involved in the stabilization, solidification and leaching processes are not yet fully understood.

2.3.1 Analytical Techniques Employed in Studying the Mechanisms of Waste Containment in Cement Matrices

The evaluation of a containment system requires a large number of analytical tools to provide insight into the nature of the surface and the bulk chemistry involved. Each characterization method has its own set of limitations that prevents a complete answer to most questions concerning a complex heterogeneous system such as OPC. Thus, in understanding the chemistry of waste and coupled cement/waste chemistries, a large group of characterization tools is needed. Many of the techniques discussed in Section 2.2.3 are also used to study the solidification/stabilization processes. Ideally, a comprehensive characterization procedure should encompass: *Physical* (macroscopic, microscopic and morphological) characterization using SEM, STEM and TEM; *molecular* characterization (Nuclear Magnetic Resonance (NMR), Fourier Transform Infrared Spectroscopy (FTIR) and X-ray Absorption Fine Structure (EXAFS)); *bulk* characterization (XRD, EDS and/or

EELS) and *surface* analysis through the use of X-ray Photoelectron Spectroscopy (XPS), Auger Electron Spectroscopy (AES), Ion Scattering Spectroscopy (ISS) or Secondary Ion Mass spectroscopy (SIMS). Many of the techniques listed above provide complementary information (Cocke [1990]).

X-ray photoelectron spectroscopy (XPS) is primarily a surface characterization technique that probes the electronic structure of an atom. It probes the first 1-2 nm of the surface and by penetrating the surface by ion milling, compositional depth profiles can be obtained. XPS involves the measurement of the kinetic energy (E_k) of core electrons ejected from an atom by monochromatic x-ray radiation. The binding (or ionization) energy (E_b) of the ejected phototelectron is determined by the relation in Equation 2.7 (Briggs and Seah [1990]);

$$E_k = h\nu - E_b - \phi_{sp} \tag{2.7}$$

$h\nu$ is the photon energy and ϕ_{sp} is the spectrometer work function. A change in the effective charge on an atom leads to chemical shifts in the various core level binding energies and therefore the onset of core to conduction band transitions at a particular core loss edge. It is therefore possible to detect changes in the bonding characteristics of the hydration products in the presence of heavy metal ions (Vempati et al. [1990]). This technique has proved valuable in understanding the reaction mechanism during the pre-induction period (Jawed et al. [1983]).

Features associated with X-ray absorption fine structure (EXAFS) and extended energy loss fine structure (EXELFS) spectroscopy emanate from the crystallographic or short range order (for amorphous materials) about the ionized atom (Okamoto et al. [1992]). While the core electron excitation source in EXAFS is usually high energy synchrotron radiation, high energy electrons are used for excitation in EXELFS (EELS detectors are usually incorporated in modern TEMs).

Basically, when a core electron is excited from a central atom, the total energy transferred is usually in excess of the ionization energy. The surplus energy is radiated as an electromagnetic wave which is elastically scattered by neighbouring atoms (Joy et al. [1986]). The interference between the outgoing and the scattered waves produces the weak modulations observed above the core edge. These vary with the path length of the excited electrons. The modulations are then Fourier transformed into k-space (wavenumber - $1/\lambda$) giving the radial distribution function of the atoms surrounding the central atom. Coordination number and bond lengths can be deduced from the procedure.

These techniques have not found wide applications in cement mainly because of the very weak signal of the fine structures of interest (especially in EXELFS of Si K-edge) and peak overlaps.

More often, investigators complement leaching studies with electron microscopy (SEM, TEM/STEM) and microanalyses, XRD, FTIR, XPS and NMR spectroscopy.

2.3.2 Overview of Stabilization/Solidification Mechanisms in Cement

Two broad mechanisms have been identified by various authors as being responsible for the containment of heavy metal ions in cement, cement/flyash or cement/sodium silicate matrices (Glasser et al. [1993], Means et al. [1995]). These are; encapsulation (physical trapping) and chemical fixation. On the microscopic scale, encapsulation involves trapping a metal ion in the crystal lattice of the cement hydration products without chemical bonding. Chemical fixation entails interaction between the metal ions and cement products of hydration. Tashiro et al. (1977) suggested a chemical fixation mechanism in which the metal ion is incorporated in the C-S-H gel through vicarious replacement or isomorphous substitution (solid solution) and formation of metal complexes. Heavy metals contained in cement can exhibit either or both of these mechanisms. Moreover, each heavy metal has specific overall mechanisms of containment leading to variations in the leachability of different heavy metals. Standard leaching tests on cement/heavy metal containment systems show the dominating influence of pH and to an extent, type and solubility of the heavy metal salt, cement paste formulation, particle size, acid flux through the waste/cement matrix and the time of contact on the leachability of the heavy metal ions from the cement matrix (Thomas et al. [1981], Bishop et al. [1983], Bishop [1988], Zamorani and Sheik [1989]). By complementing leaching studies with electron microscopy and microanalyses, both microstructural and microchemical information are obtained.

Mercury (Hg) has been reportedto be encapsulated and retained in the pore solution, making it accessible to leachants (Poon et al. [1985a, 1986]). In another paper by the same authors (Poon et al. (1985b), it was suggested that Hg may be partially chemically fixed because a dramatic rise of Hg in the leachate is observed below pH 7, which coincides with the breakdown of the Aft (ettringite) phase in cement. More recently, however, McWhinney et al. (1990), using EDS and XPS, noted that Hg exists as precipitated mercuric oxide (HgO) and not a complex of the hydration products. Mercuric oxide (HgO) seems to be closely associated with $CaCO_3$ or CH. Existence of HgO and not a complex of the hydration products strongly suggests that physical sorption processes are mainly

responsible for the containment of Hg in a cement matrix. For Hg and other metals, which are physically entrapped in the cement matrix, Poon et al. (1985b) suggested that reduced leachability is achieved by reducing porosity, through the addition of pulverized flyash or fumed silica.

A study by Thomas et al. (1981) reveals that Pb (a hydration retarder) added as soluble lead nitrate forms precipitates which are mixed Pb compounds without specific stoichiometry and deposited mainly in a colloidal gelatinous form around cement grains. Cocke et al. (1989) using XPS, ISS and EDS, observed that Pb is preferentially deposited on the surface of cementitious materials. This observation coupled with the fact that Pb salts such as carbonates and silicates are extremely insoluble (because of their low surface energies), strongly supports the coating of cement particles by Pb compounds. The surface coating which acts as a barrier to water, extends the setting time, thereby allowing the segregation of C-S-H as observed in the SEM. Cartledge et al. (1990) inferred from leaching, calorimetry and NMR studies that Pb is ineffectively contained in both cement and silicate/flyash modified cement pastes. FTIR and NMR studies (Ortego et al. [1991]) reveal that when Pb-OPC samples are subjected to an acetic acid leaching solution of the EPA-TCLP (Toxicity Characteristic Leaching Procedure), silicate polymerization is slightly enhanced. The acidic leachant neutralizes the basic Pb compounds surrounding cement grains, and the leaching rate is primarily determined by the solubility of the lead compounds in acid media. The strong acid (H^+) introduced into the matrix displaces metal (X) ions (Ca^{2+}, impurity cations or toxic metal ions) which form coordinate covalent bonds with the silicate oxygens (Lewis base sites). The metal ions thus displaced, dissolve in the leaching solution. A reactive silanol group is formed which condenses and produces longer and/or branched silicate structures as illustrated in Equation 2.8 (Ortego et al. [1991]).

$$\equiv\text{Si-O-X} + \text{H}^+(\text{aq}) \rightarrow \equiv\text{Si-O-H} + \text{X}^+(\text{aq}) \qquad (2.8)$$

The cross linked silicate species (Q_4), similar to amorphous silica, is the most prominent specie and tends to destroy the cement matrix. This theory may also apply to metal ions that form coordinate covalent bonds with the silicate oxygens.

Another hydration retarder that forms a protective membrane around cement grains is Zn. It forms a $CaZnO_2$ precipitate from the hydrolysis of $Zn(OH)_2$ (Thomas et al. [1981], Jawed et al. [1983], Poon et al. [1985b]). Poon et al. (1985b) using SEM and XRD observed that C-S-H gel does not form until after 2 days, indicating that C-S-H does

not participate in the fixation of Zn. The absence of CH in the solidified matrix also indicates complete consumption of Ca^{2+} by $Zn(OH)_2$ to form $CaZnO_2$.

A series of leaching experiments by Montgomerry et al. (1988), on OPC and OPC containing soluble sodium silicate, indicate that the release of certain heavy metals from the cement matrix is low and based on the pattern of release, the heavy metals could be classified into two distinct groups. The first group, comprising Zn, Pb and Cd, gave pH dependent releases under equilibrium leaching test conditions, suggesting that the metals are bound in the cement matrix as insoluble hydroxides or oxyanions at high pH. The second group, consisting of copper and nickel, are released throughout the leaching test (amount released from the OPC/silicate is greater than that released in OPC) indicating that the metals are complexed by ligands present in the sludge and therefore soluble under alkaline as well as acid leaching conditions. Zamorani and Sheik (1984) recently showed that nickel, added in the form of $NiCl_2$, precipitates $Ni(OH)_2$ which shows low solubility in high pH media, comparable with cadmium.

When introduced as a soluble salt to an OPC paste, $Cd(OH)_2$ is precipitated (Bishop et al. [1983], Bishop [1988], Montgomerry et al. [1988], Zamorani and Sheik [1989], Cartledge et al. [1990]). NMR and SEM studies by Cartledge et al. (1990) show $Cd(OH)_2$ precipitates surrounded by CH and C-S-H. They concluded that $Cd(OH)_2$ possibly acts as nucleation sites for both C-S-H and CH. Leaching studies coupled with SEM and STEM microanalyses conducted by Heimann et al. (1991) also confirmed that Cd is effectively retained in OPC, showing no sensitivity to leachate pH in contrast with the suggestion by Montgomerry et al. (1988) that cadmium dissolution is pH dependent when present in a sludge containing other heavy metals such as Zn, Pb, Ni and Cu. This indicates a probable dependence of leachability on the cumulative effects of all ions present in the sludge.

Heimann et al. (1991) investigated the leachability of vanadium when added as soluble sodium orthovanadate to OPC, SRPC (sulphate resistant Portland cement)/flyash and alumina cement. Even though a comprehensive conclusion cannot be drawn from the work reported, leaching studies show very low losses of V from OPC. This has been attributed to the formation of insoluble calcium hydroxyvanadate [$Ca(VO_4)_3OH$] at high leachate pH. This phase has not been observed in the TEM. The concentration of V in the leachate is related to that of Si, but not Ca, suggesting that V is associated with leachable C-S-H but not the Ca-rich CH or $CaCO_3$. Vanadium is also detectable in low levels in the hydration products of alumina cement.

Chromium stabilization in cement/alite has been investigated by numerous authors. When added in the hexavalent form (Cr^{6+}), Cr is leached from standard leachate solutions especially at high Cr^{6+} concentrations (Bishop [1988], Heimann et al. [1991], Ivey et al.

[1993], Kindness et al. [1994]). Kindness et al. (1994) reported that Cr^{6+} is immobilized in an OPC/blast furnace slag blend (1 : 9). No Cr was detected when the pore fluid was extracted and analyzed after hydration for 250 days. They also reported the ability of blast furnace slag to reduce Cr^{6+} to Cr^{3+}. However, no standard leachate test was conducted to determine its stabilization potential. Cr^{3+} is better contained and more leach resistant in cement matrices than Cr^{6+}. When chromium is added as Cr^{3+}, the initial concentration of Cr^{3+} in the leachate decreases with increasing surface area of cement/heavy metal admixture. Bishop et al. (1988) attributed this to the higher leachate pH around smaller particles. This occurs because small particles were found to leach alkalinity more rapidly than large ones. Leaching studies by Roy et al. (1991) also indicate that Cr^{3+} concentration in the leachate does not become noticeable until a breakdown in the C-S-H occurs through Si dissolution. This further supports the likelihood that Cr is incorporated in the C-S-H phase. Detailed leaching and SEM/STEM microanalysis by Heimann et al. (1991) and Ivey et al. (1993) indicate that Cr^{3+} dissolves in all the hydration products of cement (CSH, CH and $CaCO_3$). When added in high concentrations (1.0 M Cr^{3+}), highly leach resistant chromium rich regions are identifiable. In addition, Cr^{3+} appears to substitute for Si^{4+} in the C-S-H. The charge deficiency may easily be balanced by H^+ or other cations present as impurities in alite. FTIR and SEM studies by Mollah et al. (1992) lend credence to Cr^{3+} substitution for Si^{4+}, with K^+ acting to compensate for charge deficiencies. The silicate vibrations are modified in the presence of Cr^{3+} ions. Also, an earlier similar observation was made by Tashiro et al. (1977), differing only in the latter's inference that Cr^{3+} substitutes for both Ca^{2+} and Si^{4+}. Butler et al. (1993) studied the OPC/Cr(III) system using ^{29}Si NMR. They reported that Cr(III) retarded the polymerization of the orthosilicate (Q_o) units because Q_1 and Q_2 units were absent in the solidified matrix. In an extensive TEM and XRD investigation by Kindness et al. (1994), C_3S, CH, C_3A and C-S-H were doped with 0.0019 M and 0.0048 M Cr^{3+} at a w/s ratio of ~ 100. The CH/Cr^{3+} system hydrated at 55°C indicated the formation of a compound similar to $Ca_2Al(OH)_7.3H_2O$. The compound was fitted to a hexagonal cell and the formula $Ca_2Cr(OH)_7.3H_2O$ was proposed. At 25°C, an isomorph of $Ca_2Al_2O_5.3H_2O$ was observed (Ca/Cr = 0.28). All XRD reflections are broad and diffuse. Similar products were observed in the C_3A/Cr^{3+} systems. Based on these observations, it was concluded that Cr^{3+} could substitute for Al in most of the calcium aluminate hydrate phases present in OPC. In C_3S/ Cr^{3+} experiments however, a crystalline phase (Ca : Cr ~ 0.74) with ~2% Si was observed. The Si was attributed to contribution from neighbouring C-S-H (x-ray microanalysis in the TEM). XRD indicated the formation of $Cr(OH)_3.3H_2O$. $Cr(OH)_3.3H_2O$ was also observed to form in C-S-H/Cr^{3+} systems. No evidence of Cr incorporation in C-S-H was found. It is somewhat difficult to

relate these findings to previous ones because of the high w/s ratio employed in synthesizing the hydrated phases.

2.3.3 Solution Chemistry of Chromium

2.3.3.1 Hydrolysis of Cr(VI) (CrO_3)

Chromium trioxide is a covalent linear polymer of chromium and oxygen atoms with two additional oxygen atoms attached to each Cr (Wilberg [1965]). The structure is made up of distorted CrO_4 octahedra with a Cr-O bond length of ~ 1.8 Å. CrO_3 dissolves readily in water giving a strong acid;

$$(CrO_3)_n + nH_2O \rightarrow nH_2CrO_4 \tag{2.9}$$

$$nH_2CrO_4 \Leftrightarrow nH^+ + nHCrO_4^- \tag{2.10}$$

In an alkaline solution typical of hydrating cement matrices, chromates are formed. These contain CrO_4^{2-} in which the Cr is tetrahedrally coordinated.

$$HCrO_4^- + OH^- \Leftrightarrow CrO_4^{2-} + H_2O \tag{2.11}$$

Only CrO_4^{2-} ions exist at pH > 8. Calcium chromates are yellow and slightly soluble in water. The solubility product of $CaCrO_4$ is 0.023 mol^3l^{-3} (Keller [1967]).

In acids, chromates are converted to dichromates. In the pH range 2-6, $HCrO_4^-$ and $Cr_2O_7^{2-}$ are in equilibrium;

$$2\,HCrO_4^- \Leftrightarrow Cr_2O_7^{2-} + H_2O \tag{2.12}$$

2.3.3.2 Hydrolysis of Cr(III)

The hydrolysis of Cr(III) is very complex and has generated controversial hypotheses in recent years. When a Cr(III) salt such as $Cr(NO_3)_3.9H_2O$ is hydrated, a violet solution containing hexaquo ions is formed $[Cr(H_2O)_6]^{3+}$. The hexaquo ion is quite acidic with a pK_a ~ 4 and has a tendency to form polynuclear complexes containing OH^- bridges, such as depicted in Equations 2.13 and 2.14 (Greenwood and Earnshaw [1984]):

$$2[Cr(H_2O)_6]^{3+} \xleftrightarrow{2H^+} 2[Cr(H_2O)_5OH]^{2+} \quad (2.13)$$

$$\updownarrow$$

$$(H_2O)_4Cr(OH)_2Cr(H_2O)_4]^{4+} + 2H_2O \quad (2.14)$$

As the pH is raised, further deprotonation and polymerization can occur. At pH ~ 5-10, octahedral layers of $Cr(OH)_3.3H_2O$ precipitate (green). The solubility product of Cr_2O_3 at pH 5 is $6.7x10^{-31}mol^3l^{-3}$ at 25°C (Larsen [1965]). Rai et al. (1987) found that at pH > 10.5, $Cr(OH)_3.3H_2O$ dissolves forming $Cr(OH)_4^-$ which remains the only species at high pH. Spiccia and Marty (1986) also reported the formation of an 'active $Cr(OH)_3.3H_2O$'. In the active chromium hydroxide, octahedral $Cr(OH)_3(OH_2)_3$ units are linked through hydrogen bonds between the OH^- and H_2O ligands of adjacent chromium centres without any bridging OH^- ligand.

Aging at room temperature transforms the monomeric hydroxide into an amorphous phase of unknown composition (Giovanoli and Stadelmann [1973]). Subsequently, aggregation of pairs of active monomers, through H-bonding, forms singly OH^- bridged dimer hydroxides. Formation of higher oligomers was also reported. For example, dimer + dimer → tetramer or trimer + trimer → hexamer (Rotzinger et al. [1986]). Typically after aging the active monomer hydroxide at pH 10.63 for 72 hours, the product comprises ~ 48% monomer, 28.2% low oligomers (dimers, trimers and tetramers) and 21.8% high oligomers (pentamer, hexamer and other soluble oligomers).

At high pH, many investigators do not share the view that $Cr(OH)_4^-$ is the main species. Chromatographic studies have shown that in strongly alkaline solutions (pH ~ 14) deprotonation of the hexaquo ion forms $Cr(OH)_4(OH_2)_2^-$ ions, which are rapidly transformed into polynuclears (Giovanoli and Stadelmann [1973], Rotzinger et al. [1986], Spiccia and Marty [1986], Spiccia et al. [1987]).

Silanol groups are known to act as ligands in complex formation with transition metals in the same way as water does (James and Healy [1972], Olsen and O'melia [1973], Schindler et al. [1976]). In a review, Iler (1979) observed that SiO_2 suspended in a solution of most polyvalent ions including transition metal ions begins to adsorb metal ions when the pH is raised to within 1 - 2 points below the pH at which the metal hydroxide starts to precipitate. The silanol group in SiO_2 solution gradually replaces the coordinated

water. Both mono and bidentate silanol ligands have been observed (Schindler et al. [1976]).

If Cr(III) is introduced as $Cr(H_2O)_4Cl_2)Cl.2H_2O$, $[Cr(H_2O)_4.Cl_2]^+$ (dark green) and Cl^- are the main ionic species.

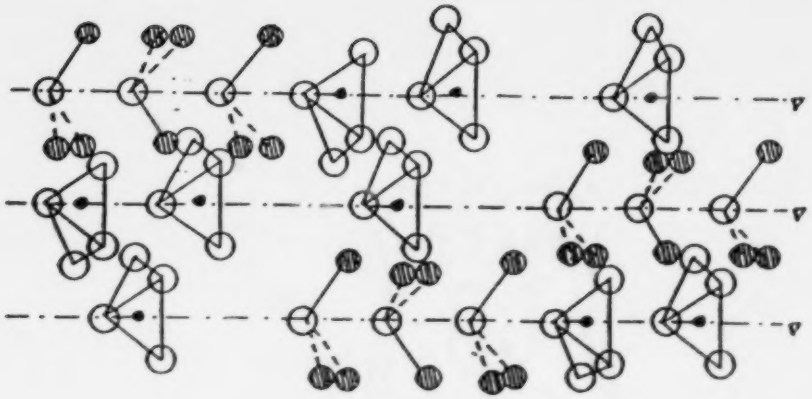

Fig. 2.1 Jeffery's C_3S structure showing the ac projection (Reproduced with permission from Handke and Jurkiewicz [1979])

● - silicon; ⊗ - calcium; ○ - oxygen.

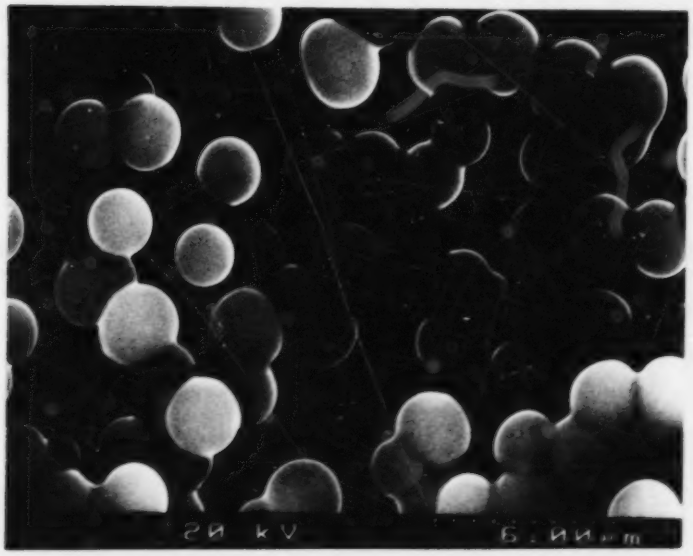

Fig. 2.2 Scanning electron micrograph of anhydrous C_3S.

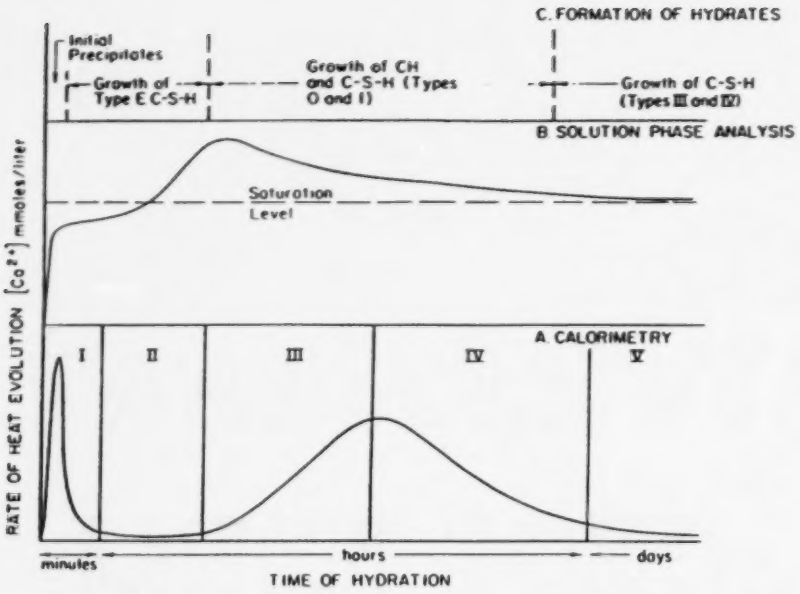

Fig. 2.3 Schematic representation of changes taking place in the C_3S - water system (water/solid ratio < 1.0) - (Reproduced with permission from Jawed et al. [1983])

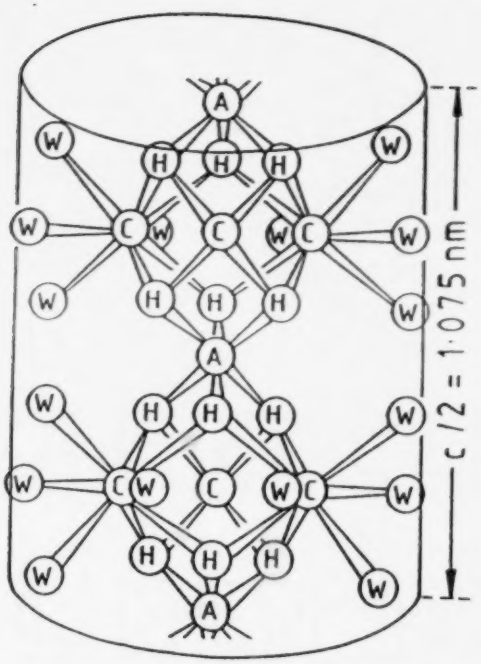

Fig. 2.4 Crystal structure of ettringite. Part of a single column in $(11\bar{2}0)$ projection; A = Al, C = Ca, H = O of an OH group, W = O of an H_2O molecule (Reproduced with permission from Taylor [1990]).

		Approximate Chemical Shift Ranges (ppm)
(H) O (H)OSiO(H) O (H)	Q_0 (0Al)	-69 to -75
(H) O (H)OSiO(Si) O (H)	Q_1 (0Al)	-79
(H) O (H)OSiO(Si) O (Si)	Q_2 (0Al)	-85
(Al) O (H)OSiO(Si) O (Si)	Q_2 (1Al)	-82
(Al) O (Si)OSiO(Si) O (Si)	Q_3 (1Al)	-93

Fig. 2.5 ^{29}Si chemical shift ranges of aluminosilicates. Si(nAl) designates the SiO_4 tetrahedron connected through shared oxygen atoms with $nAlO_4$ tetrahedra in the aluminosilicate framework.

Chapter 3 Experimental Techniques

3.1 Production of Tricalcium Silicate

Stoichiometric ratios of analytical reagent grades of $CaCO_3$ (500 g) and SiO_2 (100 g) were mixed in a rotary shaker for 12 hours to ensure homogenization. The mix was calcined in alumina crucibles at 1000 °C for four hours. The calcined mix was then transferred to a graphite crucible. Prior to sintering in a controlled atmosphere Brew high temperature furnace, the sample was degassed for about one hour at 1000 °C after which the furnace was backfilled with argon. The sample was sintered at 1600 °C for 24 hours. The sintered product (C_3S) usually has some carbon adsorbed on the surface in contact with the graphite crucible. This can be removed by decarbonation at 600 °C for 90 minutes. The colourless product obtained was ground in a ball mill with alumina balls for ~ 10 hours. The ground product was sealed in a polyethythene container and stored under vacuum. Inadequate degassing may cause oxidation of the graphite crucible forming carbon monoxide. The reducing atmosphere changes the thermodynamics of C_3S formation. An unidentified green carbonaceous substance was observed in inadequately degassed samples. This could not be removed even after re-sintering in a platinum crucible at 1450 °C.

3.1.1 Determination of Particle Size

About 1mg of C_3S was dispersed in acetone. A drop of the supernatant solution was then placed on a stub impregnated with carbon. This was fitted into an SEM sample holder and observed in the secondary electron mode. The experiment was carried out in triplicate and the particle sizes averaged. The observed range was 2 - 5 μm with a mean of 2.5 μm.

3.1.2 Determination of Free Lime (CaO)

The Franke extraction procedure was used to determine the amount of free lime present in the ground C_3S (Pressler et al. [1961]). This involves refluxing 0.1 g C_3S in 100 ml of a solution containing ethylacetoacetate in isobutyl alcohol (3:20) for 60, 90 and 120 minutes. The solution was allowed to cool and filtered with an 0.45 μm cellulose acetate membrane filter. The residue was washed with 50 ml isobutyl alcohol. The filtrate was then titrated with 0.2 M perchloric acid to a reddish tinge. 10 - 12 drops of 0.1 g

thymol blue dissolved in 100 ml isobutyl alcohol was used as the indicator. The neutralization reaction reduces to:

$$2HClO_4 + Ca(OH)_2 \rightarrow Ca(ClO_4)_2 + 2H_2O \quad (3.1)$$

The free lime was obtained by extrapolating the wt% CH of the 3 runs to zero time. The free lime in the C_3S produced (Section 3.1) was found to be less than 0.1 wt%.

3.2 Preparation of Chromium doped Samples

Table 3.1 shows the concentrations of the chromium solutions used in the stabilization/solidification experiments. Reagent grade chromium salts were obtained from Aldrich Chemicals (Wisconsin, USA). Chromium nitrate ($Cr(NO_3)_3.9H_2O$) and chromium chloride ($Cr(H_2O)_4Cl_2)Cl.2H_2O$) were used to simulate Cr(III) wastes, while chromium trioxide was used to simulate Cr(VI) wastes.

Table 3.1 Hydration experiments detailing concentrations of chromium solutions and hydration times

Solution		*Molarity*	*Hydration Period (m-minutes; h-hours; d-days)*					
(Solution/C_3S ~ 0.5 by wt)		*(M)*	*5m*	*6h*	*24h*	*72h*	*60d*	*240d*
Cr(III)	Chromium nitrate	0.1			*		*	
		1			*		*	
		2	*	*	*	*	*	
		2.75						*
	Chromium chloride	0.1			*		*	
		1			*		*	
Cr(VI)	Chromium trioxide	0.1			*		*	
		1			*		*	
		2	*	*	*	*	*	
Standard	Distilled water				*		*	*

* - *Hydration periods of sample.*

Ten grams of C_3S was separately mixed with 5 ml of each chromium solution to make a paste. Due to variations in the densities of different chromium solutions, the wt% of the Cr solutions will vary. To serve as a standard, 5 ml of distilled water was also mixed with 10 g of C_3S. The paste was cast into plastic molds and stored in a humidifying chamber plugged with ascarite and flushed with N_2. Curing under N_2 is essential because carbonation occurs much faster in the relatively small laboratory samples than in the very large quantities of waste/cement containment systems encountered in practice. Part of the 2.75 M Cr(III) pastes was stored in sealed plastic bottles, isolated from the humidifying atmosphere to which the other pastes were exposed.

Also shown in Table 3.1 are the hydration periods. Except for the 60 and 240 day old samples, all other samples were injected with isopropyl alcohol to stop the hydration reaction. This was followed by evacuation in a vacuum dessicator for 18 hours. The 60 and 240 day old samples were simply evacuated for 24 hours. All samples were stored in a vacuum dessicator prior to analysis.

3.3 X-ray Diffraction

3.3.1 Routine Identification of Samples

X-ray diffraction patterns were recorded on a Rigaku X-ray Diffractometer equipped with a rotating anode. All experiments were carried out with CuK_α radiation at 40 kV and 110 mA. The solidified sample was ground with a mortar and pestle and spread on a glass slide coated with a thin layer of petroleum jelly. The diffractometer was scanned from 5 - 60 °2θ, with a step scan of 0.1° for 5 seconds. This procedure was used to characterize C_3S and to determine the phases present in the hydrated paste. The preliminary identification enables the use of the right primary standards for quantitative analysis.

3.3.2 Quantitative X-ray Diffraction Analysis

3.3.2.1 Preparation of Standards

To quantify the phases present in the hydrated samples, the following standards were required:

a. Distilled water/C_3S: C_3S, CH, $CaCO_3$.

b. Cr(III)/C_3S: C_3S, CH, $CaCO_3$, calcium chromium hydroxide hydrate (Ca : Cr = 3:1), calcium chromium hydroxide hydrate (Ca : Cr = 2:1).

c. Cr(VI)/C_3S: C_3S, CH, $CaCO_3$, $CaCrO_4.2H_2O$ (Ca : Cr = 1:1), $Ca_2CrO_5.3H_2O$ (Ca : Cr = 2:1).

C_3S was taken from the stock kept under vacuum. $CaCO_3$ was from the same batch as the starting material for C_3S preparation.

Commercial analytical reagent grade calcium hydroxide was found unsuitable because of the very small crystallite size. This introduced excessive broadening of the CH peaks unmatched by those of the hydrated pastes. To obtain calcium hydroxide, $CaCO_3$ was calcined at 1000 °C until a constant weight was achieved. The resulting CaO was transferred to a stoppered flask and hydrated in excess distilled water for 24 hours. The slurry was filtered in a CO_2 free environment (glove bag) and dried at 105 °C for 1 hour. A N_2 purged Thermolyne 21100 tube furnace was used for this purpose.

The powder diffraction pattern of the Cr(VI) doped C_3S paste shows the formation of two different compounds; $CaCrO_4.2H_2O$ (Ca/Cr = 1) and $Ca_2CrO_5.yH_2O$ (Ca:Cr = 2). $CaCrO_4.2H_2O$ is well characterized (Powder Diffraction File [37-1367]), while the diffraction pattern of $Ca_2CrO_5.yH_2O$ does not match any compound in the powder file.

To produce pure $CaCrO_4.2H_2O$ and $Ca_2CrO_5.yH_2O$, stoichiometric ratios of $Ca(OH)_2$ and 2 M H_2CrO_4 were mixed according to the reactions:

$$Ca(OH)_2 + H_2O + CrO_3 \rightarrow CaCrO_4.2H_2O \qquad (3.2)$$

$$2Ca(OH)_2 + yH_2O + CrO_3 \rightarrow Ca_2CrO_5.(2+y)H_2O \qquad (3.3)$$

The solutions were filtered and dried at 50°C.

Two compounds were also detected in the Cr(III) doped pastes. The first, $[Ca_3Cr(OH)_6(NO_3)_3]_2.(12+x)H_2O$, has a diffraction pattern which matches $[Ca_6Al_2O_5(NO_3)_3]_2.xH_2O$ (Powder Diffraction File [28-0208]). The diffraction peaks of $[Ca_6Al_2O_5(NO_3)_3]_2.xH_2O$ are broad and diffuse. There was no indexing or determination of the lattice parameters by the authors. The chemical formula does not reflect the coordination of the metal ions. A pure sample of the Cr analogue was produced by reacting 2 M chromium nitrate with CH (Ca/Cr ratio = 3). Unlike the Cr(VI) compounds, the compound obtained from the reaction of CH/Cr(III) strongly depends on the concentration of the starting chromium nitrate.

The second compound with Ca/Cr = 2 could not be synthesized from numerous trials with varying concentrations and Ca:Cr ratios.

Five grams of each primary standard was mixed with 1 g of rutile (internal standard). The primary standard mix was packed with alumina balls in a 75 ml

polyethylene bottle and tumbled in a rotary shaker. Cyclohexane was used as a grinding aid. Grinding for 2 hours was found to be necessary to reduce the particle sizes to between 1 - 3 μm with virtually no contamination by the alumina grinding balls.

5 grams of each hydrated sample was ground in a similar manner with 1 g of rutile.

3.3.2.2 Data Collection and Analysis

The data collection strategy is similar to that used by Gutteridge (1984). The sample was loaded from the back (Klug and Alexander [1984]) into a 20 mm x 3 mm cylindrical hole drilled into a glass slide. The slide was positioned on the sample stage such that the glass was out of the beam path during data collection. For all samples, diffraction intensities were obtained between 5 and 55 °2θ at 40 kV and 110 mA. The diffractometer was step scanned at 0.05 ° for 10 seconds. For the primary standards, the background was fitted with a cubic spline and subtracted. In the hydrated samples, the amorphous C-S-H diffuse halo was simulated and subtracted from the pattern.

Also using a cubic spline interpolation routine, the rutile (110) peak was aligned to 27.4501 ± 0.0005 °2θ. This resulted in 5000 data points. Each pattern was collected in triplicate. The rutile (110) peak was then normalized to 1000 counts. A linear least squares equation was used to fit the 5000 equations generated as shown below.

$$\sum_{i=1}^{5000}(y_i)_s = \sum_{j=1}^{M} w_j(y_i)_j + c_i \qquad (3.4)$$

$(y_i)_s$ is the ith data point of sample s, $(y_i)_j$ is the ith data point of the primary standard j, w_j is the weight fraction of the primary sample j in the sample, M is the number of primary standards and c is the contribution of the background to the ith data point. It also accounts for the amorphous halo. The coefficients w_j in the equation are obtained using a Gaussian elimination routine. The amorphous C-S-H was obtained by difference (1 - sum of w_i). The reliability (R) is given as:

$$R = \frac{\sum_{i=1}^{5000}\left[(y_i)_s - (\sum_{j=1}^{M} w_j(y_i)_j + c_i)\right]^2}{\sum_{i=1}^{5000}\left[(y_i)_s - c_i\right]^2} \qquad (3.5)$$

The background subtraction routine was performed with a dedicated x-ray diffraction program Jade+ (Materials Data Inc. CA). The alignment and least square routine are part of a macro written within a graphing program (Igor Pro 2.0.4).

3.4 Electron Microscopy

3.4.1 Scanning Electron Microscopy

A Hitachi S-2700 scanning electron microscope equipped with a Link eXL energy dispersive spectrometer (EDS) was used for microstructural and microanalytical characterization of the hydrated samples. Polished and fractured sections were characterized.

Because of the high porosity of the partially and fully hydrated pastes, polished sections were usually impregnated prior to grinding and polishing. Otherwise the pores may entrap grinding and polishing abrasives. A low viscosity epoxy (EpoThin - TechMet Ont.) was used for this purpose. The following procedure was adapted:

a. Remove a small sample prior to grinding.
b. Coat a polyethylene cup - 10 ml capacity and 2.5 cm diameter with a thin film of mold release.
c. Immerse fragments or powder in a freshly mixed epoxy + hardener.
d. Place the container with the contents in a vacuum bell jar and evacuate (Epoxy will boil under vacuum and will overflow if too full).
e. Boil for 2 - 3 minutes.
f. Slowly release the vacuum, allowing atmospheric pressure to force the epoxy into the sample.
g. Cure for 24 hours and cut with a saw to expose the sample fragments.
h. The cut surface is ground with lapping oil on a cast iron disc impregnated with diamond for about 3 minutes. Remove grits with isopropyl alcohol.
i. Rough polish on a microcloth (nylon) with 6 μm diamond paste for about 5 minutes and final polish for 2 - 3 minutes on a soft cloth impregnated with 1 μm diamond paste.
j. Clean surface with isopropyl alcohol.

It is important to use oil as water will react with unhydrated C_3S or dissolve soluble components especially in the Cr(VI) doped samples. The use of SiC is also discouraged

since some pores will escape impregnation and entrap SiC. EDS analysis of the region affected will be misleading as Si is present in most of the phases.

The polished section was then stored under vacuum prior to carbon coating. SEM analysis was performed in both the secondary electron (SE) and backscattered electron (BSE) imaging modes. Carbon coating is essential to eliminate charging and x-ray attenuation during EDS compositional analysis.

EDS microanalysis was carried out with a windowless detector. Apart from detecting oxygen, the extent of carbon contamination and carbonation of CH could also be monitored. This is in spite of the uniform carbon coating on the surface. An accelerating voltage of 20 kV was used for all data collection mainly because 20 kV was used to collect the spectra of the virtual standards supplied with the detector. X-ray data was acquired for 100 seconds live time at > 2500 cps. There was no need to collect standard spectra for quantitative analysis as the Ca/Si and Ca/Cr ratios were accurate to within ± 0.05. This was based on the correlation between the known Ca/Si ratio in the unreacted C_3S present in most of the samples and Ca/Cr ratio of $CaCrO_4.2H_2O$ in the Cr(VI) doped samples. Quantification was done using the phi-rho-z routine. Ca, Si and Cr were analyzed based on stoichiometry of their oxides and normalized to 100 atom %. The atom % of the 3 elements totals about 45%. The remaining was attributed to unanalyzed oxygen. Because the phases are hydrates, the actual concentrations are incorrect but the elemental ratios are accurate. X-ray maps were also obtained for some of the phases. To obtain a good signal to noise ratio, the beam current was increased such that the count rate was > 5000 cps. The collection strategy for line scans is similar to x-ray maps.

Freshly fractured sections were carbon coated and examined at 20 kV in the secondary electron mode. Qualitative EDS analysis was usually obtained by analyzing relatively flat regions. The x-ray data collection method is the same as that adopted for the polished samples.

3.4.2 Transmission Electron Microscopy

Characterization in the TEM was done on a JEOL 2010 transmission electron microscope equipped with a Noran Ge energy dispersive detector. The method described by Ivey et al. (1989) was used for the preparation of thin sections. Prior to thinning, hydrated samples were impregnated with a low viscosity epoxy as previously described in Section 3.4.1. The impregnated sample was ground to ~ 5 mm thickness and mounted on a heated cast iron block with Crystal Bond low melting point wax. On cooling, an ultrasonic disc cutter was used to cut several 3 mm discs from the sample. The wax was

removed by remelting and dissolving in acetone followed by a wash in isopropyl alcohol. The discs were then ground to about 250 μm with 5 μm SiC abrasives lapped with oil. Using a Gatan 656 dimpler, the 250 μm disc was dimpled on both sides with a bronze wheel (6 μm and 1 μm diamond pastes in oil) until a hole ~ 0.75 mm formed at the centre. The surface was polished with a soft cloth wrapped around a dimpling wheel and impregnated with 0.25 μm diamond paste. The dimpled sample was then supported with copper grids and ion-milled in a Gatan Duomill for 3 - 5 hours. The sample was carbon coated prior to characterization in the TEM. Large thin areas are usually revealed at 200 kV.

The probe size used for compositional analysis was ~ 10 nm and data was collected for 100 seconds live time. Quantification is simpler than in the SEM since for a thin specimen, absorption and florescence effects are negligible. The ratio of two elements will then be proportional to their x-ray intensities (134):

$$\frac{C_A}{C_B} = k_{A/B}\frac{I_A}{I_B} \tag{3.6}$$

C_A and C_B are the concentrations in weight % of elements A and B, I_A and I_B are the respective x-ray intensities and $k_{A/B}$ is the Cliff-Lorimer factor. The k-factor was determined by analyzing areas containing unhydrated C_3S and $CaCrO_4.2H_2O$.

3.5 Molecular Spectroscopy

3.5.1 Fourier Transform Infrared (FTIR)

Powdered samples < 5 μm were used for both FTIR and Raman Spectroscopy. The classical disk technique was used with cesium iodide pellets to prepare FTIR samples. The spectra were collected on a Nicolet 750 Magna spectrometer between 200 and 4000 cm^{-1}. Assignments of vibrational frequencies were made by using the correlation table (Nyquist [1971]) and the results of other investigators referenced earlier. However, the vibrational frequencies of the new compounds were partially assigned by deuteration of the OH^- groups (Ryskin [1974]). Specifically, this was done for the calcium chromate hydrates [Cr(VI)] and calcium chromium hydroxide hydrates [Cr(III)].

Calcium deuteroxide [$Ca(OD)_2$] was prepared by calcining $CaCO_3$ at 1000°C in a N_2 purged furnace. The CaO produced was cooled to room temperature in a glove bag while maintaining a constant flow of N_2. Excess D_2O was added to CaO in a stoppered

flask and allowed to stand for about 12 hours. The solution was filtered and dried at 105°C to remove excess D_2O. The purity of the $Ca(OD)_2$ formed was monitored with XRD.

To prepare $CaCrO_4.2D_2O$ and $Ca_2CrO_5.3D_2O$ from $Ca(OD)_2$ and a 2 M CrO_3 solution (D_2CrO_4), the following was done:

a. 2 g of CrO_3 was dissolved in D_2O and made up to 10 ml.
b. 0.304 g of $Ca(OD)_2$ was added to 1 ml of the CrO_3 solution to form $Ca_2CrO_5.3D_2O$ (Ca/Cr ratio = 2).
c. 0.304 g of $Ca(OD)_2$ was added to a 2 ml CrO_3 solution to produce $CaCrO_4.2D_2O$.

In the case of calcium chromium hydroxide hydrate, the water was partially substituted by D_2O;

a. 20 g $Cr(NO_3)_3.9H_2O$ was dissolved in D_2O and made up to 25 ml to obtain 2 M chromium nitrate solution.
b. 0.456 g of $Ca(OD)_2$ was added to 1 ml of the solution (Ca/Cr ratio = 3) to form calcium chromium deuterate hydrate.

XRD analysis indicated the same structure as their hydrated counterparts. All the samples were ground to < 5 μm before FTIR analysis.

3.5.2 Nuclear Magnetic Resonance

Powdered samples were also used for ^{29}Si solid state magic angle spinning nuclear magnetic resonance spectroscopy (^{29}Si MAS NMR). The high resolution solid state NMR spectra were recorded at 59.63 MHz on a Bruker M SL-300 spectrometer. Samples were spun at 4.5 KHz at the magic angle to the external field. A relaxation delay of 10 seconds was used for all the samples. About 5000 scans were usually collected. This yielded a satisfactory signal to noise ratio in most cases. Q_8M_8 (Trimethylsilyl ester of the four ring octameric silicate) was used as the secondary standard. Its major ^{29}Si chemical shift was assigned as +11.5 ppm downfield from TMS (tetramethylsilane). Identification of the different silicate polyhedra was made based on the works of Lipmma et al. (1980, 1982).

Ratios of the Q_1 (dimer) to Q_2 (polymer) were obtained by fitting a Voigt function to the peaks and integrating.

3.6 Leaching Studies

Leaching tests were carried out on the 240 day old hydrated pastes using the EPA Standard Characteristic Leaching Procedure (TCLP - (EPA [1986])). A sample was ground to less than 0.5 mm and leached with acetic acid (pH 2.88). 200 ml of acetic acid was added to the 10 g sample in a high density polyethylene bottle. The bottle and its contents were agitated in a rotary shaker at 30rpm for 18 hours. A Perkin-Elmer 4000 atomic absorption spectrometer (AAS) was used to analyze the leachate solution. The leachate was acidified with 1 M HNO_3 to bring the pH to below 3. This prevents precipitation of the metal ions prior to analysis.

To obtain the composition of the solid residue, the flux method (Ingamells and Pitard [1986]) was used:

a. 20mg of the sample was weighed into a platinum crucible and 140mg of lithium metaborate was added ($LiBO_3$ added as a fluxing agent).
b. The mixture was heated at 1000°C in a muffle furnace for 45 minutes.
c. After cooling, 20 ml of 4% HNO_3 was added to dissolve the glass. Stirring with a magnetic bar greatly accelerates the dissolution process.
d. The solution was diluted appropriately for analysis in the AAS.

The composition of the unleached samples was also determined in a similar manner. XRD and FTIR were used to characterize the leached samples as previously described for the unleached hydrated samples.

Chapter 4 Results and Discussions

4.1 X-ray Powder Diffraction

X-ray powder diffraction was used to investigate the composition of the hydrated chromium doped C_3S pastes and the rate of formation of crystalline hydration products.

In a blank (C_3S/water) paste, calcium hydroxide begins to appear within a few hours, and in a few days a diffuse band at ~ 28 - 31 °2θ corresponding to amorphous C-S-H starts to form. The completely hydrated paste comprises CH, C-S-H and some $CaCO_3$ formed as a result of partial carbonation of CH. The presence of $CaCO_3$ depends greatly on the hydration environment. The diffraction patterns of anhydrous C_3S and a fully hydrated blank paste are shown in Fig. 4.1.1.

In the following sections, the development of the crystalline phases in Cr(III) and Cr(VI) doped C_3S pastes is monitored and compared to the normal hydration products of C_3S. Attempts were made to quantify some of the crystalline phases.

Unless otherwise stated throughout the text, elemental ratios are in atom %.

4.1.1 Trivalent Chromium Doped C_3S Pastes

Cr(III) solutions containing 0.1 M, 1 M, 2 M and 2.75 M were separately mixed with C_3S in a solution to solid ratio of ~ 0.5. The resulting pastes contained 0.17, 1.63, 3.11 and 4.11wt% chromium respectively. To enhance identification of chromium containing compounds, 2 M Cr(III) pastes were used to monitor the formation of these compounds.

Fig. 4.1.2 shows the x-ray powder patterns of 2 M Cr(III) pastes hydrated for varying times. The strong peaks at 27.4, 36.1, 41.2 and 54.3 °2θ are due to rutile (TiO_2), added to all the pastes as a standard. The presence of equal amounts of a standard enabled peak alignment and quantification of the crystalline phases. Within the first five minutes of reaction, no extra peaks apart from the starting C_3S peaks were observed even though some C_3S had reacted. (The container holding the mixture became hot due to the liberated heat of dissolution.) After 6 hours, a phase with the strongest peak at 10.98 °2θ began to emerge. This phase is not present in the normal hydration products of C_3S. The diffraction intensities of this phase increased continuously in the 24 hr and 72 hr old pastes. The intensity of the C_3S peaks also decreased with time. In the 60 day old paste however, another set of peaks with the most intense peak at 10.12 °2θ could be discerned. The

peaks at 18.1 and 34.1 °2θ are due to CH. In the completely hydrated 2.75 M Cr(III) paste (14 month old), exposed in a humidifying chamber, all the C_3S had reacted leaving only the amorphous C-S-H halo. The phase that was first noticed in the 6 hour old paste has dissolved completely leaving only diffraction intensities of the new phase seen in the 60 day old paste. CH was also present. X-ray microanalyses reveal that these phases contain calcium and chromium with no silicon (Section 4.2). For brevity throughout the text, the initial phase is referred to as 'early Ca-Cr complex' and the late phase as 'late Ca-Cr complex'. As could be seen from the sealed 2.75 M Cr(III) paste also hydrated for 14 months, no decomposition of the early Ca - Cr complex occurred. It was tempting to attribute this effect to carbonation of the pastes exposed to the humid atmosphere, since CO_2 is known to increase condensation of the C-S-H and reactivity of C_3S. No carbonate peaks were found in either the sealed or the exposed 2.75 M Cr(III) pastes. To establish the cause of decomposition of the early Ca - Cr complex, 2 M Cr(III) pastes were prepared and hydrated for 15 days under different conditions.

Fig. 4.1.3 highlights these experiments. Two sets of 2 M Cr(III) doped pastes were cast into plastic molds without covering and placed in a N_2 flushed humidifying chamber. One of the two sets was compacted to obtain a monolithic block of waste after setting and the other was cast straight into the mold without compaction. Two other sets were sealed in plastic bottles with only one compacted. A striking observation is the presence of the early Ca-Cr complex in the sealed pastes (A and B) and the presence of both early and late Ca-Cr complexes in the pastes exposed to the humid atmosphere (C and D). It is also apparent that the pressure exerted during compaction did not appreciably affect the course of reaction in the sealed pastes but reduced the decomposition of the early Ca-Cr complex in the exposed pastes. Water was found to collect on top of the exposed pastes with large single crystals of CH adhering to the surfaces. The presence of single crystal CH accounts for the excessive preferred orientation exhibited by the (001) CH peak at 18.1 °2θ. Some CH had also formed in the sealed pastes but not as visible single crystals obtained in the exposed pastes. These are indications that CH formed in the sealed and exposed pastes are of different origins. Since the emergence of single crystal CH coincides with the development of late Ca - Cr complex and an attendant reduction in the early Ca - Cr complex, the following reaction sequence appears most plausible;

$$\text{Early Ca - Cr complex} \xrightarrow[\text{decomposition}]{H_2O} \text{Late Ca - Cr complex} + \text{CH} + H_2O \qquad (4.1)$$

The excess water absorbed from the humidifying chamber activated the decomposition reaction. The stoichiometry of the equation was ignored because the exact chemical formulae of the Ca - Cr phases are unknown. Formation of single crystal CH and collection of water on the surfaces of solidified pastes were noticed in the 1 M, 2 M and 2.75 M Cr(III) doped pastes hydrated for longer than 72 hours.

Judging from the amorphous C-S-H halo in Fig. 4.1.3, the formation of C-S-H does not appear to be overly affected by the hydration conditions. An interesting observation was the coloration of the different Ca - Cr complexes. The paste hydrated for 5 minutes was deep green while the pastes containing the early Ca - Cr complex had a distinct purple tinge. A gray coloration was observed in pastes containing the late Ca - Cr complex.

The diffraction patterns of the Ca - Cr complexes did not match any previously characterized Ca - Cr phase in the powder file. The diffraction pattern of the early Ca - Cr complex closely matched the pattern of $Ca_6Al_2O_5(NO_3)_3.xH_2O$. However, no symmetry or lattice parameter determination was carried out for this phase. Only peak positions were identified. The chromium analogue (Fig. 4.1.4) was produced by reacting 2 M chromium nitrate with CH as shown in equation 4.2.

$$6Ca(OH)_2 + 2Cr(H_2O)_6^{3+} + 6(NO_3)_3^- + xH_2O \rightarrow [Ca_3Cr(OH)_6.(NO_3)_3]_2.12+xH_2O \quad (4.2)$$

This is similar to ettringite which has a formula; $[Ca_3Al(OH)_6.12H_2O]_2.(SO_4)_3.2H_2O$. The OH^- ions are coordinated to aluminum and four water molecules are coordinated to the calcium atoms alongside the four OH^- ions shared with the $Al(OH)_6^{3-}$ octahedra. The presence of octahedral $Cr(OH)_6^{3-}$ units was confirmed with infrared spectroscopy in Section 4.3.1. Several unsuccessful attempts were made to produce single crystals to facilitate structure determination with x-ray diffraction. Shown in Tables 4.1.1 and 4.1.2 are the d-spacings of the Ca - Cr complexes. The compositions of the 2 M pastes hydrated for varying times are shown in Table 4.1.3. The rate of C_3S dissolution, and the rate of formation of early Ca - Cr complex are shown in Fig. 4.1.5.

Table 4.1.1 X-ray powder diffraction data of early calcium - chromium complex (Ca:Cr = 3).

d(nm)	*I(fix)*	*I(var)*
0.805	100	51
0.501	14	11
0.474	35	30
0.426	36	35
0.403	18	18
0.376	6	6
0.364	45	51
0.314	20	26
0.304	3	4
0.293	54	76
0.275	9	13
0.268	46	71
0.264	7	11
0.245	5	8
0.240	1	1
0.237	11	19
0.233	56	100
0.230	9	16
0.215	45	86
0.211	19	37
0.199	5	10
0.196	3	6
0.188	13	28
0.187	14	31
0.185	24	53
0.184	7	15
0.179	6	14
0.176	7	16
0.170	2	5

Table 4.1.2 X-ray powder diffraction data of late calcium - chromium complex (Ca: Cr = 2).

d(nm)	*I(fix)*	*I(var)*
0.873	66	32
0.431	100	98
0.292	59	85
0.276	31	47
0.242	57	100

Table 4.1.3 QXRD of 2 M Cr(III) pastes hydrated for varying times

Sample	*C_3S (wt%)*	*$Ca(OH)_2$ (wt%)*	*Early Ca-Cr complex*	*Late Ca-Cr complex*	*Reliability*
2MC3-5MIN	62.0	n.d*	n.d	n.d	0.02
2MC3-6H	51.1	n.d	7.22	n.d	0.03
2MC3-24H	48.1	n.d	8.6	n.d	0.02
2MC3-72H	37.2	n.d	12.9	n.d	0.03
2.75MC3-14M (sealed)	n.d	2.4	28.6	n.d	0.03

* n.d - not detected.

4.1.2 Effects of Varying Cr(III) Concentrations on Hydration Reactions

Enumerated in Table 4.1.4 are the compositions of 0.1 M and 1 M Cr(III) doped pastes. These pastes were hydrated for 24 hours and 60 days to identify specific effects of increasing Cr(III) concentrations on the reaction mechanism. Both chromium nitrate and chloride were used to better understand the role of the anion. Fig. 4.1.6 shows the diffraction patterns of 24 hour old 0.1 M and 1 M Cr(III) pastes. In the 0.1 M chromium nitrate and chromium chloride pastes, none of the Ca-Cr complexes were observed within the detection limit of the x-ray diffractometer.

The overall diffraction patterns are similar to the 24 hour old blank paste with only CH and unreacted C_3S prominent. A small amorphous C-S-H halo had also started forming. In the 1 M chromium nitrate however, a weak peak at ~ 11 °2θ indicates the presence of early Ca-Cr complex. This peak is located at 11.2 °2θ in the 1 M chromium

chloride paste. The shift is not unexpected as Cl^- modifies the structure of the Ca-Cr complex. After 24 hours, very little CH has formed in the 1 M Cr(III) pastes and none in the 2 M Cr(III) paste. As shown in Table 4.1.3, no CH was observed even after 72 hours in the 2 M Cr(III) paste. It is obvious that the early Ca-Cr complex formed preferentially to CH which did not start forming until all the available chromium has been consumed, hence the inhibition of CH with increasing chromium concentrations. If this is the case, the early C-S-H formed prior to complete consumption of chromium would have a lower Ca/Si ratio than the C-S-H formed in the blank paste.

The diffraction patterns of the 60 day old pastes are shown in Fig. 4.1.7 and the composition of the phases in Table 4.1.4. The diffraction patterns of the 0.1 M Cr(III) pastes are similar to the 60 day old blank paste with the amorphous C-S-H halo, CH and unreacted C_3S peaks dominating the powder patterns. In the 1 M chromium pastes, most of the C_3S have reacted leaving strong CH and very weak Ca-Cr complex peaks. The most obvious is the late Ca-Cr complex peak at 30.6 °2θ riding on the amorphous C-S-H halo. The peak at 11.2 °2θ in the 1 M chromium chloride paste remained. It is obvious from Table 4.1.4 that even at low concentrations, chromium accelerates the hydration reaction of C_3S. The relative effect on amorphous C-S-H could not be directly implied from x-ray powder diffraction. However, the Ca/Si ratio could be calculated for the blank at all ages and the 0.1 M Cr(III) solutions at 24 hours when negligible amounts of Ca-Cr complexes are formed.

The following mass balance was used to obtain the Ca/Si ratio in the C-S-H;

$$(Ca)_T = Ca_{C3S}(wt\%\ C_3S) + Ca_{CH}(wt\%\ CH) + Ca_{CaCO3}(wt\%\ CaCo_3) + Ca_{C\text{-}S\text{-}H}(wt\%\ C\text{-}S\text{-}H) \quad (4.3)$$

$$(Si)_T = Si_{C3S}(wt\%\ C_3S) + Si_{C\text{-}S\text{-}H}(wt\%\ C\text{-}S\text{-}H) \quad (4.4)$$

$(Ca)_T$ and $(Si)_T$ are the wt% of Ca and Si in the original mixture (1 g C_3S + 0.5 ml H_2O) respectively. Ca_{C3S}, Ca_{CH}, Ca_{CaCO3} and $Ca_{C\text{-}S\text{-}H}$ are the wt% Ca in unreacted C_3S, CH, $CaCO_3$ and C-S-H. The components in parentheses are the wt% of the phases obtained from QXRD. The mass balance of Si follows the same trend. All the terms are known except $Ca_{C\text{-}S\text{-}H}(wt\%\ C\text{-}S\text{-}H)$ and $Si_{C\text{-}S\text{-}H}(wt\%\ C\text{-}S\text{-}H)$. The Ca/Si ratio can thus be easily calculated without using the unreliable wt% C-S-H obtained by difference from 100% in the quantitative x-ray diffraction procedure.

For the partially and fully hydrated blank pastes, the average Ca/Si ratio obtained was 1.94 ± 0.05. This is similar to a value of 1.99 obtained by several investigators (Taylor [1990]). The relatively low reliability values in some of the patterns is mainly due to the C-S-H standard used to simulate the amorphous halo and the possibility of amorphous chromium compounds present especially during the early hydration periods. A typical least squares fit result is shown in Fig. 4.1.8 for the 14 month old 2.75 M Cr(III) pastes.

Table 4.1.4 QXRD analyses of partially hydrated 0.1 M and 1 M chromium pastes

Sample	*C_3S (wt%)*	*$Ca(OH)_2$ (wt%)*	*$CaCO_3$ (wt%)*	*Ca/Si*	*Reliability*
Bl-24H	72.2	9.5	n.d	1.95	0.016
0.1MCC3-24H	65.4	11.2	n.d		0.018
0.1MCN3-24H	68.3	8.6	0.3		0.009
0.1MC6-24H	68.9	4.2	n.d		0.009
1MCC3-24H	61.6	2.7	n.d		0.019
1MCN3-24H	67.9	n.d	n.d		0.007
1MC6-24H	70.4	0.7	n.d		0.016
Bl-60D	44.5	17.7	0.8	1.98	0.007
0.1MCC3-60D	36.3	18.7	2.3		0.018
0.1MCN3-60D	33.0	20.75	0.8		0.007
0.1MC6-60D	55.2	8.2	1.0		0.008
1MC6-60D	41.2	6	n.d		0.015
1MCC3-60D	2.9	12.6	0.3		0.005
1MCN3-60D	1.2	13.2	n.d		0.006
Bl-14M	7.6	31.9	1.7	1.89	0.014

4.1.3 Hexavalent Chromium Doped C_3S Pastes.

CrO_3 solutions containing 0.1 M, 1 M and 2 M were used as was the case with Cr(III) pastes. Fig. 4.1.9 shows the diffraction patterns of 2 M Cr(VI) pastes hydrated for varying times. The paste hydrated for 5 minutes shows unreacted C_3S and strong peaks at 11.1, 20.7 and 22.4 °2θ, matching $CaCrO_4.2H_2O$ in the powder file. As more C_3S reacted

and dissolved in the pore solution, $CaCrO_4.2H_2O$ disappeared in the 6 hour old and subsequent pastes, replaced by another phase with diffraction intensities at 15.5, 28.5 and 34.6 °2θ (3 most intense). No matching compound was found in the powder file. To produce the pure phase, CH was reacted with 1 M CrO_3 solution (Ca:Cr = 2) according to equation 4.4;

$$2Ca(OH)_2 + CrO_3 + xH_2O \rightarrow Ca_2CrO_5.yH_2O \qquad (4.4)$$

$y = 2+x$.

$CaCrO_4.2H_2O$ was produced in the same manner with a Ca:Cr ratio of 1.

The d-spacings of this phase are shown in Table 4.1.5. Good single crystals could not be produced with conventional techniques. Unlike the early Ca-Cr complex which increased with age, $Ca_2CrO_5.yH_2O$ reached a maximum at 6 hours (18.1 wt%) and decreased to 10.8 wt% at 60 days. The appearance of CH at 72 hours coincides with a rapid decrease in the amount of $Ca_2CrO_5.yH_2O$.

The amount of $CaCrO_4.2H_2O$ formed at 5 minutes is 8.8 wt%. The maximum amount of $CaCrO_4.2H_2O$ that could be formed based on the Cr concentration in the original mix is 12.06 wt%. Obviously not all the chromium has reacted within 5 minutes.

It is reasonable to assume that all the Cr has reacted at 6 hours to form $Ca_2CrO_5.yH_2O$ (18.1 wt%, shown in Table 4.1.6). The number of moles of lattice water in $Ca_2CrO_5.yH_2O$, (y) was calculated based on this assumption.

For a 0.5 ml 2 M Cr(VI) solution,

the number of moles of Cr = $(2 * 0.5 \times 10^{-3}) = 0.001$ mole

the mass of $Ca_2CrO_5.yH_2O$ = [0.001 * (230.176 + Total molar mass of H_2O)] (4.5)

= 0.181*1.5757 (wt % $Ca_2CrO_5.yH_2O$ * Total mass of initial mixture).

Total molar mass of H_2O = 55.026

$\therefore$ y = 55.026/18.016 = 3.05

The formula is thus $Ca_2CrO_5.3H_2O$.

Table 4.1.5 X-ray powder diffraction data of $Ca_2CrO_5.3H_2O$

d(nm)	*I(fix)*	*I(var)*
0.571	47	25
0.518	18	11
0.408	40	30
0.402	60	46
0.364	48	41
0.344	12	11
0.313	100	100
0.30	50	52
0.284	18	20
0.268	5	5
0.263	4	4
0.259	61	73
0.257	39	47
0.251	15	18
0.243	33	42
0.239	19	25
0.233	26	35
0.229	14	19
0.226	4	5
0.222	13	18
0.216	26	37
0.204	7	10
0.201	18	28
0.199	22	34
0.198	21	33
0.195	3	4
0.189	2	3
0.185	4	6
0.184	11	18
0.182	45	77
0.181	43	74
0.178	28	49
0.172	7	12
0.171	18	32

The compositions of the 2 M Cr(VI) pastes are listed in Table 4.1.6. Fig. 4.1.10 shows the rate of consumption of C_3S and formation of the calcium chromates. The CrO_4^{2-} ions released by $Ca_2CrO_5.3H_2O$ during the course of hydration may be forming an amorphous material not detected by powder diffraction techniques or they may be incorporated in the tetrahedral silicate sites in the C-S-H.

Table 4.1.6 QXRD of 2 M Cr(VI) pastes hydrated for varying times

Sample	*C_3S (wt%)*	*$Ca(OH)_2$ (wt%)*	*$CaCrO_4.2H_2O$ (wt%)*	*$Ca_2CrO_5.3H_2O$ (wt%)*	*Reliability (Equation 3.5)*
2MC6-5MIN	72.6	n.d	8.8	n.d	0.01
2MC6-6H	52.4	n.d	n.d	18.1	0.01
2MC6-24H	41.1	n.d	n.d	16.3	0.02
2MC3-72H	32.4	1.3	n.d	12.4	0.03
2MC6-60D	19.0	4.5	n.d	10.8	0.04

4.1.4 Effect of Varying Cr(VI) Concentrations on Hydration

No calcium chromate peaks were found in the 0.1 M Cr(VI) pastes hydrated for 24 hours (Fig. 4.1.11). Strong peaks of $Ca_2CrO_5.3H_2O$ could be seen in the 1 M and 2 M pastes. As expected, very small amounts of CH formed compared to the blank and 0.1 M pastes, since $Ca_2CrO_5.3H_2O$ is preferentially precipitated from the pore solution. In the 60 day old 1 M and 2 M pastes shown in Fig. 4.1.12, relatively large amounts of CH have formed and a marked reduction in $Ca_2CrO_5.3H_2O$, similar to the trend in 2 M Cr(VI) pastes, is evident. As was the case with Cr(III) pastes, increasing Cr(VI) concentrations inhibit the formation of CH.

4.2 Microstructure and Composition of Undoped and Chromium Doped C_3S Pastes

4.2.1 Microstructure of Undoped C_3S Pastes

Scanning electron microscopy studies of fracture surfaces provide valuable microstructural information about the development of hydration products of tricalcium silicate paste. In a C_3S paste hydrated for 24 hours (comprising the induction and acceleratory periods), the microstructure is dominated by fibrous C-S-H (Type I) radiating into the pores from the anhydrous C_3S grain. These fibres could be as long as 1.5 μm as shown in the SEM micrographs in Figs. 4.2.1a and b. The honeycomb or reticular network structure (Type II) observed by several investigators (Taylor [1990]) during the early hydration period could not be distinguished from the fibrous structure. CH plates formed from the supersaturated pore solution appeared with different morphologies. The bright CH in the back scattered electron image (Fig. 4.2.2a) probably assumed a flaky form

as a result of the drying procedure to stop hydration. The dark featureless region is also CH. A low magnification backscattered electron image of the section in contact with the mold is shown in Fig. 4.2.2b. The bright plates are primarily CH. Water trapped between the paste and the mold during compaction was responsible for the large size of the plates.

As the reaction lapses into the deceleratory and steady state stages, more CH and fibrous C-S-H are formed. A shrinking pore volume and a reduced pore solution contribute to the condensation of the silicate units to form polymeric C-S-H (pentameric and octameric silicate chains (Taylor [1990])). The polymeric silicate units are termed 'inner C-S-H' or Types III and IV. The morphology resembles tightly packed equant grains. 60 day old C_3S paste consists of fibrous C-S-H and well defined massive hexagonal CH crystals sandwiched between the C-S-H grains. A typical SEM micrograph showing these features is displayed in Fig. 4.2.3. Also shown in Fig. 4.2.4 is a TEM micrograph of 60 day old paste comprising the dense inner C-S-H and the porous outer C-S-H. The outer C-S-H fibres were found to decompose rapidly at 200 kV. The tightly packed structure is best seen in the polished 14 month old C_3S paste shown in Fig. 4.2.5. Region A is mainly unreacted C_3S (Ca/Si ratio = 2.95) while region B, covering about 60% of the micrograph is C-S-H. The phase (C) running along the boundaries is CH. It is, however, difficult to differentiate the inner C-S-H from the outer C-S-H in this paste.

At best, x-ray microanalysis of fracture surfaces gives semiquantitative results, because the x-rays generated within the excitation volume also excite x-rays from surrounding structures. The x-rays generated in the excitation volume can also be absorbed by the surrounding structures. Polished and thin sections provide better quantification of the composition. Because the samples analyzed contain hydration water, only elemental Ca/Si ratios could be calculated with acceptable accuracy. To enhance the precision of the elemental ratios, unreacted C_3S regions were used as standards for both polished and thin samples. Fig. 4.2.6 shows the relationship between Ca and Si in the 14 month old blank pastes with an average C-S-H Ca/Si ratio of 1.61 $\pm$ 0.15 and ranging between 1.46 and 1.84. The Ca/Si mole ratios are tabulated in Table 4.2.1. A wider range of Ca/Si ratio was obtained with TEM thin sections using a 10 nm electron probe size as opposed to x-ray microanalysis in the SEM (Tungsten filament) where the minimum lateral beam spread could be as high 1 µm. The Ca/Si ratio has been found to vary from 0.8 to 1.5 in 1 day old pastes, and 0.5 to 2.0 in 60 day old pastes.

Table 4.2.1 Average Ca/Si ratios in hydrated blank and chromium - doped pastes

Sample	*SEM Ca/Si atom ratio*	*TEM Ca/Si atom ratio*
Bl-24H	1.65 ± 0.02	1.10 ± 0.35 (0.83 to 1.49)
Bl-14M	1.61 ± 0.15	1.24 ± 0.54 (0.52 to 2.04)
0.1MCN3-24H	1.60 ± 0.05	1.15 ± 0.16 (0.95 to 1.30)
0.1MCN3-60D	1.54 ± 0.05	n.d*
0.1MCC3-60D	1.51± 0.04	n.d
1MCN3-24H	1.87 ± 0.07	n.d
1MCN3-60D	n.d	1.5 ± 0.4 (0.8 to 2.0)
2MCN3-5MIN	n.d	1.7 ± 0.3 (1.12 to 2.06)
2MCN3-24H	n.d	1.04 ± 0.18 (0.83 to 1.48)
2MCN3-60D	n.d	a) 0.48 ± 0.09 (0.39 to 0.62)
		b) 1.59 ± 0.35 (0.88 to 2.18)
2.75MCN3-14M	1.83 ± 0.15	n.d
1MC6-24H	1.80 ± 0.13	n.d
1MC6-60D	1.81 ± 0.11	n.d

** n.d - not determined*

4.2.2 Microstructure and Composition of Cr(III) Doped Paste

Fig. 4.2.7 shows an SEM micrograph and EDS spectra of a fractured 1 day old 0.1 M Cr(III) chloride paste. The fibres that dominated the blank paste appeared to take a honeycomb form typical of Type II C-S-H (A and D). Well defined CH crystals have also formed within the first day of hydration reaction (regions B and C). In addition to the honeycomb structure, structures resembling flowering buds were also found in the 1 day old 0.1 M Cr(III) nitrate pastes. This phase was not present in either the blank or the 0.1 M Cr(III) chloride pastes. The SEM micrographs of these regions are displayed in Fig. 4.2.8. The formation of honeycomb C-S-H in place of fibres signifies the modifying

effects chromium has on the morphology of the hydration products. Likewise, the presence of chlorine in the EDS spectra of C-S-H regions of 0.1 M Cr(III) chloride paste, and the differences in the types of C-S-H formed in the nitrate and chloride pastes, indicate that the anion plays a crucial role in hydration reactions. Chloride ions are known to be better hydration accelerators than nitrate ions.

The 60 day old pastes of both 0.1 M chromium nitrate and chloride are similar with honeycomb C-S-H dominating the microstructure (Figs. 4.2.9 and 4.2.10). The average Ca/Si ratios are 1.54 and 1.51 for chromium nitrate and chloride respectively. No Cr was found in the C-S-H regions analyzed. X-ray microanalysis in the TEM gave a Ca/Si of 1.15 ± 0.16 with values ranging from 0.95 to 1.30 (0.1 M chromium nitrate). As in the blank pastes the 60 day old 0.1 M chromium doped pastes were much less porous than the 1 day old pastes.

As the chromium concentration is increased, more distinct Cr - containing phases were observed. Fig. 4.2.11 shows an SEM micrograph of 1 M chromium nitrate hydrated for 24 hours. In place of the fibrous or honeycomb C-S-H that characterized the 1 day old blank and 0.1 M Cr(III) pastes, rods up to 4 μm long and 0.4 μm wide dominated the microstructure. The growth of C-S-H and CH was hindered as significantly lower amounts of these phases were detected relative to the blank and 0.1 M Cr(III) pastes. As could be seen from Fig. 4.2.11, the C_3S - like grains (C) are devoid of fibrous C-S-H. X-ray microanalysis of the C_3S - like grain indicate a Ca/Si ratio of ~ 1.8. TEM studies revealed these rods to be amorphous (Fig. 4.2.12) and comprised of only Ca and Cr in highly variable ratios. In about six spots analyzed in a rod, the Ca/Cr mole ratio varied from 0.2 to 3.5 (Table 4.2.2). Some amorphous C-S-H regions were also found to contain variable chromium concentrations. The rods were not seen in the 1 M chromium chloride pastes hydrated for 1 day, where chromium was found to be associated with C-S-H. In the 60 day old 1 M Cr(III) nitrate and chloride pastes, the Cr - rich rods were not observed in the dense microstructures shown in Figs. 4.2.13 and 4.2.14. As could be seen from the EDS spectra, both pastes contain large crystals of Cr - free CH and Cr containing featureless C-S-H gel. The small Cr blips in these spectra were most likely derived from the surrounding Cr - containing C-S-H phase. The chromium distribution in 1 M Cr(III) nitrate paste is depicted in the x-ray maps of a typical polished section (Fig. 4.2.15). Cr-rich phases were seen to form mainly in the pores, like CH. The average Ca/Cr ratio in the Cr-rich regions is 1.93. The contrasts of the elemental maps were separately adjusted to improve the signal to noise ratio. The TEM micrograph in Fig. 4.2.16 revealed two types of C-S-H. The denser C-S-H (A) is the inner product and has a

Ca/Si ratio of ~ 1.5 ± 0.4 with a range between 0.8 and 2.0 and very little Cr. The Cr - containing C-S-H phase (B) has a Ca/Si ratio ranging from 0.8 to 3.2 and high Cr concentrations. Since no CH was found in this region to account for the increase in Ca/Si ratio, some of the Ca must be associated with Cr and some Cr is possibly incorporated within the C-S-H network . The absence of Cr in the late inner C-S-H suggests that most of the Cr not forming Ca-Cr rods is associated with the C-S-H formed during the early stages of hydration.

Table 4.2.2 Average Ca/Cr ratios in chromium - doped pastes

Sample	*Ca/Cr mole ratio (Range)*
1MCN3-24H	Highly variable (0.2 to 3.5)
1MCN3-60D	1.93 ± 0.11
2MCN3-5MIN	2.92 ± 0.08
2MCN3-24H	2.0 ± 0.4 (1.53 - 2.46)
2MCN3-60D	2.2 ± 0.5 (1.47 - 2.79)
2.75MCN3-14M (Exposed)	1.95 ± 0.15 (TEM) 1.94 ± 0.08 (SEM)
1MC6-60D	2.06 ± 0.04
2MC6-5MIN	1.02 ± 0.09
2MC6-24H	1.38 ± 0.09

The 2 M Cr(III) pastes offer a more comprehensive observation of the formation of the hydration products. Shown in Fig. 4.2.17 is a TEM micrograph of 2 M Cr(III) nitrate paste hydrated for 5 minutes. The phase is primarily C-S-H containing Cr in variable concentrations. Localized regions containing only Ca/Cr, in other areas studied, have a Ca/Cr mole ratio of 2.92 ± 0.08. This is an indication that some early Ca-Cr complex has started forming despite its absence in the x-ray diffraction pattern. Fig. 4.2.18 shows the relationship between the elemental concentrations in the C-S-H. The Ca/Si ratio in these regions ranged from 1.12 to 2.06 with an average of 1.7 ± 0.29. This is similar to the

range obtained in Cr free regions in the blank and lower chromium doped C_3S. As can be seen from Fig. 4.2.18, Cr concentrations are high in the analyzed areas indicating that most of the Cr was associated with C-S-H within the first few minutes of hydration. After 24 hours, a large amount of C_3S has reacted and well defined Ca-Cr rods could be discerned in the SEM micrograph shown in Fig. 4.2.19. Typical microstructures are shown in the TEM micrographs in Fig. 4.2.20. X-ray microanalysis of the phase in Fig. 4.2.20a revealed a C-S-H with an average Ca/Si ratio of 1.04 ± 0.18, and a range between 0.83 and 1.48. Very little Cr was observed in this area. Fig. 4.2.20b contains Ca and Cr with very little Si and an average Ca/Cr mole ratio of 2.0 ± 0.4, ranging between 1.53 and 2.46. The relationships between the constituents of the analyzed phases are shown in Fig. 4.2.20c.

The Cr containing regions are explicitly delineated in the 60 day old 2 M Cr(III) paste. Fig. 4.2.21a shows a fine C-S-H gel containing chromium and an unusually high Si concentration. The average Ca/Si ratio is 0.48 ± 0.09 with a narrow range between 0.39 and 0.62 (Table 4.2.1). The more porous C-S-H in Fig. 4.2.21b has a higher Ca/Si ratio, but similar variable Cr concentrations, with a Ca/Si ratio of 1.59 and ranging from 0.88 to 2.18. This is similar to the Ca/Si ratio obtained in the blank and the Cr-doped pastes discussed earlier in this section. Fig. 4.2.22 shows a TEM micrograph of the Ca-Cr rods. These amorphous rods have a variable Ca/Cr ratios varying between 1.47 and 2.79 with an average of 2.23. Considering the x-ray diffraction studies which identified both early and late Ca - Cr complexes at this stage, this Ca/Cr variation was not unexpected as both are located within the pores. No trace of Si was observed in the EDS spectra of these rods. The low Ca/Si ratio observed in the C-S-H in Fig. 4.2.21a was most probably due to the depletion of the Ca from C-S-H used for the formation of Ca-Cr complexes. The lower Ca concentration in this phase leads to increased condensation of such silicate units. This deduction is verified by FTIR and NMR studies in Sections 4.3 and 4.4. Fig. 4.2.23 shows the relationships between the constituents of the analyzed areas.

The microstructure of the 2.75 M Cr(III) paste stored in the humidifying chamber for 14 months is similar to the 60 day old pastes. Fig. 4.2.24 shows a TEM micrograph of a Cr -rich amorphous gel. The average Ca/Cr ratio is 1.67, ranging between 0.82 and 2.37. The Ca/Si ratio in this area is greater than 5. Since some of the Ca is associated with Si, the actual Ca/Cr ratio would be lower than 1.67. The EDS spectra of the sites with the lowest and highest silicon concentrations are also shown in Fig. 4.2.24. Fig. 4.2.25 shows Ca-Cr rods with a Ca/Cr mole ratio of 1.95 ± 0.15. The distribution of Cr in

several phases analyzed (C-S-H with or without Cr and Ca - Cr rods) are plotted in Fig. 4.2.26.

Analysis of a polished section of 14 month old 2.75 M Cr(III) paste in the SEM revealed some interesting microstructures. The Ca-Cr phase appeared as distinct flakes and it is located in the pores surrounding C-S-H grains, as shown in a low magnification micrograph of the 14 month old 2.75 M Cr(III) paste (Fig. 4.2.27). The darker phase is primarily C-S-H containing Cr in small but variable quantities. The line scan shown in Fig. 4.2.28 revealed the elemental composition of the phases. It is obvious that the C-S-H in the bottom left corner contains more Cr than the C-S-H (mid centre) surrounded by Ca-Cr flakes. The relationship between the Ca/Cr and Ca/Si ratio in the randomly selected regions is shown in Fig. 4.2.29. The analyzed spots were randomly chosen. The Ca/Si mole ratio of the Cr free clusters in the lower right region is 1.83 ± 0.15 and the Ca/Cr ratio of the Si - free Ca-Cr rods is 1.94 ± 0.08 (upper left clusters). An interesting observation was the Ca/(Cr+Si) mole ratio which was fairly constant between 1.39 and 2.30 with a mode at 1.89. Coupled with the observed data points between C-S-H and Ca-Cr rods, one might suggest that Cr substitutes for Si in the C-S-H gel, however, equally probable is the random distribution of Ca-Cr complex in C-S-H on a microscale. The highly variable Cr concentration in the C-S-H phases observed in the TEM data, however, indicates that either possibility might be far-fetched. The evidence points more towards the localized incorporation of chromium within the C-S-H network.

The synthesized early Ca-Cr complex (Ca/Cr = 3) was also analyzed in the TEM. The complex appeared as well formed rods similar to the Ca - Cr rods in the Cr(III) pastes (Fig. 4.2.30). As obtained in the Cr-doped pastes, the rods are mostly amorphous (few diffraction spots hinting at some crystallinity) with highly variable Ca/Cr ratios. The x-ray diffraction pattern indicates a strongly crystalline structure without an amorphous halo. The source of this anomaly is not known but the variable Ca/Cr ratio in the rods might account for the short range disorder. Ten different spots were analyzed giving a Ca/Cr ratio ranging from 0.39 to 2.86. On the other hand, the same sample analyzed in the SEM gave an average Ca/Cr ratio of 3.05 using crystalline $CaCrO_4.2H_2O$ as a standard.

The following points are evident from the SEM and TEM x-ray microanalysis:

- The early Ca-Cr complex has a Ca/Cr ratio of ~ 3 while the late complex has a Ca/Cr atom ratio of ~ 2.

- The Cr in the C-S-H appeared to be randomly incorporated into the C-S-H without substituting for either Ca or Si. Since the Cr - containing C-S-H appears as a single

phase, chemical incorporation of Cr in the C-S-H gel is more likely than a physical mixture of amorphous $Cr(OH)_3.3H_2O$ or calcium chromium complex on a fine scale. Random incorporation of $Cr(OH)_4^-$ in the tetrahedral silicate sites is expected to distort the C-S-H structure.

4.2.3 Microstructure and Composition of Cr(VI) Pastes

Similar microstructural and microanalytical strategies were employed for both Cr(III) and Cr(VI) pastes. Fig. 4.2.31 shows an SEM micrograph of a 24 hour old 0.1 M Cr(VI) paste. Cr was found to be associated with both CH and fibrous C-S-H as shown in EDS spectra in Fig. 4.2.31. The distinct nature of the hydration products without the connectivities observed in the corresponding blank and Cr(III) pastes was striking (Fig. 4.2.1 and Fig. 4.2.8). This suggested a highly porous structure. The C-S-H fibres could be seen to be shorter than the fibrous C-S-H in the blank paste. The approximate Ca/Si ratio of the C-S-H gel was found to be 1.80 ± 0.13. This porous structure persisted in the 60 day old paste as depicted in Fig. 4.2.32. The only difference between the 1 day old and 60 day old pastes being the greater amount of CH seen in the microstructure of the 60 day old paste. The average Ca/Si of the fibrous C-S-H was also found to be 1.81 ± 0.11. In analyzing these fracture surfaces, care was taken to focus the beam on relatively flat surfaces to reduce the generation of secondary x-rays from surrounding structures.

Doping C_3S with 1 M Cr(VI) solution gave microstructures similar to the 0.1 M Cr(VI). Shown in Fig. 4.2.33 is an SEM micrograph of a fractured 60 day old paste similar to 0.1 M Cr(III) pastes. The microstructure remained porous with CH and C-S-H dominating the structure. Microanalysis of the 60 day old polished sections revealed a phase containing only calcium chromate. Fig. 4.2.34 shows an x-ray map of the polished section. The phase in the top left corner of the micrograph could be seen to contain only Ca and Cr. X-ray microanalysis confirmed the Ca/Cr ratio to be 2.06 ± 0.04 (Table 4.2.2). This is in agreement with $Ca_2CrO_5.3H_2O$ predicted from XRD diffraction studies.

Shown in Fig. 4.2.35 is an SEM micrograph of 2 M Cr(VI) paste hydrated for 5 minutes. The large crystals are $CaCrO_4.2H_2O$. This was confirmed by detailed x-ray microanalysis in the TEM. Fig. 4.2.36 shows a TEM micrograph of a calcium chromate crystal. The Ca/Cr mole ratio was obtained as 1.02 ± 0.09. Some C-S-H containing Cr was also observed in the 5 minute old thin section. The Ca/Si ratio was found to be 1.69 ± 0.35. Fig. 4.2.37 depicts the compositional relationships in the phases analyzed.

After 24 hours, the $CaCrO_4.2H_2O$ crystals could not be distinguished from the regular products of hydration (Fig. 4.2.38). The rod in the lower left corner is CH. The C-S-H fibres are shortened as the volume increase associated with the formation of fibrous C-S-H appeared inhibited. This is similar to 0.1 M and 1 M Cr(VI) doped pastes. TEM/EDS analysis of the Cr containing regions revealed a phase containing primarily Ca/Cr with a ratio of 1.38 ± 0.09 (Fig. 4.2.39).

The following inferences can be drawn from the SEM and TEM x-ray microanalysis of the Cr(VI) pastes:

- The fibres associated with dimeric C-S-H are much shorter, compared to the blank pastes. This leads to the formation of highly porous Cr(VI) waste forms.
- The formation of large crystals of $CaCrO_4.2H_2O$ within the first few minutes of reaction and subsequently, $Ca_2CrO_5.3H_2O$, depends on the amount of Ca available in the pore solution to react with Cr.
- The Ca/Si ratio of C-S-H was not largely affected as was the case with Cr(III) doped pastes.

4.3 FTIR Spectroscopy

The complex structure of C_3S is manifest in its FTIR spectrum shown in Fig. 4.3.1. The free orthosilicate SiO_4^{4-} has a tetrahedral (T_d) symmetry and four normal modes of vibration namely: ν_1, symmetric stretching (811 - 854 cm^{-1}); ν_3, asymmetric stretching (873 - 997 cm^{-1}); ν_2, in plane bending (452 cm^{-1}); and ν_4, out of plane bending (513 - 525 cm^{-1}). Fortunately, the ionic nature of the Ca-O-Si bonds in calcium silicates results in the separation of internal SiO_4^{4-} vibrations between 450 and 1000 cm^{-1} and lattice vibrations normally observed below 400 cm^{-1} in the far infrared region. This makes it easy to correlate the vibrations exhibited by the silicate anions in C_3S to the normal modes of the free SiO_4^{4-} anion. Splitting of the vibrations occur owing to the low symmetry of C_3S. The vibrations are grouped in Table 4.3.1.

Atomic masses, bond force constants and molecular geometry all contribute to the vibrational frequencies observed in materials. It is thus conceivable that condensation of the silicate anions in C_3S to form C-S-H will affect the vibrational frequencies of SiO_4^{4-}. The asymmetric vibrations will be affected more because the Si atom is stationary during symmetric vibrations (ν_1 and ν_2), whereas in the asymmetric vibrations (ν_3 and ν_4), the Si atom moves with the oxygen atoms making it more sensitive to variations in bond force constants and isotopic substitution. In Si-O-Si linkages, oxygen forms two strong bonds each as strong as the terminal oxygen bond in SiO_4^{4-} (Ryskin [1974]). The increased bond force constant may shift the vibrations to higher frequencies.

The effects of chromium on the silicate tetrahedra in hydrating C_3S may be two - fold. The degree of silicate polymerization may change through competition for Ca ions without the Cr ions being chemically incorporated in the C-S-H, or Cr may substitute for Si or Ca in C-S-H as postulated by some investigators (Heiman et al. [1991], Ivey et al. [1993], Mollah et al. [1992]). In both cases, the silicate bands will be shifted. However, if in the second case, Si and Cr are connected through Ca polyhedral, Cr will have very little effect on silicate vibrations and CrO_4 vibrations in tetrahedra coordination should become active. The infrared spectra of Cr(III) and Cr(VI) doped C_3S are described in Sections 4.3.1 and 4.3.2 respectively. Factor group analyses could not be carried out on these spectra because the structures of the hydration products, mainly C-S-H, calcium chromium complexes and dicalcium chromate trihydrate, are unknown. Hence only partial assignments of the bands could be made.

Table 4.3.1 FTIR spectra assignments of C_3S and fully hydrated blank and 2 M Cr(III) doped pastes

Assignments (cm^{-1})	*C_3S*	*C_3S/H_2O blank (14 months)*	*Sealed 2.75 M Cr(III) (14 months)*	*Exposed 2.75 M Cr(III) (14 months)*
ν_2 (SiO)	452 s, b*	452 b	-	-
ν_4 (SiO)	525 vs	492 w	-	-
ν (CrO)	-		492 s	489 s
**	-	-	530, 598 s, b	543 s, b
ν_4 (CO)	-	714 w	-	-
ν_4 (NO)	-	-	717 w	-
δ (Cr-OH)	-	-	774 s	774 s
ν_2 (NO)	-	-	824 w	835 w
ν_1 (SiO)	811 s, b, 835, 845 sh	-	-	-
ν_3 (SiO)	873, 906 sh, 929 w, 939 vs, 950, 979, 997 sh	-	-	-
ν (SiOSi)	-	981 s, b	915 sh, 1000 vs, b	915 sh, 1000 vs, b
ν_1 (NO)	-	-	1047 w, sh	-
ν_3 (NO)	-	-	1329 s, 1353 s, 1425 s, 1444 s	1368 s, 1408 b
ν_1 (CO)	-	1420 vb	-	-
δ (HOH)	-	1633 w	1633 s	1633 s
ν (HOH)	-	3512 b, s	3416, 3548 s, b	3533 b
ν (OH) - (Ca-Cr complex)	-	-	3588 sp, 3606 sp	3588 sp
ν (OH)-(CH)	-	3644 sp	-	3644 sp

* *Band intensity: vs, very strong; s, strong; sh, shoulder; sp, sharp; b, broad; w, weak; vw, very weak.*

** *Unassigned bands.*

4.3.1 Chromium (III) Pastes

Also shown in Fig. 4.3.1 and Table 4.3.1 are the infrared spectra of fully hydrated pastes of the blank and 2 M Cr(III) (exposed and sealed). The spectra could be divided into four main groups:

- vibrational modes due to silicate ions
- vibrational modes due to water molecules and hydroxyl ions
- metal-hydroxyl bending vibration
- vibrational modes due to nitrate ions.

Silicate vibrations

As C_3S diminishes with time, the silicate vibrations in the Cr(III) doped spectra decrease. The symmetric SiO_4^{4-} vibrations least affected by condensation are more easily identifiable, because ν_4 (O-Si-O) overlaps with Cr-O vibrations and the ν_3 (Si-O) becomes very broad with the formation of polymeric C-S-H. In a fully hydrated blank paste, the asymmetric stretch shifted from 939 cm^{-1} to about 981 cm^{-1}. This is expected for asymmetric Si-O-Si vibrations in dimeric and polymeric C-S-H. In the Cr-doped spectra, a broader band centred around 1000 cm^{-1} is observed indicating minor differences in the silicate anion environment compared to the blank paste. The weak band at 492 cm^{-1} in the blank paste can be attributed to bending modes in the polymeric silicate units. This band cannot be compared directly to the spectra of Cr(III) doped pastes because it overlaps with a stronger Cr-O stretching vibration around 490 cm^{-1}.

Water of hydration and hydroxyl ion vibrations

The fairly strong band at 1633 cm^{-1} in all the spectra is due to bending modes in water molecules contained in the lattice. The $\nu_1 + \nu_3$ stretching vibration of lattice water in C-S-H is the broad band centred around 3510 cm^{-1} in the C_3S/water paste. Two broad bands at 3416 and 3548 cm^{-1} in the sealed Cr (III) paste indicate the presence of hydration water in the early calcium chromium complex. This is similar to the water vibrations in the calcium chromium complex produced from $CH/Cr(NO_3)_3.9H_2O$ (Ca : Cr = 3) shown in Fig. 4.3.2 and Table 4.3.2. The exposed Cr(III) paste has its water band centred at 3533 cm^{-1} (Table 4.3.1).

The hydroxyl stretch due to CH is at 3644 cm^{-1}. This is very strong in the standard C_3S/H_2O paste and visible in the exposed 2 M Cr(III) paste in agreement with XRD studies. In hydrating C_3S paste, CH is usually noticed after about 6 hours corresponding

to the termination of the induction period (Taylor [1990]). The absence of CH in the sealed Cr(III) paste is suggestive of a CH formation mechanism occurring in Cr(III) pastes different from that in normal C_3S/H_2O paste.

The very small width of the bands at 3588 cm^{-1} (FWHM = 10 cm^{-1}) and 3606 cm^{-1} (FWHM = 14 cm^{-1}) in the sealed Cr (III) paste indicate the presence of non-hydrogen bonded hydroxyl ions (OH). To further differentiate the OH bands from the broad water bands, an analogous compound to CH/Cr(III) Ca:Cr = 3 was prepared from deuterated water. This entailed reacting calcium deuteroxide with $Cr(NO_3)_3.9H_2O$ made up to 2 M with D_2O. The infrared spectrum is shown in Fig. 4.3.2. The OD bands have shifted to 2646 and 2660 cm^{-1} and a ν_H/ν_D ratio of 1.36 is typical for most transition metal hydroxides (Ryskin [1974]). Both OH and OD bands are present since the starting $Cr(NO_3)_3.9H_2O$ has some water. The fully hydrated exposed Cr(III) paste contains only one OH peak indicating a higher site symmetry of the late calcium chromium complex than the early complex.

Table 4.3.2 FTIR spectra assignments of early calcium chromium complex

Assignments (cm^{-1})	*$Ca(OH)_2$ / $Cr(NO_3)_3.9H_2O$*	*$Ca(OD)_2$ / $Cr(NO_3)_3.9H_2O$*
ν (CrO)	492 s	492 sh
δ (Cr-OD)	-	538 vs
**	530, 598 s, b	598 s, b
ν_4 (NO)	717 w	717 w
δ (Cr-OH)	774 s	774 s
ν_2 (NO)	824 w	824 w
ν_1 (NO)	1047 w, sh	1047 w, sh
ν_3 (NO)	1329 s, 1353 s, 1425 s, 1444 s	1329 s, 1353 s, 1425 s, 1444 s
ν (OD)	-	2646 vs 2660 vs
δ (HOH)	1633 s	1633 s
ν (HOH)	3416, 3548 s, b	3416, 3548 s, b
ν (OH)	3588 sp, 3606 sp	3588 sp, 3606 sp
ν (OH) - (CH)	-	3644 sp

High covalence of the M-OH (metal - hydroxyl) bond in amphoteric hydroxides transforms the OH libration frequency into bending vibrations involving M-OH bonds (Ryskin [1974]). These are normally observed between 600 and 1200 cm^{-1} and depend on the energy of the H- bonds linking the OH groups and the strength of the M-O bond (Bensted and Varma [1971]). By nature, these vibrations are not degenerate due to the lack of rotation axes among the symmetry elements of an OH site. If the OH group lies in a symmetry plane, in - plane δ(OH) and out - of - plane γ(OH) would become active (Ryskin [1974]). The nature and frequency of the vibration at 774 cm^{-1} in the Cr(III) pastes is similar to metal - hydroxyl bending modes δ(OH) in analogous complexes such as ettringite and calcium sulphoaluminate (Bensted and Varma [1973]). In the deuterated complex, this peak has shifted to 538 cm^{-1} further lending credence to the correctness of the assignment. In such a case, Cr would be in octahedral coordination as in $[Cr(OH)_6]^{3-}$. The bands at 530 cm^{-1} and 598 cm^{-1} could not be positively assigned but may correspond to independent sets of hydroxyls in the calcium chromium complexes.

The Cr - O stretching vibration is at 492 cm^{-1} in the sealed Cr(III) paste and at 489 cm^{-1} in the exposed Cr(III) paste.

Nitrate vibrations

The free NO_3^- ion has a planar D_{3h} symmetry. This gives rise to two NO stretching bands (ν_3 and ν_1) and two bending vibrations (ν_2 and ν_4) (Nakamoto [1986]). Of these, ν_2 and the doubly degenerate ν_3 and ν_4 are infrared active, while ν_1, ν_3 and ν_4 are Raman active. When the symmetry of the nitrate ion is lowered through complex formation, these vibrations may split and Raman active vibrations become active in infrared. The peaks between 1320 cm^{-1} and 1450 cm^{-1} belong to the asymmetric stretch (ν_3 NO_3^-). The bands split with age corresponding to the amount of early calcium chromium complex present in the paste (compared to the CH/Cr(III) spectrum in Fig. 4.3.2). The splitting observed in the sealed Cr(III) paste indicates a lower nitrate ion site symmetry in the early calcium chromium complex and a strongly bonded NO_3^- compared to the unsplit exposed Cr(III) paste. The presence of two doubly degenerate bands might be due to Ca and Cr coordinating NO_3^-. The band at 1047 cm^{-1} in the sealed Cr(III) paste is due to the symmetric NO_3^- stretching vibration which is only active in the infrared mode when the site symmetry of the NO_3^- ion deviates from D_{3h} due to complex formation. The bending in - plane vibrations are the sharp peaks at 824 cm^{-1} (ν_2) in the sealed paste and 834 cm^{-1} in the

exposed Cr(III) paste. Out of plane bending (ν_4 at 717 cm^{-1}) is only active in the sealed Cr(III) paste. The absence of splitting in the ν_3 (NO_3^-) and the disappearance of the ν_1 (NO_3^-) vibration in the exposed Cr(III) paste is also an indicator that the late calcium chromium complex has a higher symmetry than the early complex.

The little information obtained thus far on the structure of these complexes made further attempts to assign the remaining vibrations improper. It is, however, apparent that both complexes are primarily calcium chromium hydroxide nitrate hydrates similar to the calcium aluminate hydroxide hydrates formed in Portland cement hydration.

The vibrational bands at 1420 - 1490 cm^{-1}, 870 cm^{-1} and 714 cm^{-1} in the blank paste are due to ν_1 CO_3^{2-}, ν_2 CO_3^{2-} and ν_4 CO_3^{2-} respectively. These arise from carbonation of CH to form calcium carbonate.

4.3.1.1 Rate of Formation of Calcium Chromium Complexes in 2 M Cr(III) Pastes

The infrared spectrum of the exposed 2 M Cr(III) doped pastes hydrated for 5min, 6 hrs, 24 hrs, 72 hrs and 60 days are shown in Fig. 4.3.3. The progress of hydration could be followed by the decreasing intensities of the silicate bands and the emergence of vibrational modes of calcium chromium compounds.

The lattice water bending vibration at 1640 cm^{-1} in the spectra decreases with age. It is plausible that excess water is rejected during the formation of calcium chromium complexes from Ca^{2+}, OH^- and $[Cr(H_2O)]^{3+}$ present in the pore solution. This is in agreement with the reaction proposed in Equation 4.1 pertaining to the dissolution of early Ca-Cr complex to give the late Ca-Cr complex, CH and water. It was observed that the samples hydrated in a humidifying chamber actually bled water even after one year. The CH band at 3644 cm^{-1} became noticeable only in the 60 day old paste suggesting that high concentrations of Cr inhibits the formation of CH.

In contrast to the H_2O bands which decrease with age, the intensities of the sharp OH bands at 3588 and 3606 cm^{-1} increase with age and coincide with the appearance and development of the strong δ(Cr-OH) bending vibration at 774 cm^{-1}. The intensities of the ν(OH) stretching vibrations increased continuously up to 72 hours and decreased in the 60 day old paste. These bands were completely merged in the completely hydrated exposed 2.75 M Cr(III) paste (Fig. 4.3.1).

The nitrate bands also change with time. Splitting of the $\nu_3(NO_3^-)$ became more evident as the concentration of the early complex increases in the system. As was the case with ν(OH) bands, less splitting was observed after 60 days and almost insignificant in the fully hydrated paste. Similarly, the $\nu_1(NO_3^-)$ at 1047 cm^{-1} increased up to 72 hours and became smaller in the 60 day old sample. It appeared inactive in the fully hydrated exposed Cr(III) paste.

4.3.1.2 Effects of Cr(III) Concentrations on the C_3S Hydration

Fig. 4.3.4 and Table 4.3.3 show the spectra and spectra assignments of 0.1 M, 1 M, 2 M and blank pastes hydrated for 24 hours. Blank and 0.1 M Cr(III) pastes possess identical silicate and lattice water vibrations. Both have quite strong CH vibrations at 3644 cm^{-1}. No CH was formed within 24 hours in the 1 M and 2 M Cr(III) doped pastes. Both chromium chloride and chromium nitrate gave similar results. This is in agreement with the XRD results discussed in Section 4.1. In the 2 M Cr(III) paste, the asymmetric silicate stretch is much broader than in the other spectra pointing to a greater condensation of the silicate units with increasing chromium concentrations.

The $\nu_1(NO_3^-)$ at 1047 cm^{-1}, $\nu_4(NO_3^-)$ at 717 cm^{-1} and $\nu_1(NO_3^-)$ at 1320 - 1450 cm^{-1} are visible in all the Cr(III) nitrate spectra. A sharp $\nu(NO_3^-)$ band at 1384 cm^{-1} not present in either of the calcium chromium complexes was observed in both the 0.1 M and 1 M Cr(III) pastes. The source is uncertain. Both the 1 M and 2 M Cr(III) pastes started showing splitting of the asymmetric NO_3^- stretch within 24 hours. The ν(OH) stretching vibrations characteristic of the early calcium chromium complex are also present between 3540 and 3606 cm^{-1}. The 1 M Cr chloride paste shows a single sharp shoulder at 3571 cm^{-1}. The two broad bands at 1420 - 1490 cm^{-1} are due to $\nu(CO_3^{2-})$ stretching vibrations.

Infrared spectra of 60 day old pastes of 0.1 M, 1 M and 2 M Cr(III) pastes are shown in Fig. 4.3.5. The spectra assignments are given in Table 4.3.4. In all the samples, most of the C_3S has reacted completely as evident in the weak intensities of the symmetric stretch (ν_1) of the orthosilicate units between 811 and 854 cm^{-1}. The bands have almost disappeared in the 1 M and 2 M Cr pastes. The intense asymmetric silicate (Si-O-Si) stretch has shifted to 955 cm^{-1} in all the spectra. A broad weak band centred at 1000 cm^{-1} (Table 4.3.1) is also visible in the 1 M and 2 M Cr(III) pastes. This appears as weak shoulders in the 0.1 M and C_3S/water pastes.

Table 4.3.3 FTIR spectra assignments of 24 hour old Cr(III) pastes.

Assignments (cm^{-1})	*Blank*	*0.1 M Cr(III) nitrate*	*1 M Cr(III) nitrate*	*1 M Cr(III) chloride*	*2 M Cr(III) nitrate*
ν_2 (SiO)	452 s, b	452 b	452 b	452 b	467 b
ν_4 (SiO)	510, 522 s, b	510, 522 s,b	510, 522 s,b	510, 522 s,b	512, 528 s,b
ν (CrO)	-	-	-	-	-
ν_4 (CO)	-	-	-	-	-
ν_4 (NO)	-	-	716 w	-	716 sh
δ (Cr-OH)	-	-	-	-	776 w
ν_2 (NO)	-	-	-	-	820 s
ν_1 (SiO)	812 s, b, 836, 847 sh	810 s, b, 833, 845 sh	810 s, b, 833, 845 sh	811 s, b, 833, 846 sh	833 sh, 848 sh,
ν_3 (SiO) + ν (SiOSi)	877 sh, 906 sh, 939 s, 952 sh, 978 sh, 997 sh	874 s, 906 w, 939 s, 951 sh, 978 sh, 997 sh	874 s, 906 w, 939 s, 951 sh, 978 sh, 997 sh	872 s, b, 906 w, 940 sh, 940 sh, 979 sh, 998 sh	877 s, 941 b, 1000 vb
ν_1 (NO)	-	-	1047 w, sh	-	1047 sh
ν_3 (NO)	-	1385 vs 1416 s,b	1354 s,b 1385 sh, 1428w,b, 1445 w,b	-	1351 s, b 1437 s, b
ν_1 (CO)	1425, 1469 s, b	-	-	1386 sh, 1436 s,b 1494 s,b	-
δ (HOH)	1630 s, b	1632 s,b	1634 s,b	1634 s, b	1637 s, b
ν (HOH)	3425 s, b	3431 s,b	3420 s,b	3447s, b	3473 vs, b
ν (OH) - (calcium chromium complex)	-	-	3538 sh,b 3585 sh, b 3604 s,sh	3571 sh,b	3586 sh, w 3606 sh, w
ν (OH) - (CH)	3644 sp	3644 sp	-		-

Table 4.3.4 FTIR spectra assignments of 60 hour old Cr(III) pastes

Assignments (cm^{-1})	*Blank*	*0.1 M Cr(III) chloride*	*0.1 M Cr(III) nitrate*	*1 M Cr(III) nitrate*	*1 M Cr(III) chloride*	*2 M Cr(III) nitrate*
ν_2 (SiO)						458 s,b
ν_4 (SiO)	510 s,b	509 s, b	509 s, b	525 sh	525 sh	-
ν (CrO)	-		-	486 w,b	490 w, b	-
**	-	-	-	-	-	530 s, b
ν_4 (CO)	713 w	/13 w	713 w	-	-	-
ν_4 (NO)	-		-	716 w	-	717 s
δ (Cr-OH)	-	-	-	-	-	773 s, b
ν_2 (NO)	-	-	-	-	-	823 sh
ν_1 (SiO)	813 sh, b 833 sh, 847 sh	813 sh, b 834 sh, 847 sh	813 sh, b 833 sh, 847 sh	810 s, b, 833, 845 sh	811 s, b, 833, 846 sh	835 sp, 848 sh,
ν_2 (CO)	872 s	872 s	872 s	864 sh, b	867 sh, b	874 b
ν_3 (SiO) + ν (SiOSi)	907 sh, 960 vs, b	906 w, 958 vs, b	906 w, 958 vs, b	971 s, b	964 s, b 998 sh	918 sh 995 s, b
ν_1 (NO)	-	-	-	1047 w, sh	-	1048 sh
ν_3 (NO)	-	-	1352 w, sh 1385 w, sh	1362 sh 1386 sp,	-	1358 vs 1421, 1446 s, b
ν_1 (CO)	1427, 1472 b	1424 vs, 1479 s, b	1424 vs, 1479 s, b	1425 s, 1488 s, b	1419 s, b	-
δ (HOH)	1636 s, b	1641 s, b	1641 s, b	1634 s,b	1634 s, b	1633 s, b
ν (HOH)	3436 vs, b	3443 vs, b	3443 vs, b	3470 vs,b	3452 vs, b	3546 vs, b
ν (OH) - (Ca - Cr complex)	-	-	-	3567 sh 3587 sh 3607 sh	3571 sh,b	3588 sp 3606 sp
ν (OH) - (CH)	3644 sp	3644 sp	3644 sp	3644 sp	3644 sp	3644 sp

This peak may be attributed to the polymeric silicate units in C-S-H that forms in the late stages of hydration reaction. Going by these assignments, Cr additions seem to promote formation of highly condensed silicate species as verified by NMR studies discussed in

Section 4.4. The strong peak at 872 cm^{-1} and 1420 - 1490 cm^{-1}, are CO_3^{2-} vibrations in $CaCO_3$. With the exception of the 2 M Cr(III) paste, the broad stretching vibrations of lattice water is centred around 3500 cm^{-1} in all the 60 day old samples. The bending vibration is at 1638 cm^{-1}. The CH band at 3644 cm^{-1} is intense in all the samples but very small in the 2 M Cr(III) paste. The OH peaks due to the calcium chromium complexes are obvious in the 2 M Cr paste but barely discernible in the 1 M Cr nitrate paste.

The following assertions can be made from the infrared absorption results of Cr(III) pastes discussed above:

- Increasing chromium concentrations promotes formation of polymeric silicate units other than the dimer in C-S-H.
- Formation of CH is inhibited during the early stages of hydration. The inhibition increases with increasing chromium concentrations.
- The calcium chromium complexes are calcium chromium hydroxide nitrate hydrate complexes with $[Cr(OH)_6]^{3-}$ in octahedral positions.
- The late calcium chromium hydroxide nitrate hydrate has a higher symmetry and is more stable under normal hydration conditions than the early calcium chromium hydroxide nitrate hydrate.
- The onset of decomposition of early calcium chromium hydroxide nitrate hydrate to formation of late calcium chromium hydroxide nitrate hydrate occurs after 72 hours (within the time frame of experiments conducted).

4.3.2 Chromium (VI) Pastes

Fig. 4.3.6 shows the infrared spectra of $CaCrO_4.2H_2O$ and $Ca_2CrO_5.3H_2O$, the two calcium chromates formed in Cr(VI) doped C_3S. The spectra contains two main absorption groups: Vibrational modes due to chromate ion (CrO_4^{2-}) and water of hydration.

When tetrahedra CrO_4^{2-} retains its T_d symmetry in a compound, four vibrational modes are present (Nakamoto [1986]);

- non degenerate ν_1 symmetric stretching at 846 cm^{-1} (Raman active)
- doubly degenerate ν_2 in plane bending at 349 cm^{-1} (Raman active)
- triply degenerate ν_3 asymmetric stretching at 890 cm^{-1} (Infrared and Raman active)

- triply degenerate ν_4 out of plane bending at 349 cm^{-1} (Infrared Raman active)

However, the presence of CrO_4^{2-} in a crystalline host might lift the degeneracy due to distortion of the tetrahedra. This also causes ν_1 and ν_2 vibrations to become active in infrared, since the symmetry is lowered. In the case of $CaCrO_4.2H_2O$, (S.G. P21/* (Powder Diffraction File [37-1367])) the point symmetry is lowered to C_{2v}. A partial assignment of both spectra are shown in Table 4.3.5. The strong band at 882 cm^{-1} in $CaCrO_4.2H_2O$ was assigned to the ν_3 asymmetric stretching of the tetrahedral CrO_4^{2-} ion. There are weak shoulder bands around the 882 cm^{-1} but these are unresolved in the spectra. The peaks at 683 cm^{-1} and 572 cm^{-1} were not assigned. Sufficient distortion of the CrO_4^{2-} ion could also give dichromate-like spectra (Gadsen [1975]), with Cr-O-Cr stretching vibrations between 600 cm^{-1} and 750 cm^{-1}. The spectrum of $Ca_2CrO_5.3H_2O$ shows considerable split of the triply degenerate $\nu_3(CrO_4^{2-})$ asymmetric stretching vibration at 870, 895 and 916 cm^{-1}. The band at 837 cm^{-1} was assigned to the ν_1 symmetric stretch. The broad bands at 563, 615, 673 and 701 cm^{-1} are typical of dichromate spectra. However, the basic nature of $Ca_2CrO_5.3H_2O$ (saturated solution pH ~ 11) suggests the absence of dichromates in the compound. It is possible that strong Ca-O-Cr bonding exists in $Ca_2CrO_5.3H_2O$ similar to Cr-O-Cr linkages in dichromates. In the absence of structural data on $Ca_2CrO_5.3H_2O$, assignment of these bands is purely speculative.

In the $CaCrO_4.2H_2O$ spectrum, the δ(HOH) bending vibration is located at 1658 cm^{-1} and a broad ν(HOH) stretching vibration at 3439 cm^{-1}. The δ(HOH) in $Ca_2CrO_5.3H_2O$ is at a slightly lower wavenumber (1637 cm^{-1}) and the ν(HOH) appeared as a doublet at 3528 and 3551 cm^{-1}.

4.3.2.1 Effect of Cr(VI) Ion on Hydration of C_3S

Fig. 4.3.7 and Table 4.3.6 show the infrared spectra of 2 M Cr(VI) pastes hydrated for 5 mins, 6 hrs, 24 hrs, 72 hrs and 60 days. Unlike the case of Cr(III) where the early calcium chromium complex forms continuously with increasing dissolution of C_3S, $CaCrO_4.2H_2O$ formed within the first 5 minutes. The strong CrO_4^{2-} asymmetric stretch (ν_3) at 882 cm^{-1} overlaps with the SiO_4^{4-} stretching vibrations. This phase could not be found in all the other spectra. Vibrational modes due to $Ca_2CrO_5.3H_2O$ appeared just after 6 hours

and remained throughout the duration of the experiments. The intensities of CrO_4^{2-} and (HOH) bands remain almost constant throughout the hydration period. The ν(OH) of CH at 3644 cm^{-1} appeared in the 72 hour sample and increased with age. The broad band centred at 975 cm^{-1} in the 6 hour sample also intensified with age and was assigned to ν(SiOSi) asymmetric stretching vibration in C-S-H.

Table 4.3.5 FTIR spectra assignments of $CaCrO_4.2H_2O$ and $Ca_2CrO_5.3H_2O$

Spectra assignments (cm^{-1})	*$CaCrO_4.2H_2O$*	*$Ca_2CrO_5.3H_2O$*
**	573, 682 s, b	563
		615
		673
		701 s, b
ν_1 (CrO)	-	837 sp
ν_3 (CrO)	882 s	870 s
		895 s
		916 s
**	1440 b	1112
		1168 w, b
δ (HOH)	1658 s	1637 s
ν (HOH)	3437 s, b	3528s
		3551 s

4.3.2.2 Effect of Cr(VI) Concentrations on C_3S Hydration

Shown in Fig. 4.3.8 and Table 4.3.7 are the spectra of 1 M and 2 M Cr(VI) pastes hydrated for 24 hours. The spectrum of the blank paste was included for comparison. Apart from the ν(CrO_4^{2-}) and ν(HOH) stretching vibrations, the spectrum of 1 M Cr(VI) paste is identical to that of the blank. The appearance of a broad Si-O-Si asymmetric stretch at 975 cm^{-1} in the 2 M Cr(VI) paste (not present in the standard C_3S/H_2O paste) suggests that increasing Cr(VI) accelerated condensation of silicate units in C-S-H, during the early ages. The reduced intensity of ν(OH) of CH at 3644 cm^{-1} in the 1 M Cr(VI) paste and its absence in the 2 M Cr(VI) paste, also confirms that the rate of CH formation is dependent on the concentration of the Cr(VI) ions.

Table 4.3.6 FTIR spectra assignments of 2 M Cr(VI) pastes

Assignments (cm^{-1})	*5 minute old*	*6 hour old*	*24 hour old*	*72 hour old*	*60 day old*
ν_2 (SiO)	452 s, b	452 b	452 b	452 b	452 b
ν_4 (SiO)	522 vs	522 vs	522 vs	522 s	522 w (obtained from F-IR spectra)
**	-	673 s	673 s	673 s	673 s
ν_1 (SiO)	816 sh	816 sh	816 sh	816 sh	816 sh
ν_3 (CrO)	882 s, b	870 s	870 s	870 s	870 s
		895 s	895 s	895 s	895 s
ν_3 (SiO)	911 b	911 b	911 b	911 b	911 b
ν (SiOSi)	-	975 sh,w	975 b	975 s, b	975 s, b
**	1419 s,b	1419 s,b	1419 s,b	1419 s,b	1419 s,b
	1450 s, b	1450 s, b	1450 s, b	1450 s, b	1450 s, b
δ (HOH)	1658 s	1637 w	1637 w	1637 w	1637 w
ν (HOH)	3437 s, b	3528 s	3528 s	3528 s	3528 s
		3551 sh	3551 sh	3551 sh	3551 sh
ν (OH) - (CH)	-	-	-	3644 sp	3644 sp

In the 60 day old 0.1 M Cr(VI) paste shown in Fig. 4.3.9 and Table 4.3.8 no $Ca_2CrO_5.3H_2O$ vibrations were detected. The concentration of $Ca_2CrO_5.3H_2O$ in this paste was probably too small to be detected. In the 1 M Cr(VI) paste the doublet ν(HOH) stretching vibrations in $Ca_2CrO_5.3H_2O$ had been swamped by ν(HOH) stretching vibrations in C-S-H at 3433 cm^{-1} making them barely visible. The intensities of the CH peak at 3644 cm^{-1} also decreased with concentration as was the case at 24 hours.

Pertinent conclusions that may be drawn from the infrared spectra of Cr(VI) doped C_3S are:

- increasing Cr(VI) concentrations increases the condensation rate of silicates in C_3S.
- formation of CH begins after all the chromium has been used up to form $Ca_2CrO_5.3H_2O$.

Table 4.3.7 FTIR spectra assignments of 24 hour old Cr(VI) pastes

Assignments (cm^{-1})	*Blank*	*1 M Cr(VI)*	*2 M Cr(VI)*
ν_2(SiO)	452 s, b	452s, b	452s, b
ν_4 (SiO)	510, 522 s, b	510, 522 s,b	522 s,b
ν_1 (SiO)	812 s, b, 836, 847 sh	810 s, b, 833, 845 sh	816 sh
ν_3(CrO)	-	870 w	870 s
		895 w	895 s
ν_3 (SiO) + ν (SiOSi)	877 sh, 906 sh, 939 s, 952 sh, 978 sh, 997 sh	874 s, 906 w, 939 s, 951 sh, 978 sh	911 b 984 b
ν_1 (CO)	1425, 1469 s, b	1416, 1426s, b	1419, 1450 s, b
δ (HOH)	1630 s, b	1632 s,b	1637 s, b
ν (HOH)	3425 s, b	3440 s,b	3447s, b
		3528 w	3528 s
		3551 w	3551 sh
ν (OH) - (CH)	3644 sp	3643 sp	-

Table 4.3.8 FTIR spectra assignments of 60 day old Cr(VI) pastes

Assignments (cm^{-1})	*Blank*	*0.1 M Cr(VI)*	*1 M Cr(VI)*	*2 M Cr(VI)*
ν_2 (SiO)	452 vw	452 vw	452 vw	452 b
ν_4 (SiO)	510 s, b	510, 522 s,b	522 s,b	522 w
ν_1 (SiO)	813 sh, b, 833, 847 sh	811 sh, b, 833, 845 sh	816 sh	816 sh
ν_3(CrO)	-	-	870 w	870 s
			895 w	895 s
ν_2(CO)	872 s	872 s	873 s	
ν_3 (SiO) + ν (SiOSi)	907 sh, 960 vs, b	907 sh, , 957 vs, b	911 b 958 vs, b	911 b 975 s, b
ν_1 (CO)	1427, 1472 s, b	1419, 1450s, b	1429, 1450 s, b	1419, 1450 s, b
δ (HOH)	1636 s, b	1635 s,b	1636 s, b	1637 w
ν (HOH)	3436 vs, b	3432 s,b	3433 s, b	3433 sh, b
			3528 w	3528 s
			3551 w	3551 s, sh
ν (OH) - (CH)	3644 sp	3643 sp	3643 sp	3644 sp

4.4 Nuclear Magnetic Resonance Spectroscopy

It was found that a very long relaxation delay (up to 2 hours) was necessary to obtain good signals from the pure anhydrous C_3S. In the case of hydrated pastes containing C-S-H, however, a relaxation delay of 10 seconds gave satisfactory signals with good signal to noise ratio. Since we are primarily interested in the silicate anion structure in C-S-H, a delay time of 10 seconds was used in all the experiments. Because the ^{29}Si nuclei in monomeric SiO_4^{4-} in C_3S do not have sufficient time to relax, the Q_o signals between -69 and -74 ppm (representing monomeric SiO_4^{4-}) were not observed in all the spectra.

4.4.1 C-S-H Anion Structure of the Blank, 2 M Cr(III) and Cr(VI) Pastes.

Shown in Table 4.4.1 and Fig. 4.4.1 are the ^{29}Si NMR spectra of 2 M Cr(III) and Cr(VI) pastes. The end groups in silicate units (Q_1) containing dimeric silicate units (Si-O-Si linkages) gave a signal at about -79 ppm and middle units (Q_2) which contain polymeric silicate units especially pentamers and octamers, gave a signal at -85 ppm. These are typical of silicate units in tetrahedral coordination. The chemical shifts of octahedral silicates are usually observed to be between -200 and -250 ppm (Grimmer and Van Lampe [1986]). None was found in any of the samples investigated. Based on the observed chemical shifts which are similar for the blank, Cr(III) and Cr(VI) at all ages, it appears that very little variation exists in the silicate anion environment in the C-S-H.

However, there is a substantial difference in the linewidths of the Q_1 units in the Cr(III) pastes compared to those in the blank and Cr(VI) pastes (Table 4.4.1). The Q_2 units have comparable width in all the spectra. During the early hydration period, saturated signals from the Q_o units may be partly responsible for the line broadening in the 72 hour old 2 M Cr(III) and Cr(VI) pastes. After 60 days, virtually all the C_3S has reacted in the 2 M Cr(III) pastes and should therefore contribute very little to the Q_1 signal. Also more C_3S is consumed in the Cr(III) pastes at a given time than in either the blank or Cr(VI) pastes and their linewidths are comparatively narrower. The paramagnetic Cr^{3+} ion is thus responsible for this localized line broadening. In the Cr(III) pastes the Q_1 line broadening (given by the Full Width at Half Maximum (FWHM)) is seen to decrease with age from 6.8 ppm at 72 hours to 3.9 ppm in the fully hydrated 2.75 M Cr(III) paste. In the 60 day old 2 M Cr(VI) paste, the linewidth has reduced to 3.4 ppm from 4.9 ppm of the 72 hour old Cr(VI) sample. This is comparable to the Q_1 linewidth of the blank paste (3.0 ppm). Variations in the Q_2 signals are less pronounced in all the spectra.

As obtained from XRD and FTIR studies, the amount of C-S-H formed increases with age, as does the concentration of the Ca - Cr complexes. It is thus unlikely that Cr^{3+} in the Ca-Cr complexes, even if physically mixed on a nanoscale with the C-S-H, could be responsible for this selective broadening. An obvious deduction is the unaveraged dipolar interactions between the ^{29}Si and ^{53}Cr nuclei. Because ^{53}Cr is a quadrupolar nucleus this will not be averaged to zero by magic angle spinning (MAS). If this is the case, the line broadening should decrease with a decrease in the number of Cr nuclei in the first coordination shell of the Q_1 units. Even though the broadening is less pronounced in the Q_2 units that should have a higher local Si/Cr ratio (assuming Cr is present) and the amounts of Q_1 and Q_2 increase with age, it is improbable that Cr will be located in the first coordination shell. This will mean the formation of Si-O-Cr bonds which should give rise to distinct chemical shifts. No direct evidence of this could be seen from the spectra, however, the broad Q_1 peak could be a collection of many peaks depicting different silicate anion environments. Another indication that the broadness is induced by Cr^{3+} ions is the relatively strong spinning side bands in the 2 M Cr(III) pastes symmetrical around Q_1 and Q_2. These indicate greater chemical shift anisotropy and an attendant increased asymmetry in the C-S-H.

The broadening may thus be caused by a less direct mechanism than direct spin - spin interaction between the nuclei. A plausible explanation is that the ^{29}Si in Q_1 units are sensitive to second and further nearest neighbor interactions.

These results indicate that some Cr is randomly chemically bonded in the early dimeric C-S-H. There is however no evidence that Cr is replacing either Si or Ca. The mere fact that tetrahedrally coordinated ($Cr^{(III)}O_4$) is rarely formed shows that replacement of tetrahedral SiO_4 by ($Cr^{(III)}O_4$) is highly improbable. If this is the case, tetrahedral $Cr^{(VI)}O_4$ exclusively formed in Cr(VI) paste is more likely to replace Si. This has not been seen in these experiments.

4.5.2 Rate of Formation of Dimeric and Polymeric C-S-H

The results of trapezoidal integration of the chemical shifts are presented in Table 4.4.2. This was achieved by fitting a Voigt equation to the overlapping Q_1 and Q_2 peaks. This gives a better approximation of the area than a Lorenztial fit. The rate of formation of Q_1 and Q_2 follow the established trend in normal C_3S or Portland cement hydration. Q_1 forms first and later Q_2, both forming continuously throughout the hydration reaction period. The production of Q_1 and Q_2 units proceed at a constant rate after about 30 days (Clayden et al. [1984]). After about 180 days, when most of the C_3S has reacted, the

Q_2/Q_1 ratio obtained by several investigators is about 0.35 (Clayden et al. [1984], Taylor 1990]). This is similar to the Q_2/Q_1 ratio of 0.37 obtained in the fully hydrated blank paste used as standard in these experiments. In the 2.75 M Cr(III) fully hydrated exposed paste, the Q_2/Q_1 ratio (0.90) is higher than in either the blank or Cr(VI) paste (Table 4.4.2). This is more apparent when the amplitudes of Q_1 and Q_2 are compared in Fig. 4.4.1. The line broadening in the Q_1 units increases the area under Q_1. This effect is more noticeable in the 72 hour and 60 day Cr(III) and Cr(VI) pastes. The relative amplitudes of Q_2 to Q_1 is higher in Cr(III) than in Cr(VI), but the Q_2/Q_1 of the integrated areas are lower. An interesting observation is the Q_2/Q_1 ratio of 60 day old 2 M Cr(VI) paste (~0.5). It is apparent that more Q_2 units are also formed compared to the blank paste, reinforcing the previous conclusion from infrared analysis that condensation of the polymeric C-S-H is also increased, although not as distinct as the effect of Cr(III) pastes.

Table 4.4.1 ^{29}Si chemical shift data of partially and fully hydrated chromium doped tricalcium silicate

Sample	*Q_1 (ppm)*		*Q_2 (ppm)*	
	chemical shift	*linewidth*	*chemical shift*	*linewidth*
Blank - 14 months	-78.9	3.0	-85.0	2.6
2.75 M Cr(III) -14 months	-78.8	3.9	-85.0	3.0
2 M Cr(III) - 60 days	-78.9	5.6	-84.6	3.8
2 M Cr(III) -72 hours	-79.3	6.8	-84.2	3.2
2 M Cr(VI) - 60 days	-79.0	3.4	-85.1	3.2
2 M Cr(VI) -72 hours	-79.3	4.9	-84.8	2.4

Table 4.4.2 Integrated intensity ratios (Q_2/Q_1) of partially and fully hydrated chromium doped tricalcium silicate

Sample	Q_2/Q_1
Blank - 14 months	0.37
2.75 M Cr(III) -14 months (exposed)	0.90
2 M Cr(III) - 60 days	0.57
2 M Cr(III) -72 hours	0.30
2 M Cr(VI) - 60 days	0.51
2 M Cr(VI) -72 hours	0.23

4.5 Leaching Studies

The leaching studies carried out were not intended to primarily investigate the mechanisms of metal ion mobility in standard leaching solutions. Rather, they were aimed at confirming the similar leaching characteristics that exist between the much investigated ordinary Portland cement and tricalcium silicate.

Results of AAS analysis of leachates are shown in Table 4.5.1. These represent the approximate leachate concentrations after 18 hours of the acetic acid leaching procedure (TCLP). No Si was detected in the leachate in any of the samples (detection limit ~ 2 ppm). Similar to the established notion, Cr(III) was found to be immobile under the acetic acid leaching procedure, whereas Cr(VI) was very mobile. In the blank pastes, the high pH and Ca contents of the leachates are primarily due to the dissolution of CH and some CaO units in the C-S-H. This is evident from the reduced CH peaks in the x-ray powder diffraction patterns shown in Fig. 4.5.1 (the blank paste still has some CH with a strong (001) preferred orientation). In the leached 2.75 M Cr(III) exposed paste, in addition to dissolution of CH, most of the diffraction intensities characterizing the late Ca-Cr complex have disappeared. Coupled with the high Ca content of the leachate (higher than the Ca content in the blank leachate which has more CH), Ca ions in the complex were leached out leaving behind an amorphous chromium complex. Since an alkaline leachate solution (pH ~ 11.9) is in contact with the solid throughout the leaching experiment, insoluble chromium oxide or hydroxide complexes should be responsible for the continued immobilization. It is also possible that acetic acid acts as complexant for chromium. Identical results were obtained for the sealed 2.75 M Cr(III) paste.

Cr(VI) paste (2.75 M) presented an interesting case. The Ca/Cr mole ratio in the leachate is ~ 4.6 which is higher than the Ca/Cr ratio in $Ca_2CrO_5.3H_2O$. This shows that some of the CaO units in $Ca_2CrO_5.3H_2O$ were possibly solubilized. Moreover, the powder diffraction pattern of 2.75 M Cr(VI) paste shows only unreacted C_3S, part of which reacts with the leachant, causing more Ca ions to be present in solution. To verify whether $Ca_2CrO_5.3H_2O$ dissolved congruently or through selective dissolution of CaO and CrO_4 units, pure $Ca_2CrO_5.3H_2O$ was leached under the same conditions. The leaching results are shown in Table 4.5.1. The Ca/Cr mole ratio is ~ 3.3 suggesting an incongruent dissolution of the metal ions. The leachate pH of 12.3, measured after 18 hours is similar to the pH of the pore solution in hydrating C_3S paste. It is conceivable that dissolution of $Ca_2CrO_5.3H_2O$ is congruent when it first comes in contact with the acetic acid solution. Since the leachant does not have a buffer, increasing pH would result in an early saturation of $Ca_2CrO_5.3H_2O$ in the leachate. From thence, selective dissolution of the metal ions

might ensue. In addition to the mobility of Cr ions in $Ca_2CrO_5.3H_2O$, the highly porous structure of Cr(VI) pastes serves to increase the exposure of Cr^{6+} ions to rapid leaching.

Table 4.5.1 AAS leachate analyses of standard and Cr - doped pastes subjected to TCLP leaching.

Sample	*Ca(ppm)*	*Cr(ppm)*	*Si (ppm)*	*pH*
2.75MCN3-14M exposed	5950	0.2	< 2	12.1
2.75MCN-14M sealed	5560	0.3	<2	11.7
Early Ca - Cr complex	7390	0.2	< 2	8.8
2.75M C6- 4M	5600	1574	<2	12.6
$Ca_2CrO_5.3H_2O$	6320	2440	<2	12.3
Bl-14M	3480	<0.2	<2	12.5

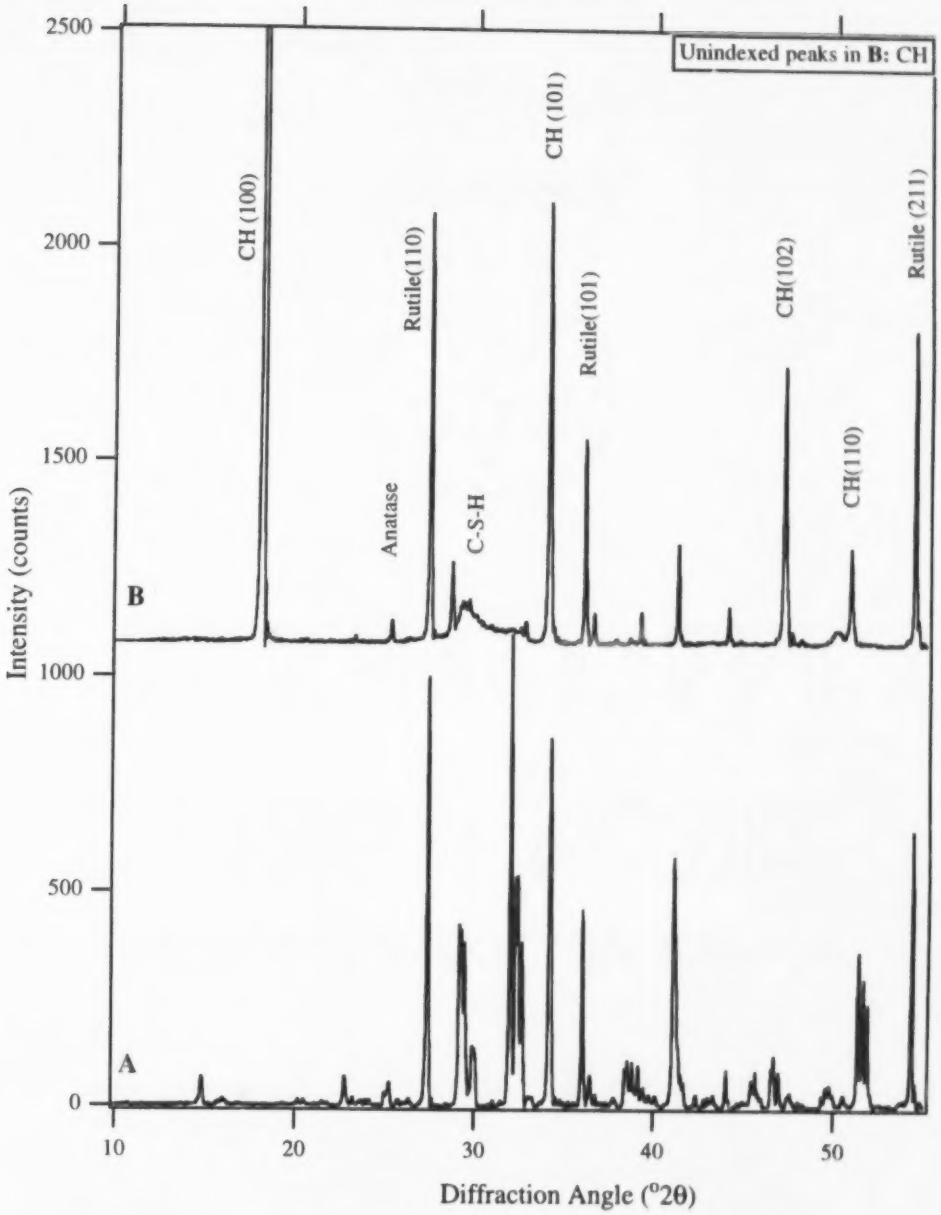

Fig. 4.1.1 XRD patterns of (A) anydrous C_3S and (B) 14 month old blank (C_3S/H_2O) paste. Anatase was an impurity in Rutile.

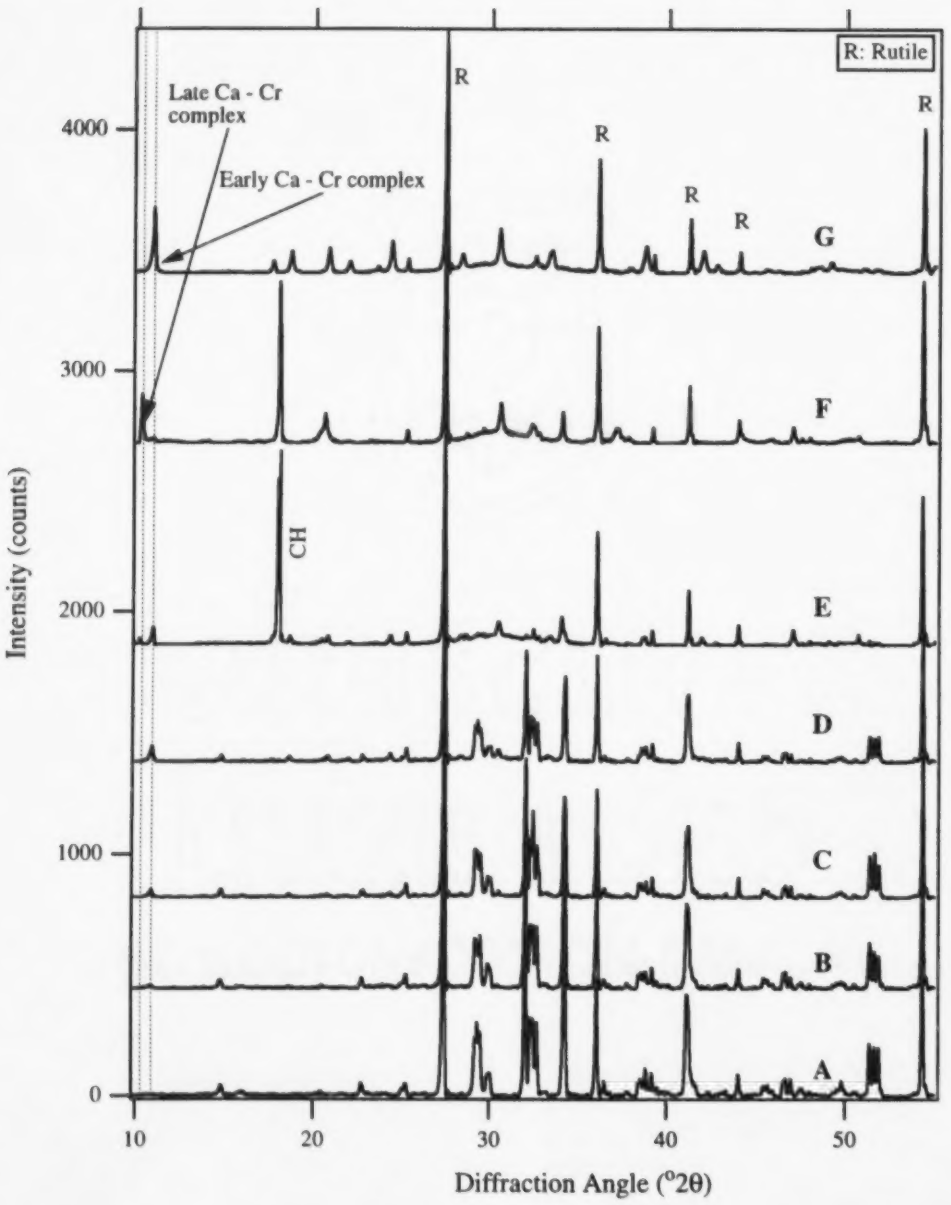

Fig. 4.1.2 XRD patterns of 2 M Cr(III) pastes hydrated for; (A) 5 minutes, (B) 6 hours, (C) 24 hours, (D) 72 hours, (E) 60 days, (F) 2.75 M Cr(III) - 14 months exposed and (G) 2.75 M Cr(III) - 14 months - sealed.

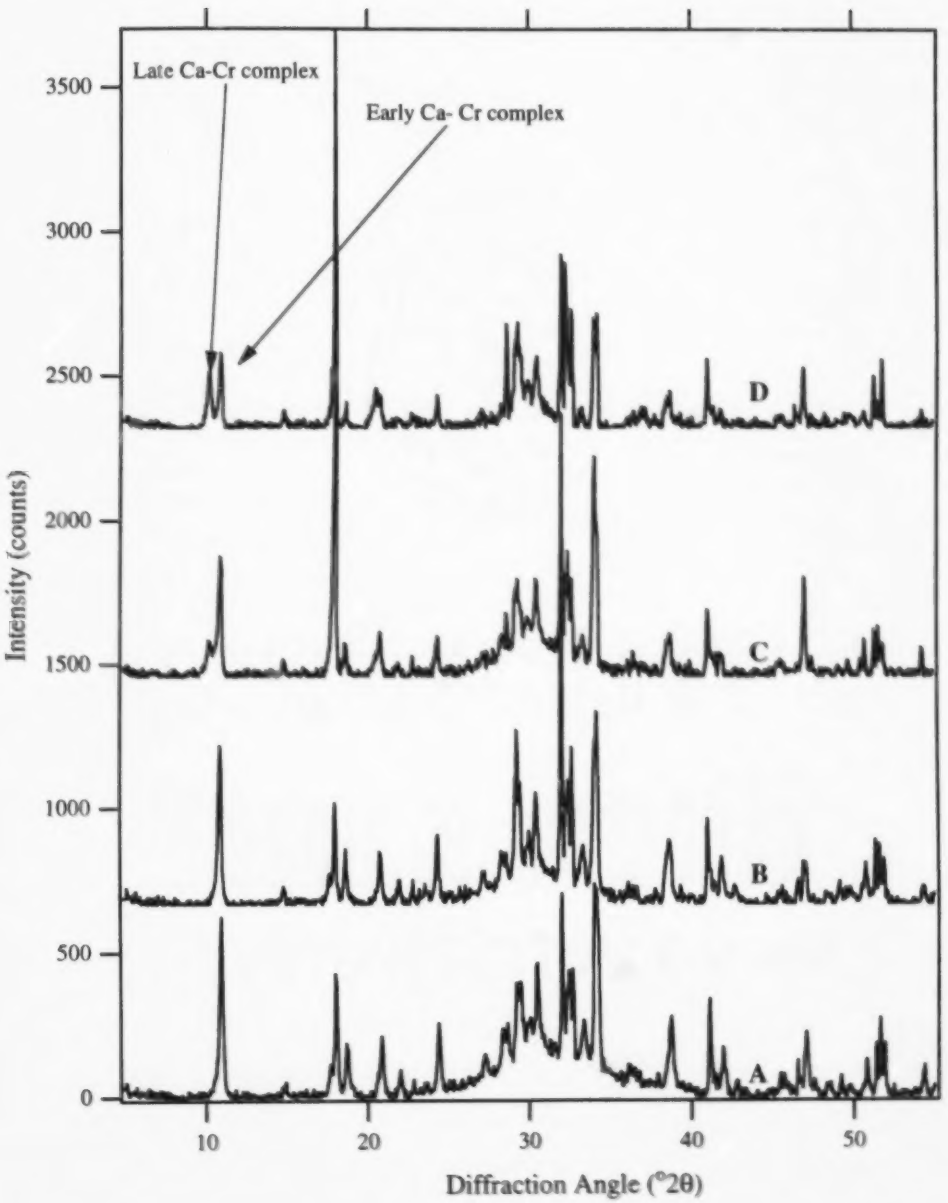

Fig. 4.1.3 XRD patterns of 15 day old 2 M Cr(III) pastes: (A) compacted-sealed, (B) uncompacted-sealed, (C) compacted-exposed and (D) uncompacted-exposed.

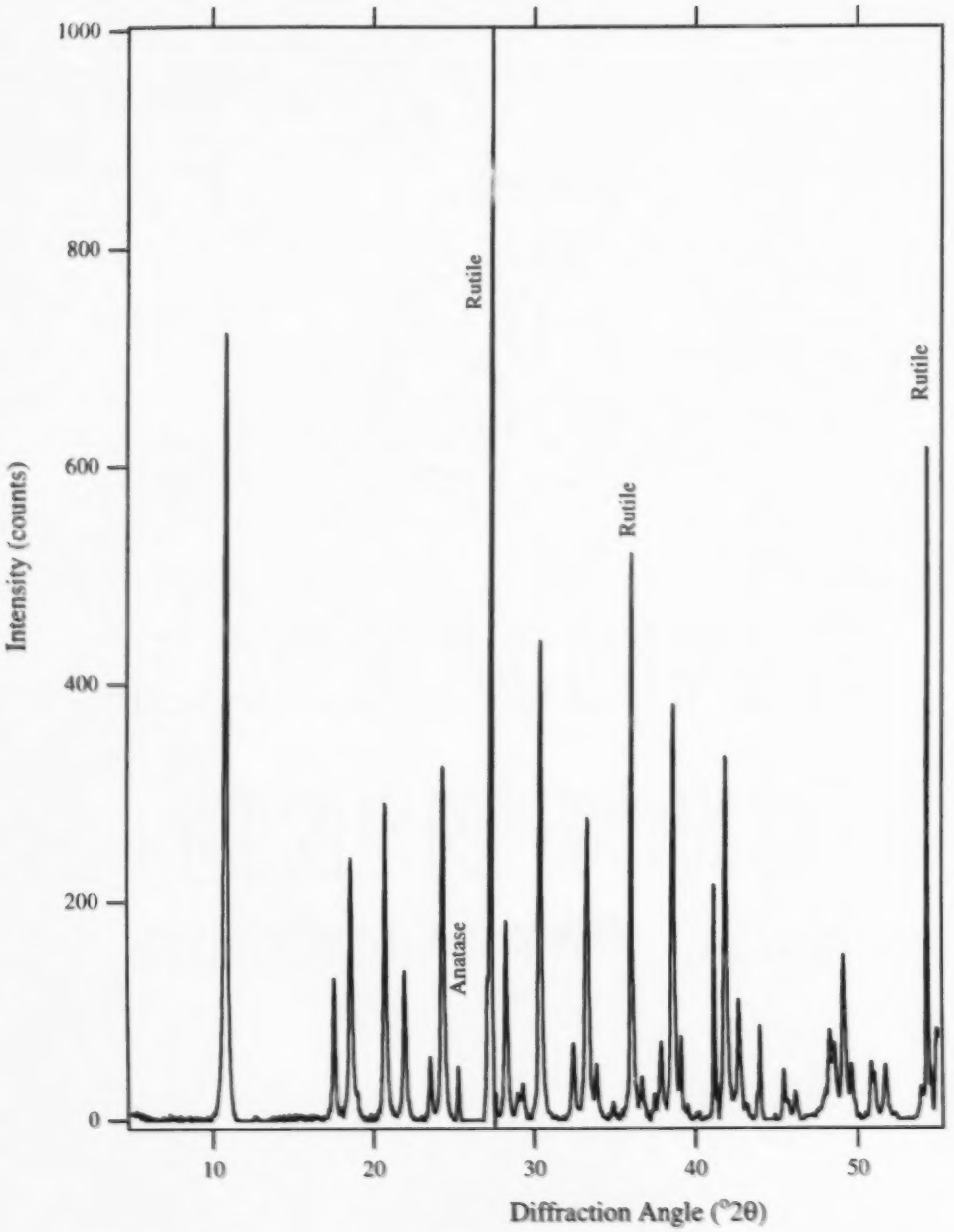

Fig. 4.1.4 XRD pattern of synthesized compound believed to be early Ca - Cr complex.

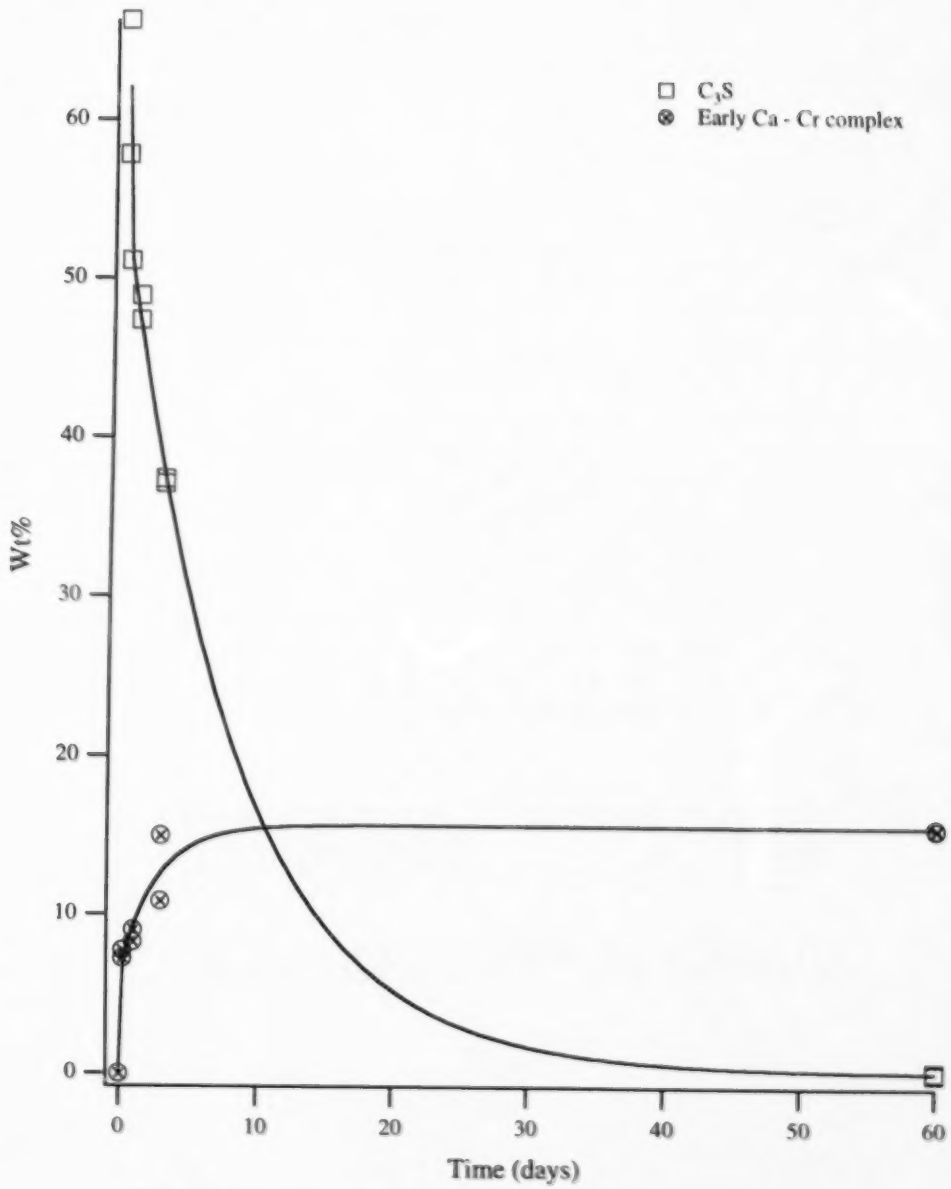

Fig. 4.1.5 Rate of reaction of C_3S and formation of early Ca - Cr complex.

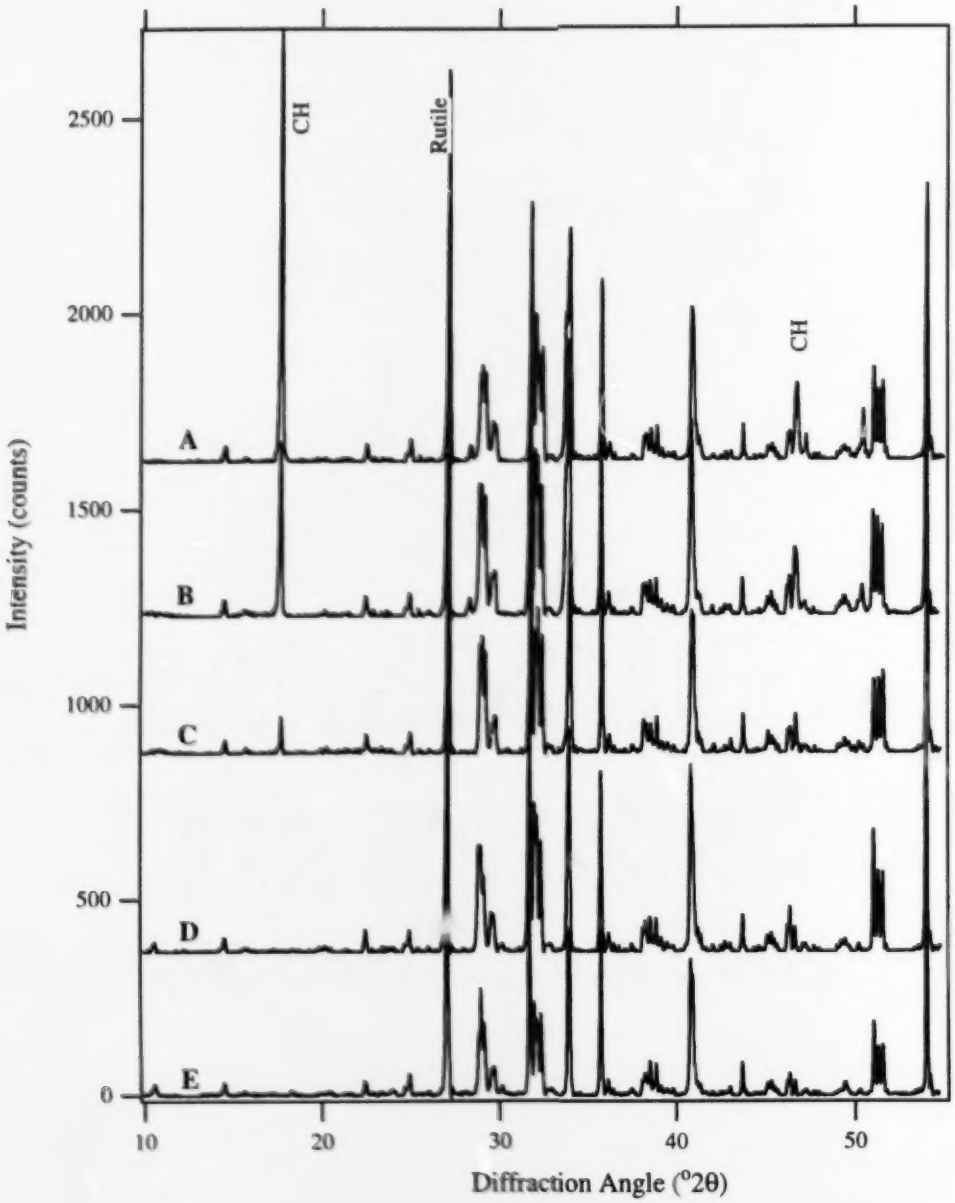

Fig. 4.1.6 XRD patterns of 24 hour old Cr(III) pastes; (A) 0.1 M Cr chloride (B) 0.1 M Cr nitrate, (C) 1 M Cr nitrate, (D) 1 M Cr chloride and (E) 2 M Cr nitrate.

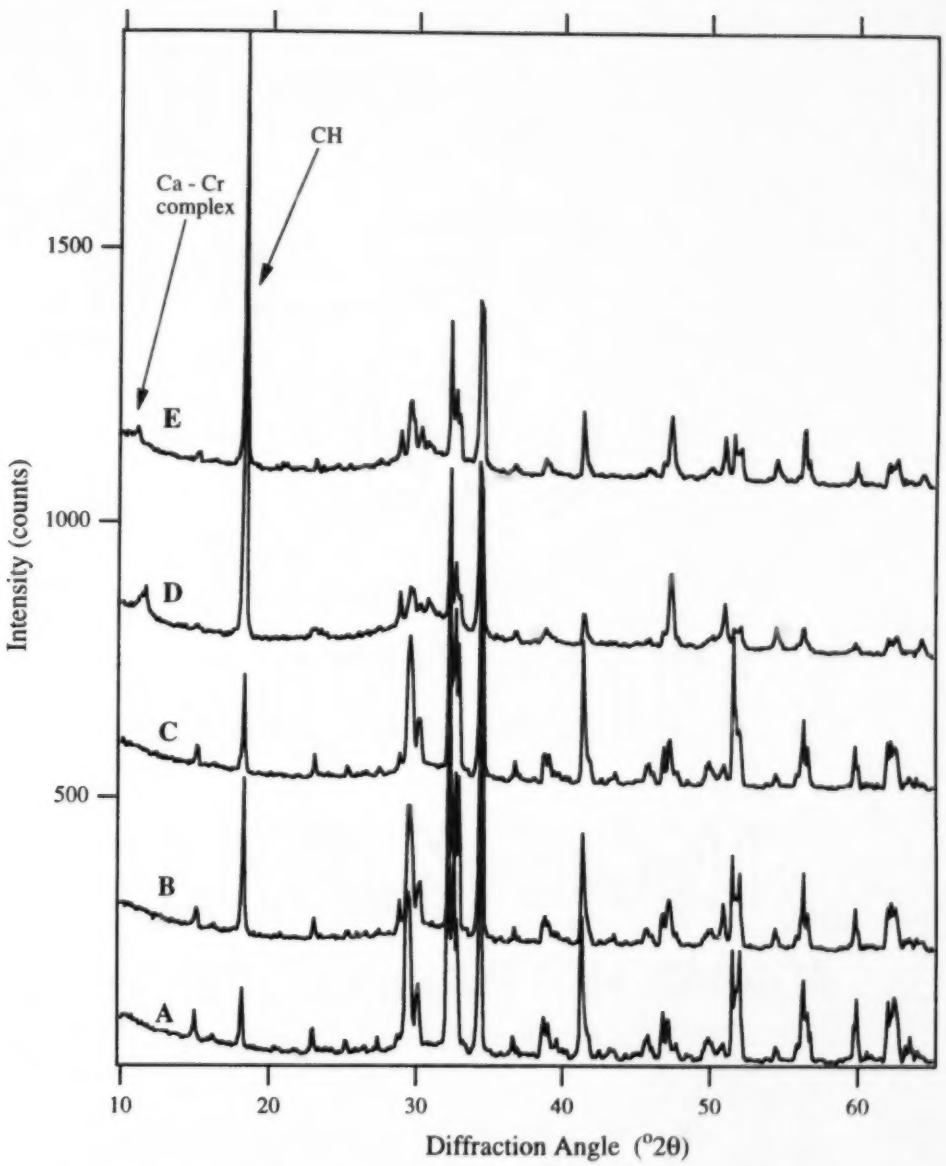

Fig. 4.1.7 XRD patterns of 60 day old blank and Cr(III) pastes; (A) Blank, (B) 0.1 M Cr chloride, (C) 0.1 M Cr nitrate, (D) 1 M Cr chloride and (E) 1 M Cr nitrate.

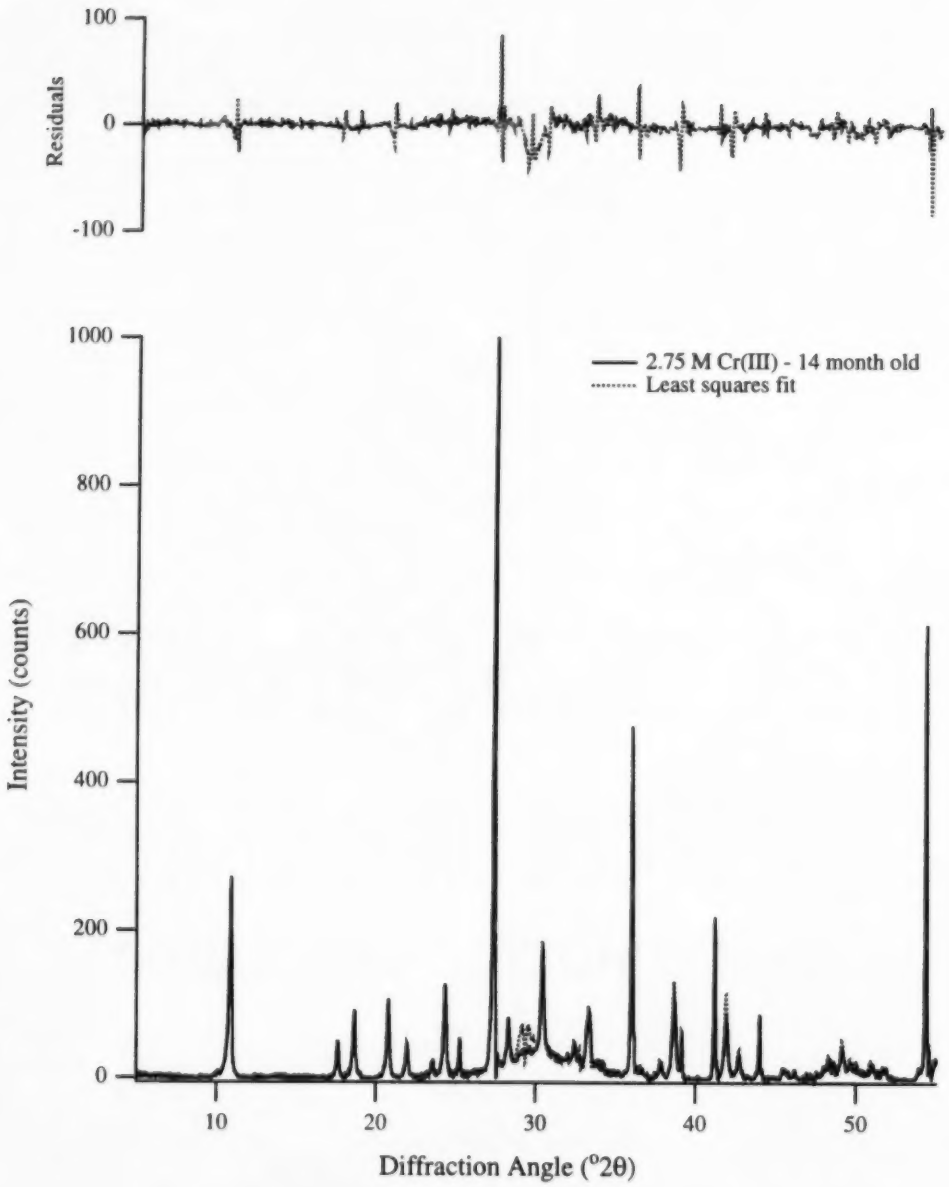

Fig. 4.1.8 QXRD analysis of 14 month old 2.75 M Cr(III) paste.

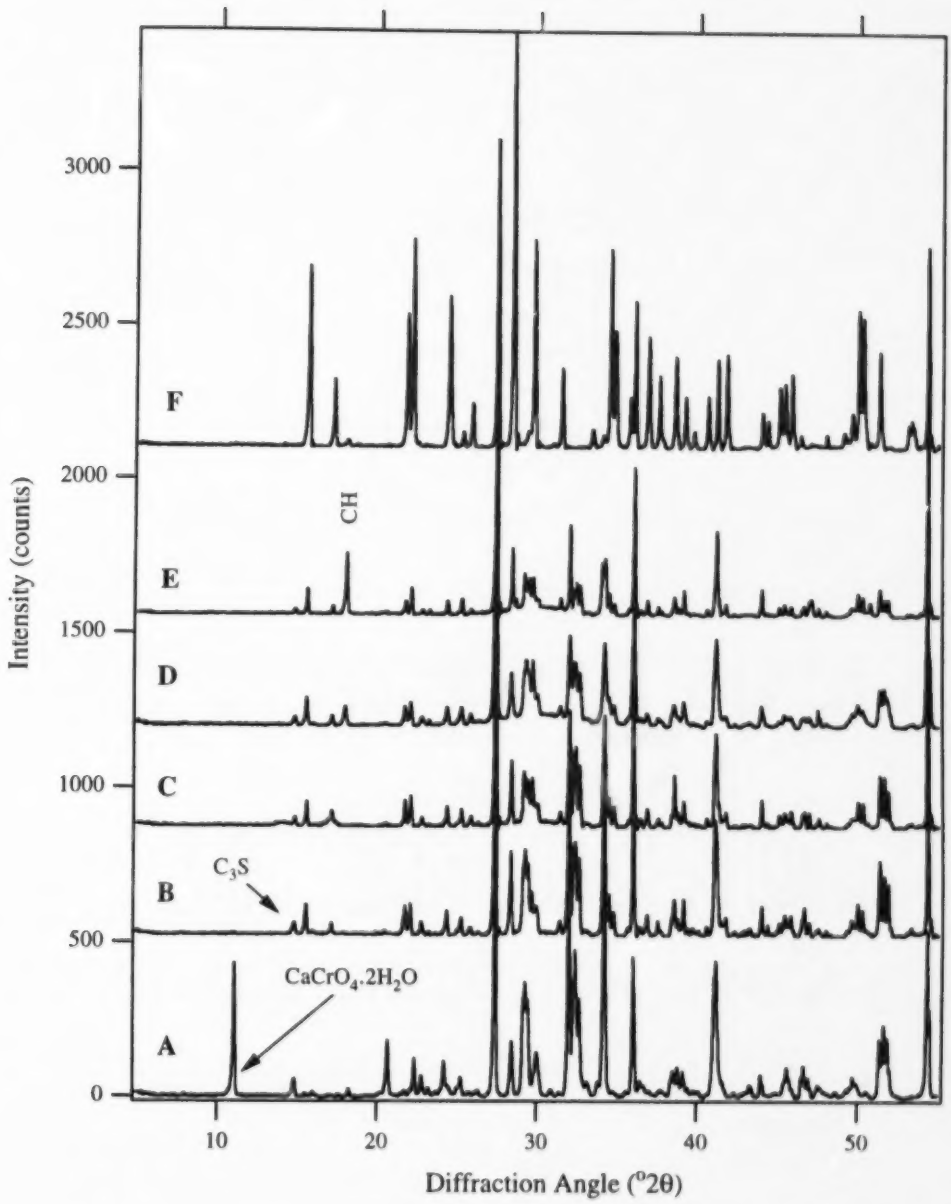

Fig. 4.1.9 XRD patterns of 2 M Cr(VI) pastes hydrated for varying times; (A) 5 minutes, (B) 6 hours, (C) 24 hours, (D) 72 hours, (E) 60 days and (F) standard $Ca_2CrO_5.3H_2O$.

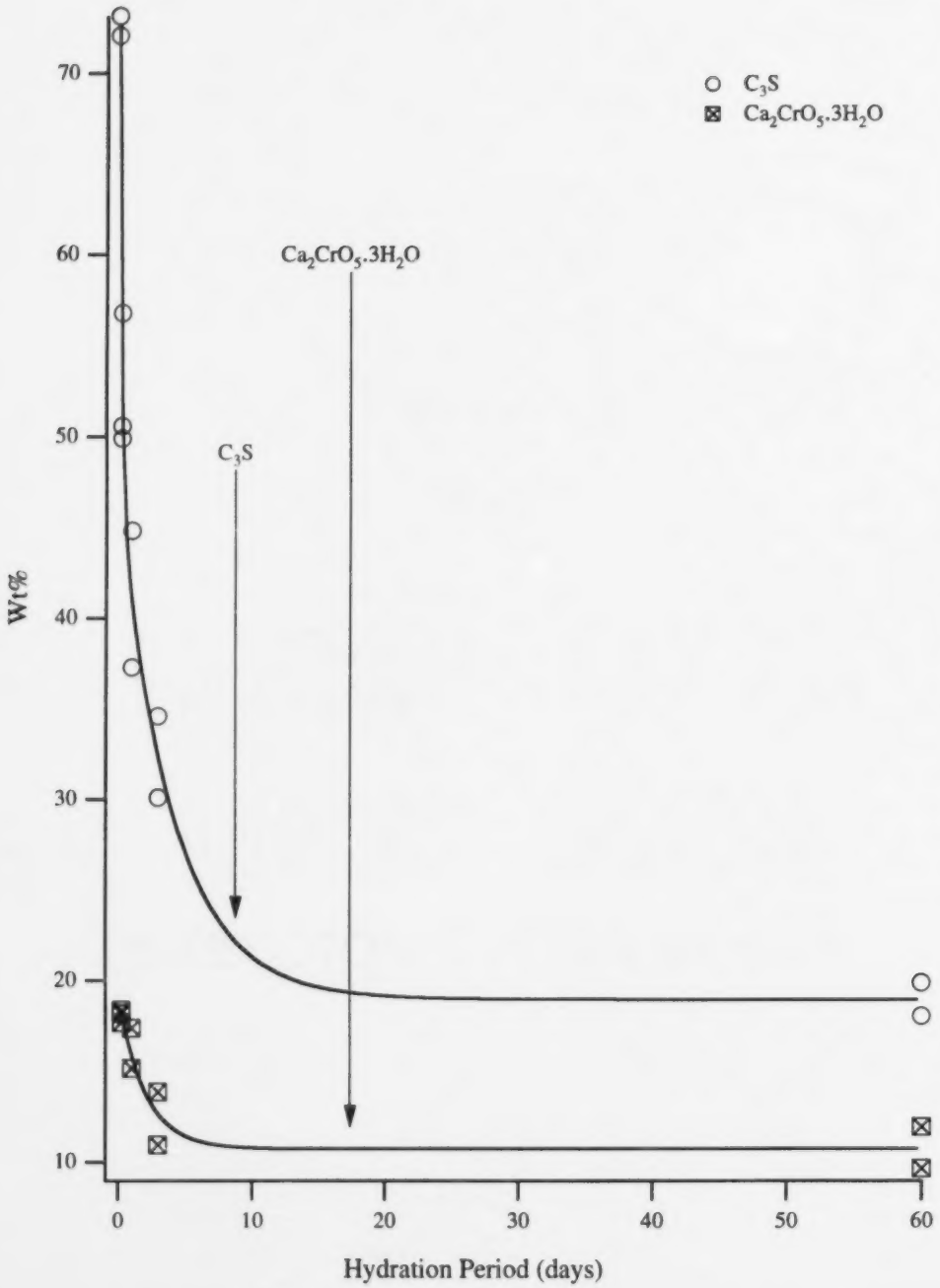

Fig. 4.1.10 Rate of reaction of C_3S and formation of $Ca_2CrO_5.3H_2O$.

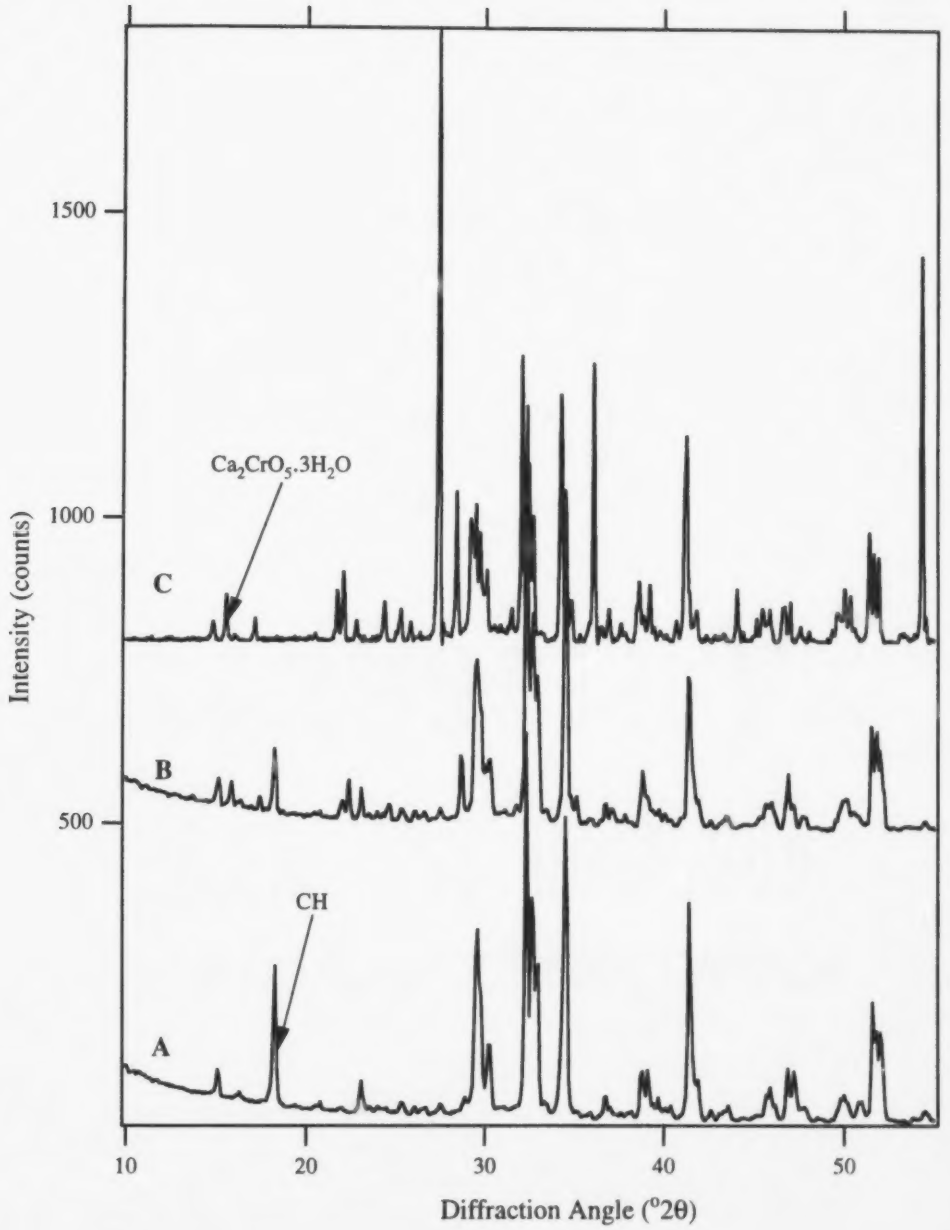

Fig. 4.1.11 XRD patterns of 24 hour old Cr(VI) pastes; (A) 0.1 M, (B) 1 M and (C) 2 M. Rutile was not added to 0.1 M and 1 M pastes.

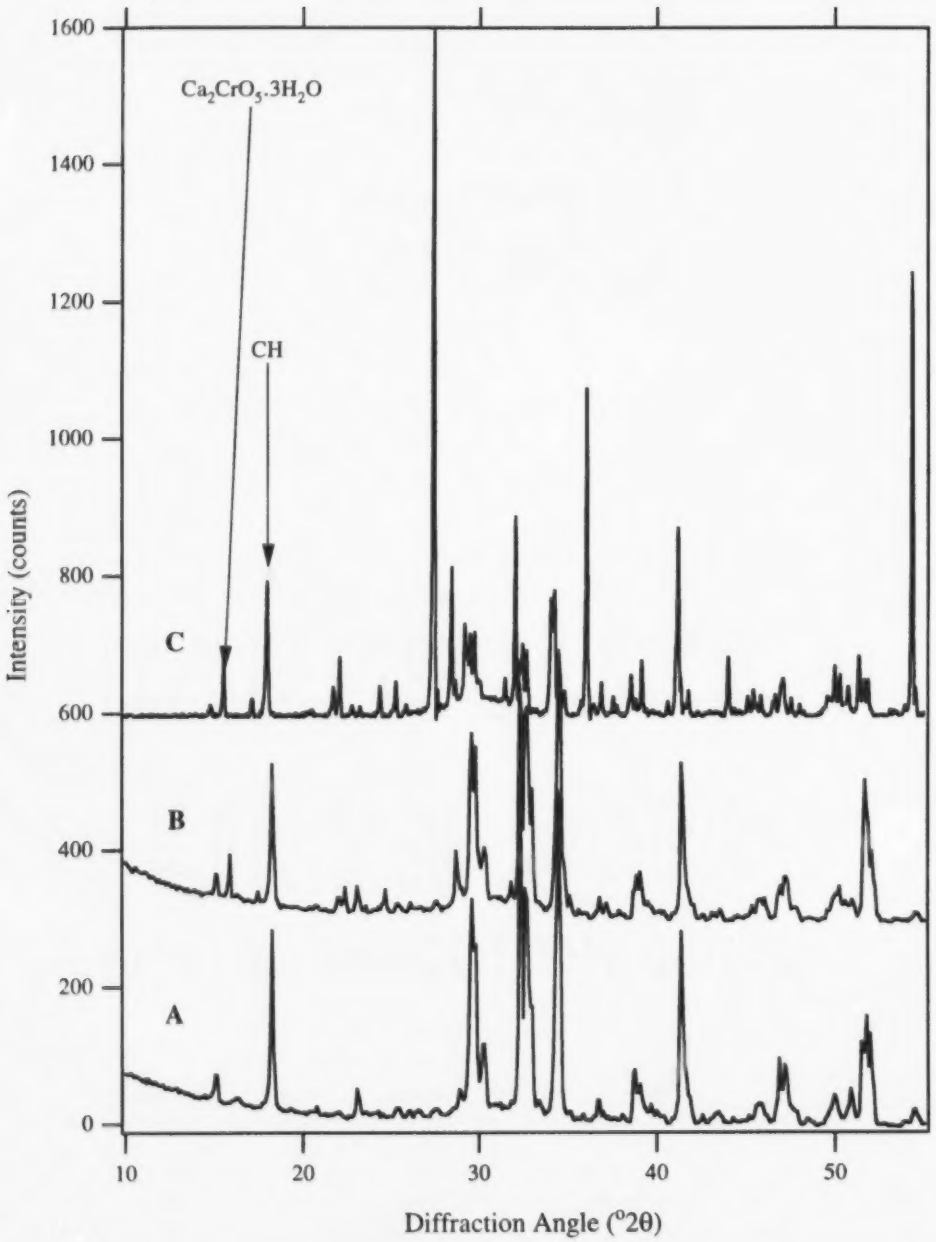

Fig. 4.1.12 XRD patterns of 60day old Cr(VI) pastes; (A) 0.1 M, (B) 1 M and (C) 2 M. Rutile was not added to 0.1 M and 1 M pastes.

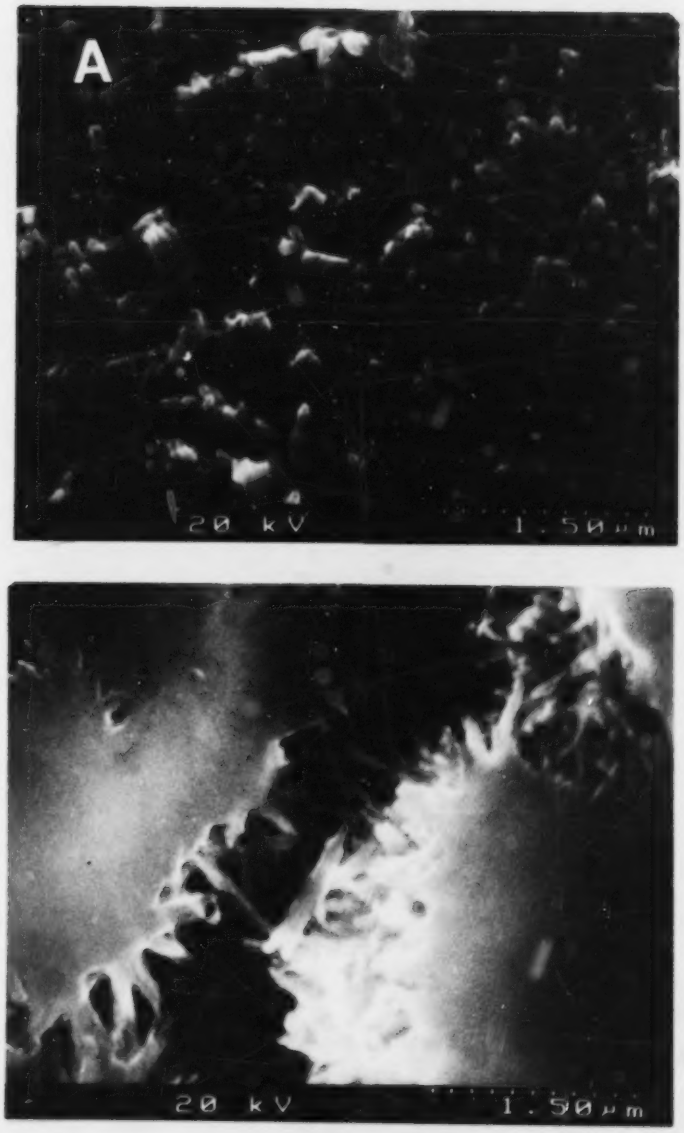

Fig. 4.2.1 SEM micrographs of a blank paste hydrated for 24 hours showing fibrous C-S-H; (A) fracture surface, (B) flat surface (surface in contact with the plastic mold).

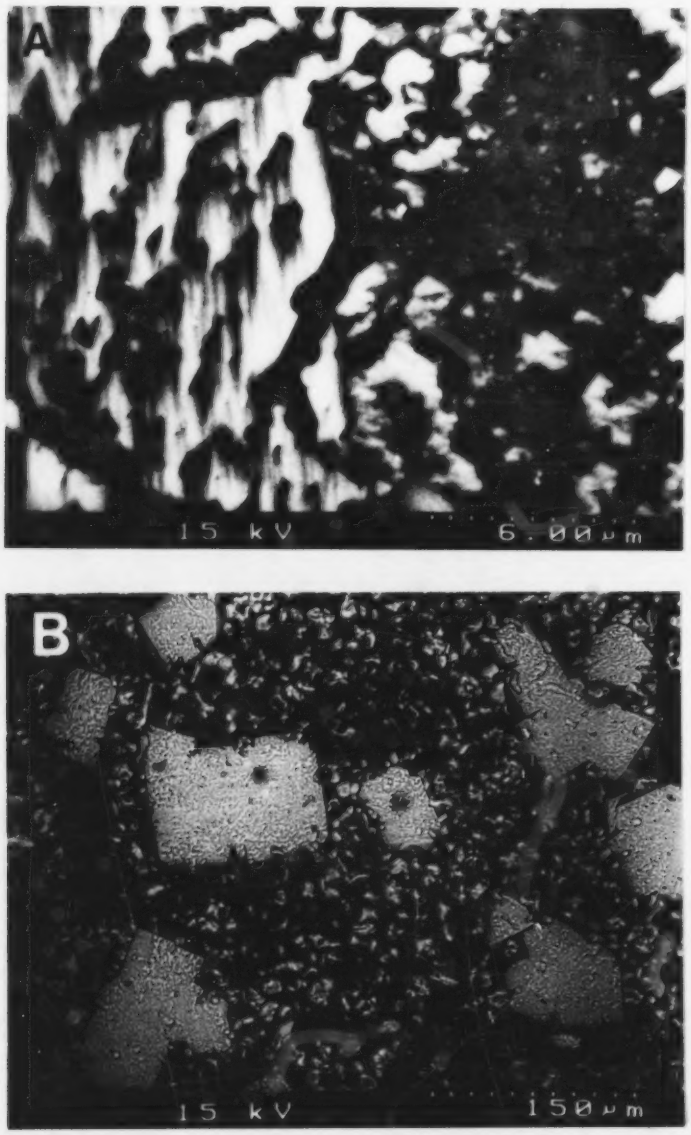

Fig. 4.2.2 Backscattered electron micrographs of a 24 hour old blank paste; (A) The featureless dark region and the flaky bright phase are different morphologies of CH. (B) Low magnification backscattered electron image. The well formed large bright structures are CH in contact with the plastic mold.

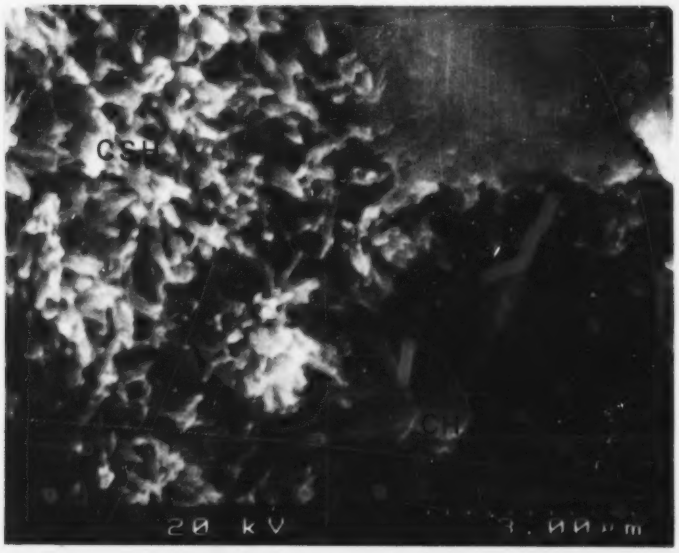

Fig. 4.2.3 SEM micrograph of a blank paste hydrated for 60 days showing fibrous C-S-H and CH.

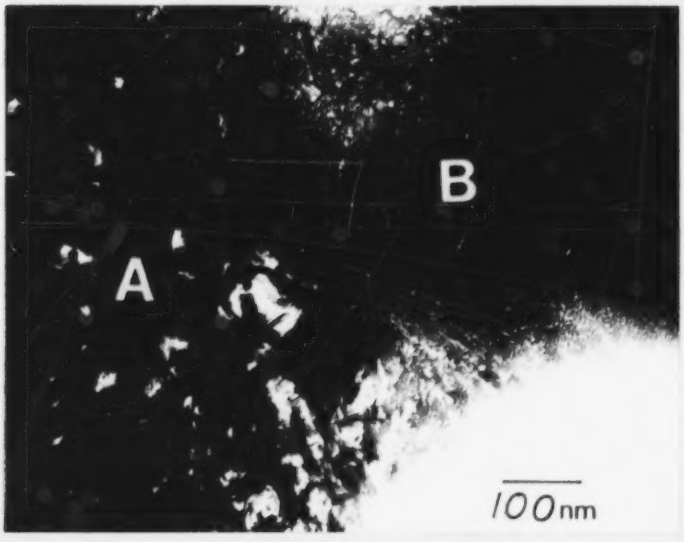

Fig. 4.2.4 TEM micrograph of a blank paste hydrated for 60 days showing early fibrous C-S-H (A) and the denser late C-S-H (B).

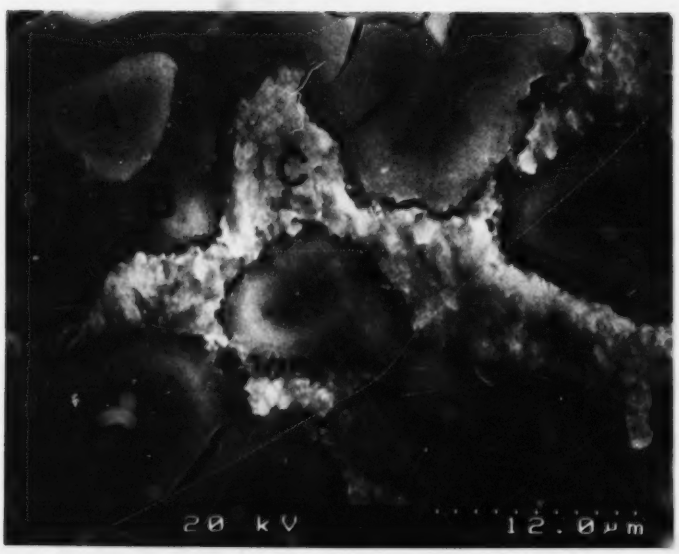

Fig. 4.2.5 SEM micrograph of a polished blank paste hydrated for 14 months showing; (A) unreacted C_3S, (B) C-S-H and (C) CH.

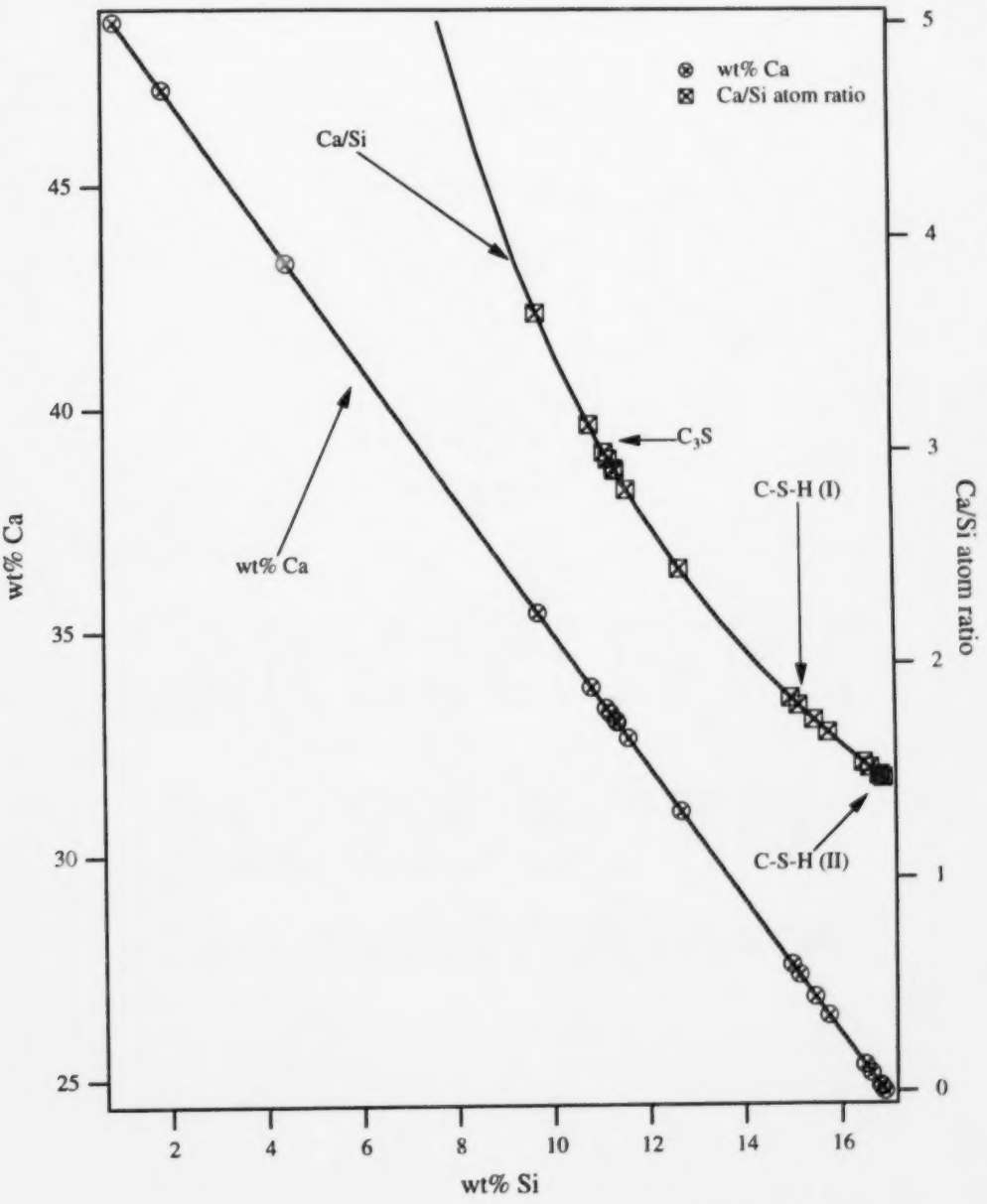

Fig. 4.2.6 X-ray microanalysis of fully hydrated blank (C_3S) pastes showing the relationship between the hydration products.

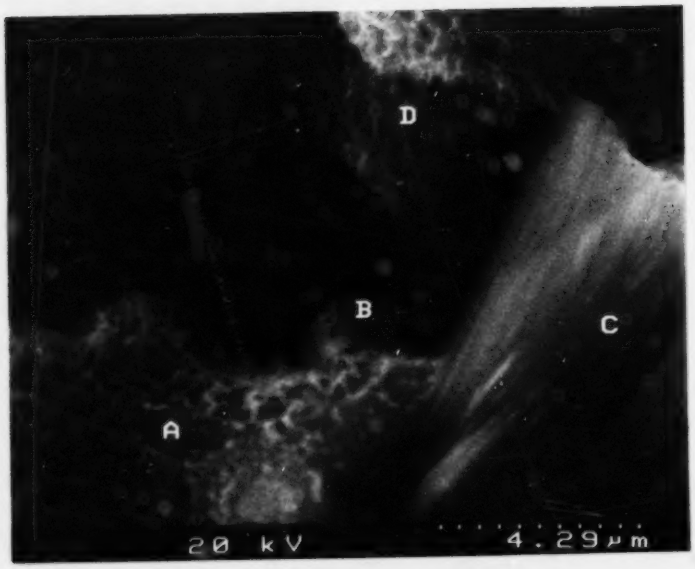

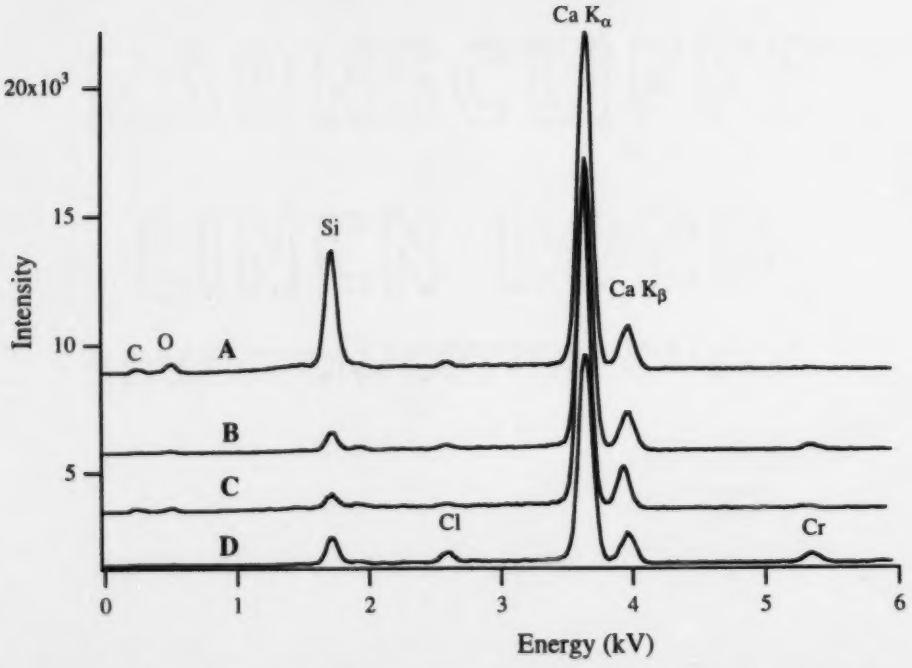

Fig. 4.2.7 SEM micrograph and EDS spectra of 0.1 M Cr(III) chloride hydrated for 24 hours.

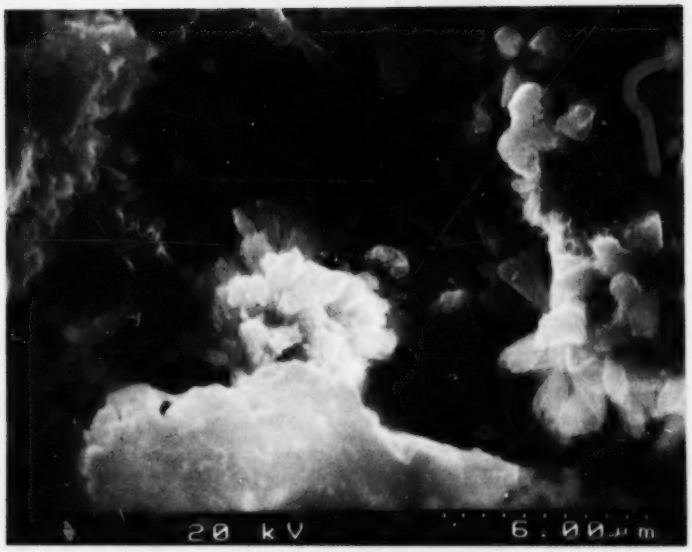

Fig. 4.2.8 SEM micrograph of 24 hour old 0.1 M chromium nitrate showing the different morphologies assumed by early C-S-H.

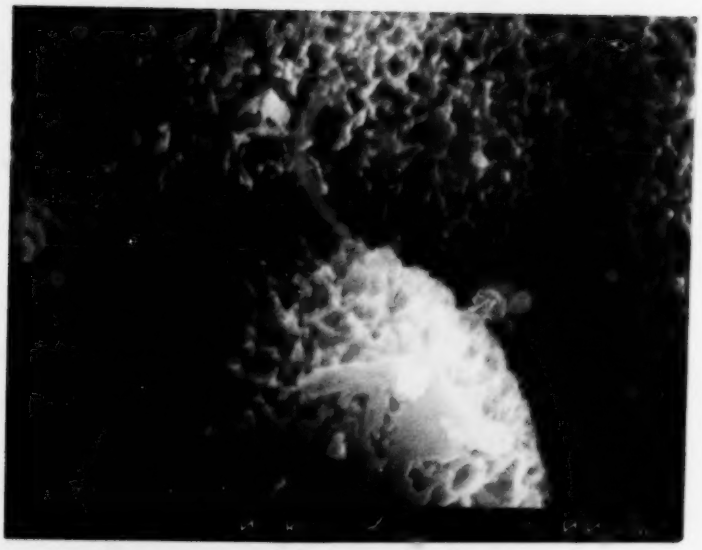

Fig. 4.2.9 SEM micrograph of a 60 day old 0.1 M chromium nitrate showing the honeycomb morphology of the early C-S-H.

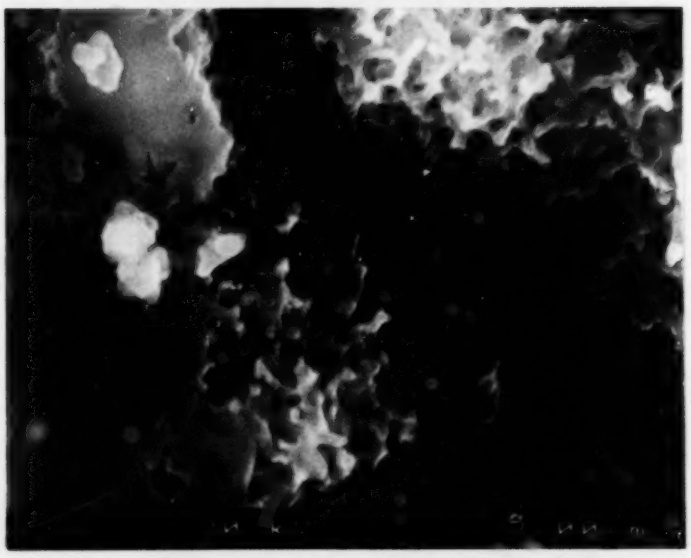

Fig. 4.2.10 SEM micrograph of a 60 day old 0.1 M chromium chloride paste showing the honeycomb morphology assumed by the early C-S-H.

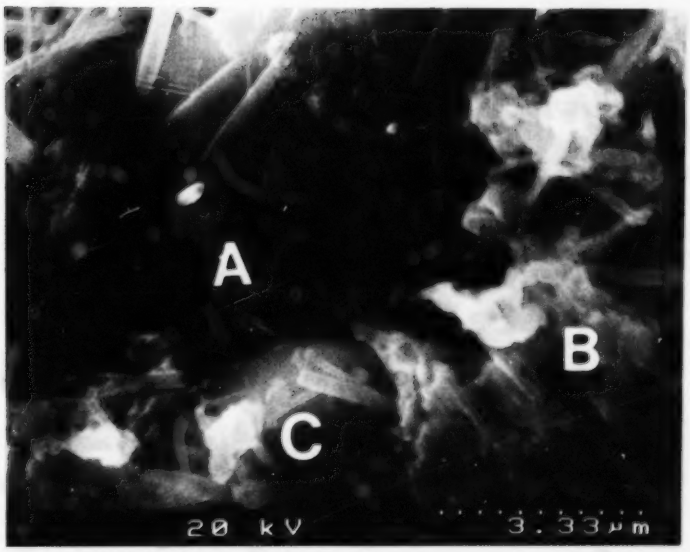

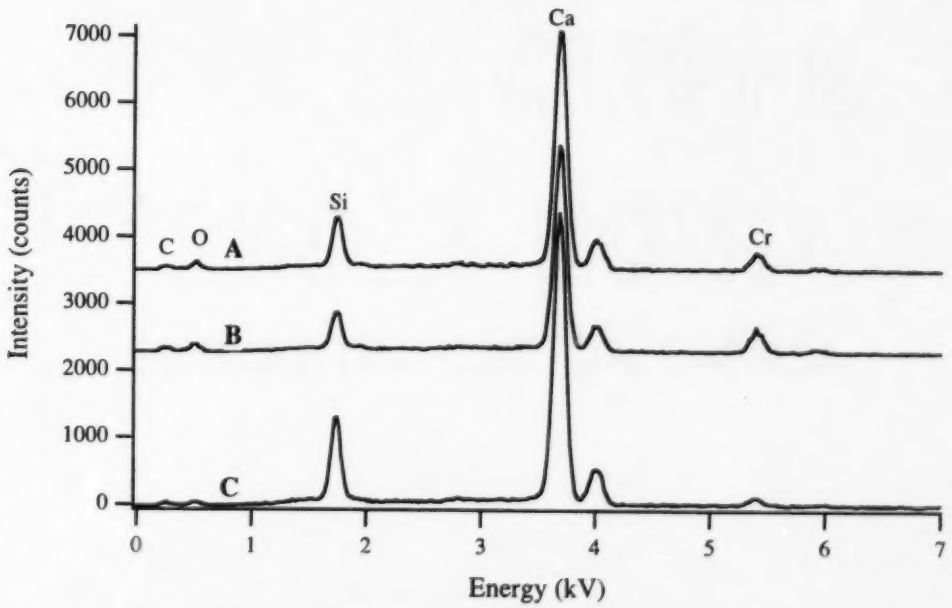

Fig. 4.2.11 SEM micrograph and EDS spectra of a fractured 24 hour old 1 M Cr(III) nitrate paste; (A) Early Ca - Cr complex rod, (B) Cr-containing C-S-H gel, and (C) C-S-H (small Cr peak possibly from surrounding structures).

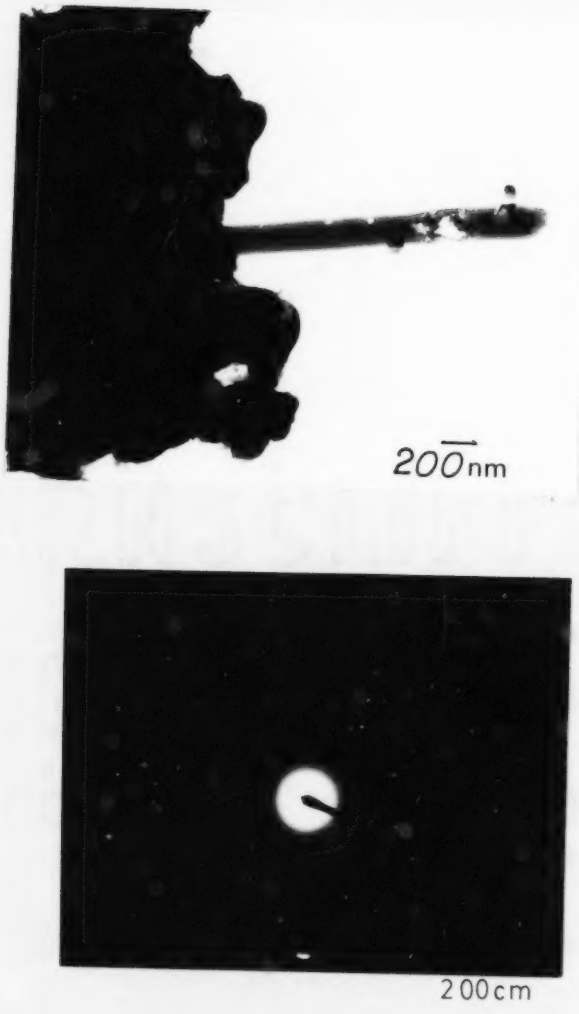

Fig. 4.2.12 TEM micrograph and SAD pattern of 1 M Cr(III) nitrate hydrated for 24 hours highlighting the early Ca-Cr rods amorphous structure.

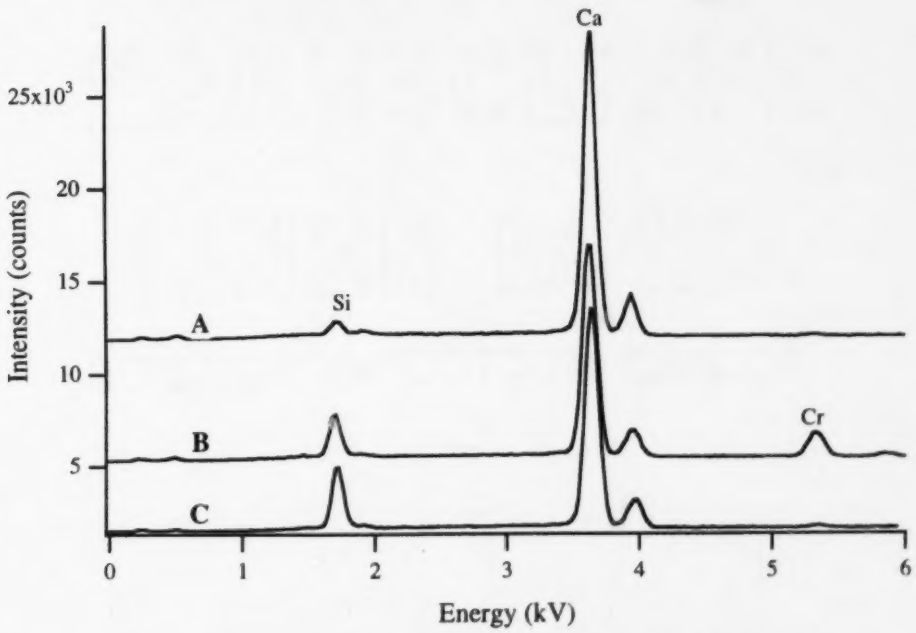

Fig. 4.2.13 SEM micrograph and EDS spectra of 60 day old 1 M Cr(III) nitrate paste showing; (A) CH, (B) Cr - rich C-S-H and (C) C-S-H.

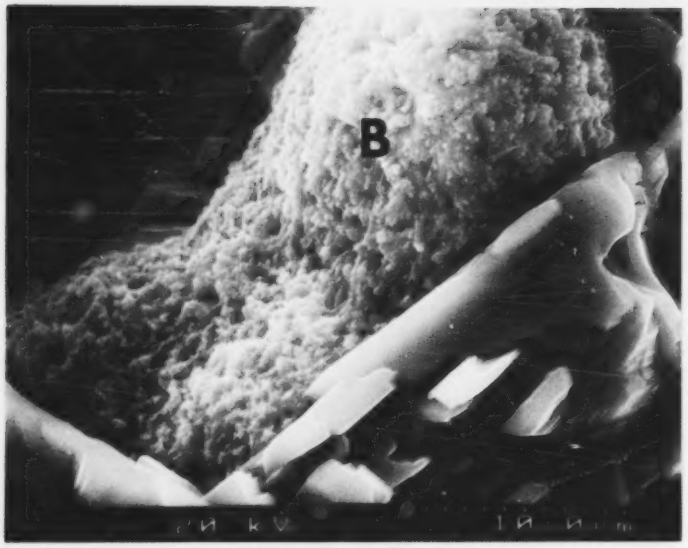

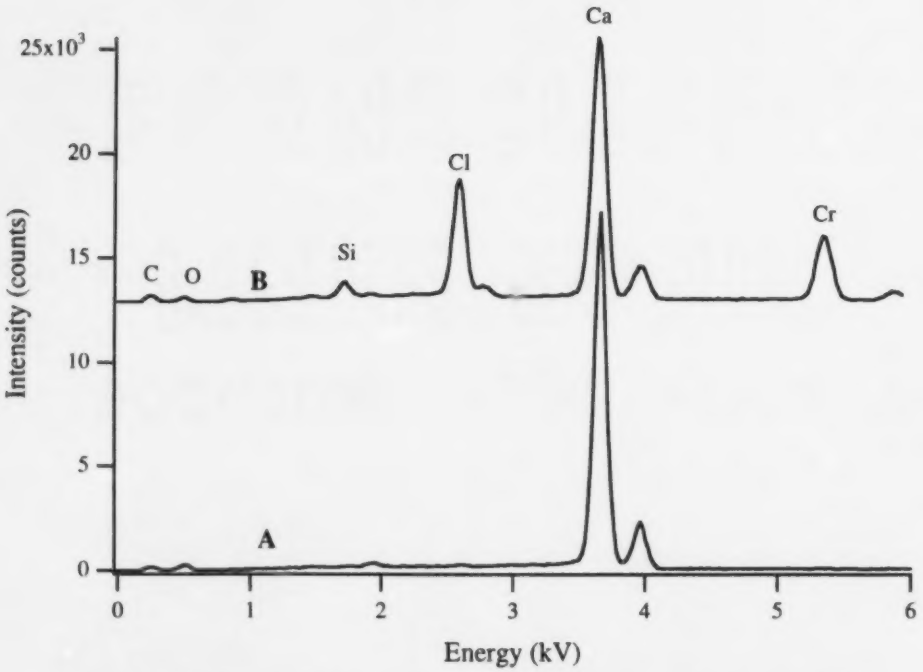

Fig. 4.2.14 SEM micrograph and EDS spectra of a fractured 60 day old 1 M Cr(III) chloride paste; (A) CH and (B) C-S-H.

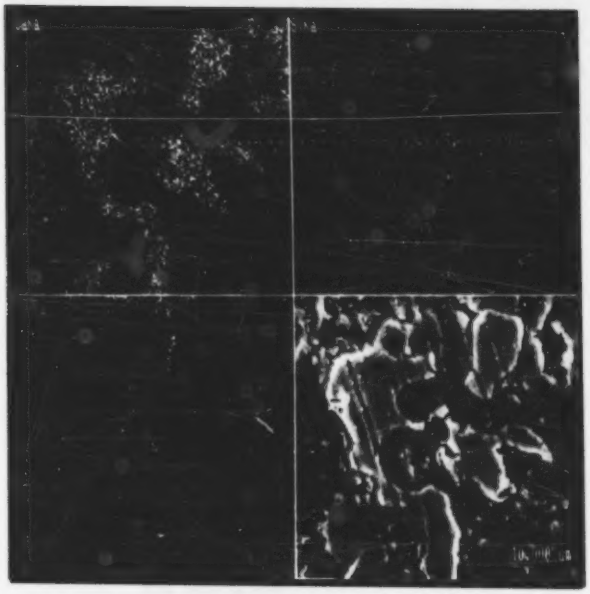

Fig. 4.2.15 X-ray map of a polished 1 M Cr(III) nitrate paste hydrated for 60 days, showing the distribution of Ca, Si and Cr in the reaction products.

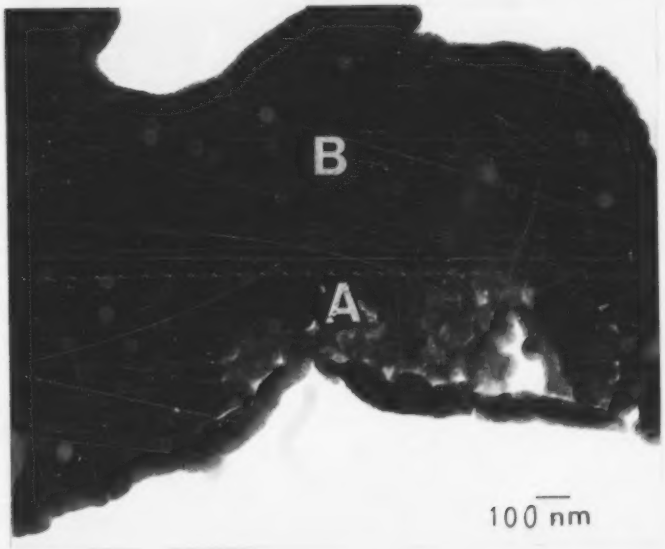

Fig. 4.2.16 TEM micrograph of a 60 day old 1 M chromium nitrate paste showing; (A) Cr - rich C-S-H and (B) Cr free C-S-H.

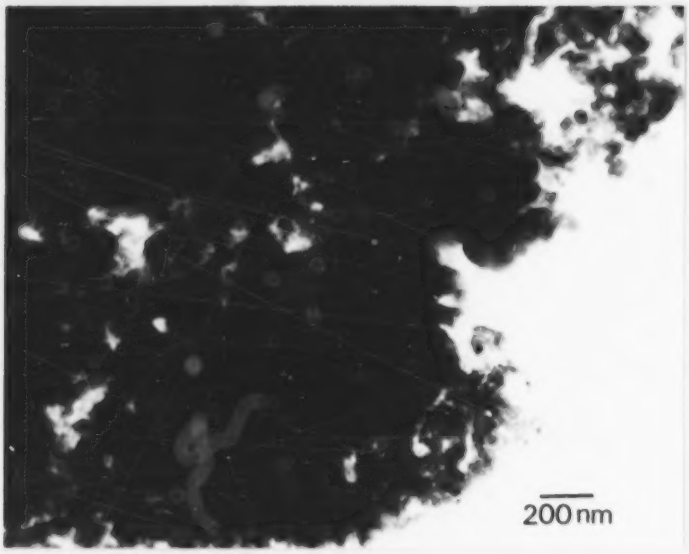

Fig. 4.2.17 TEM micrograph of a 5 minute old 2 M Cr nitrate paste showing a C-S-H region containing variable Cr concentrations.

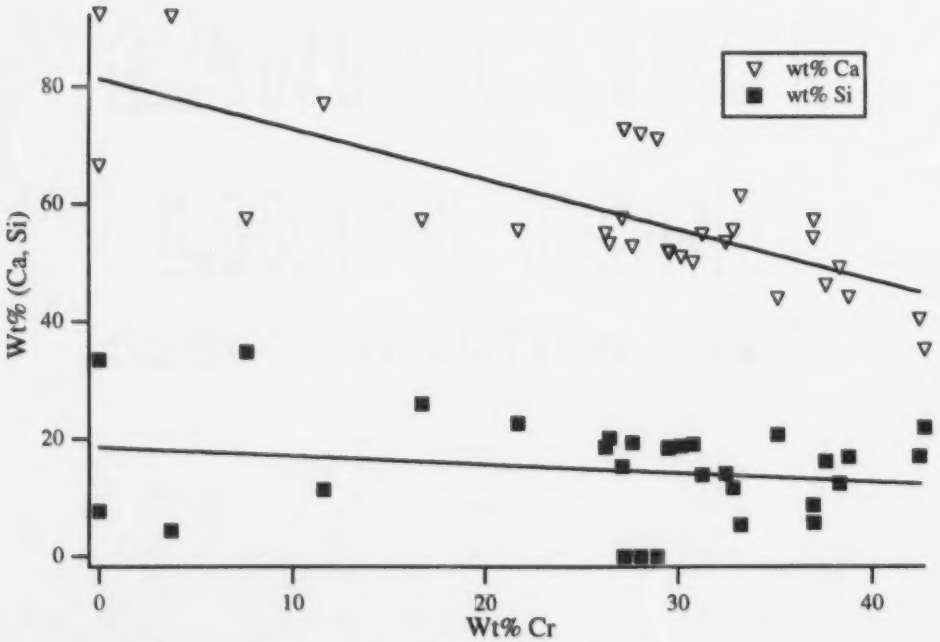

Fig. 4.2.18 Variation of Ca and Si with Cr in a 5 minute old 2 M Cr(III) paste.

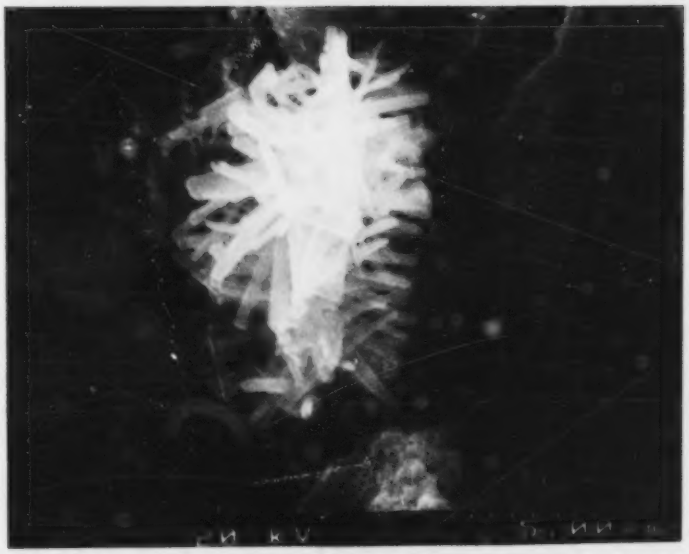

Fig. 4.2.19 SEM micrograph of a 24 hour old 2 M chromium nitrate paste showing early Ca - Cr complex crystals (white crystals).

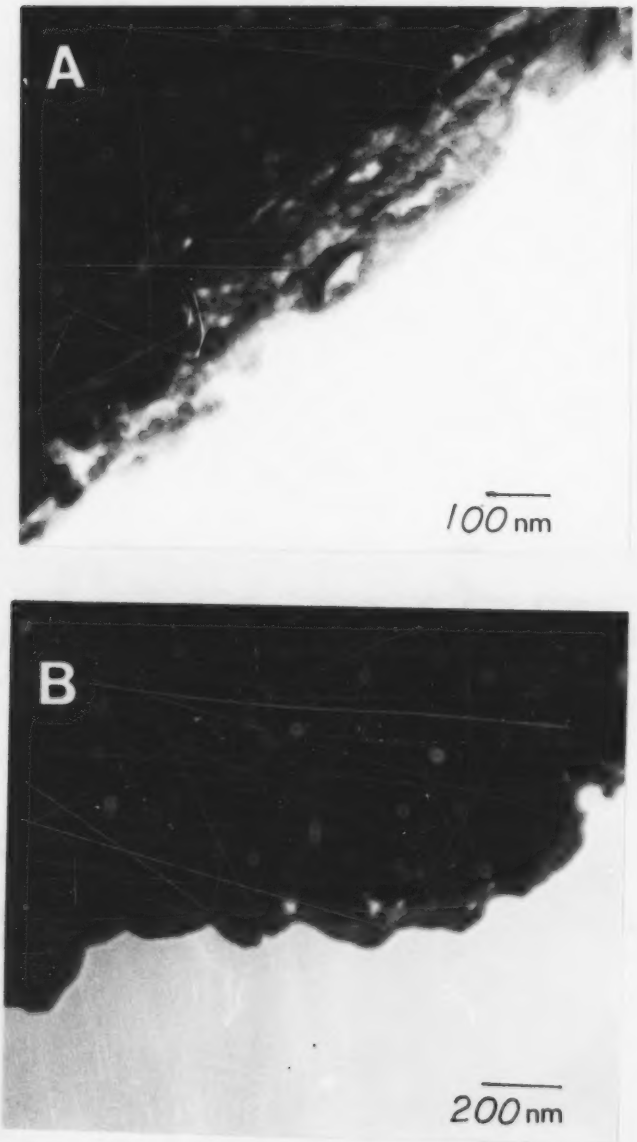

Fig. 4.2.20 TEM micrographs of a 24 hour old 2 M chromium nitrate paste; (A) Cr - free C-S-H and (B) Si - free Ca - Cr phase.

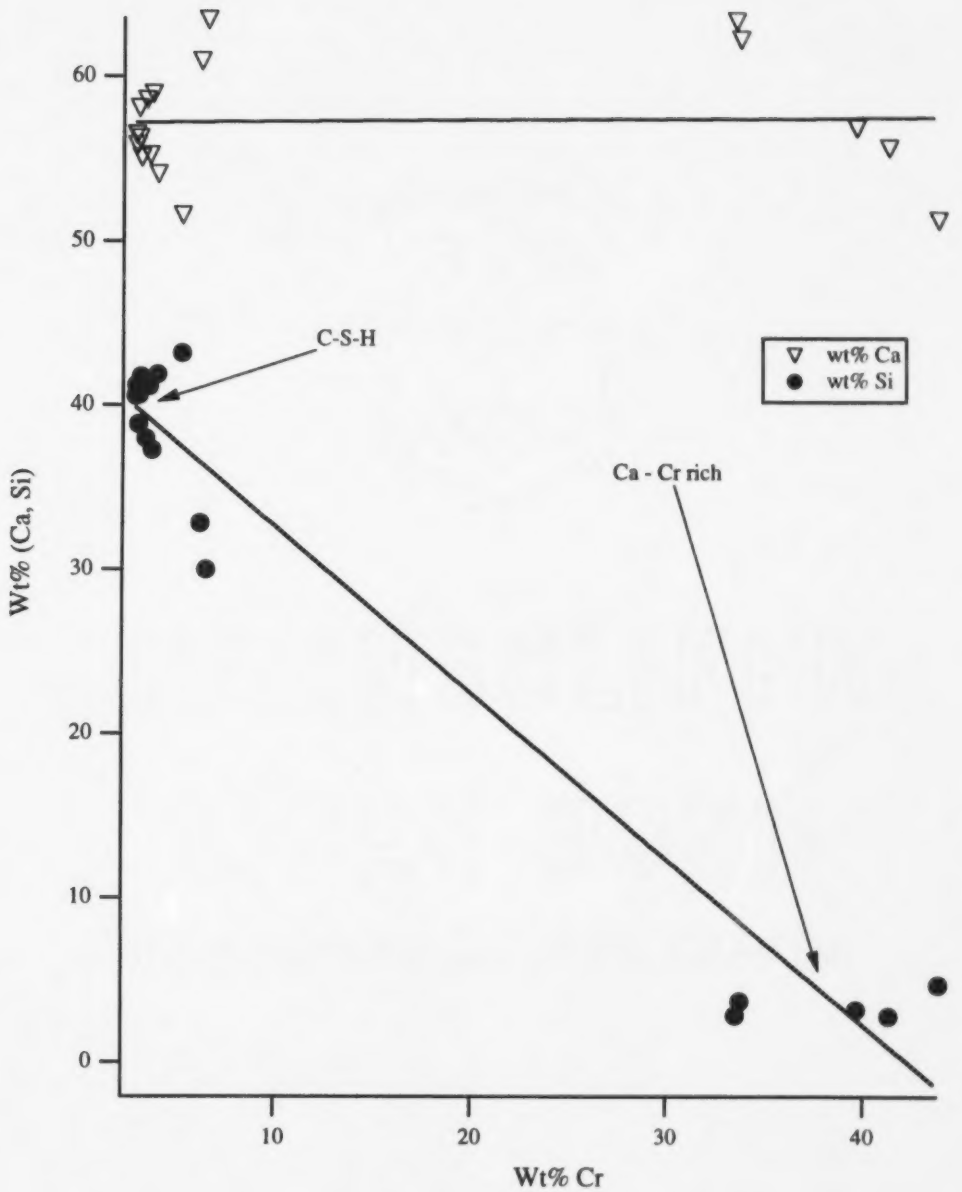

Fig. 4.2.20 c Variation of Ca and Si with Cr in a 24 hour old 2 M Cr(III) paste (EDS of CH and C_3S excluded).

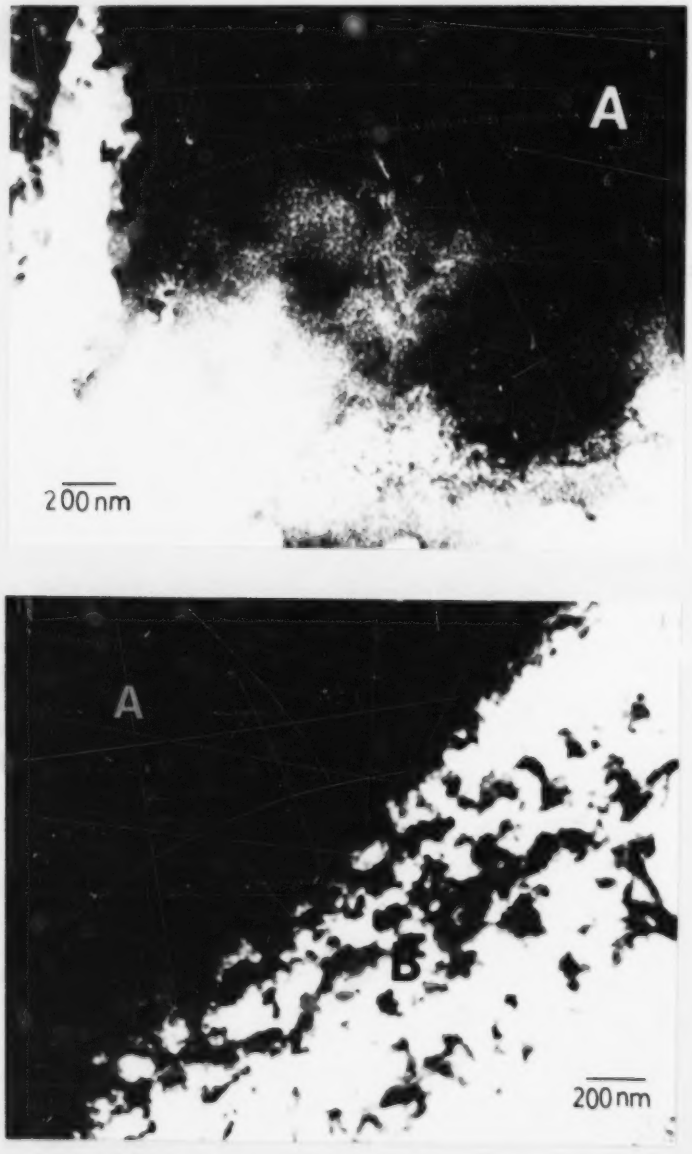

Fig. 4.2.21 TEM micrographs of a 60 day old 2 M chromium nitrate paste; (A) high Si C-S-H with variable Cr content and (B) normal C-S-H region also containing variable high concentrations of Cr.

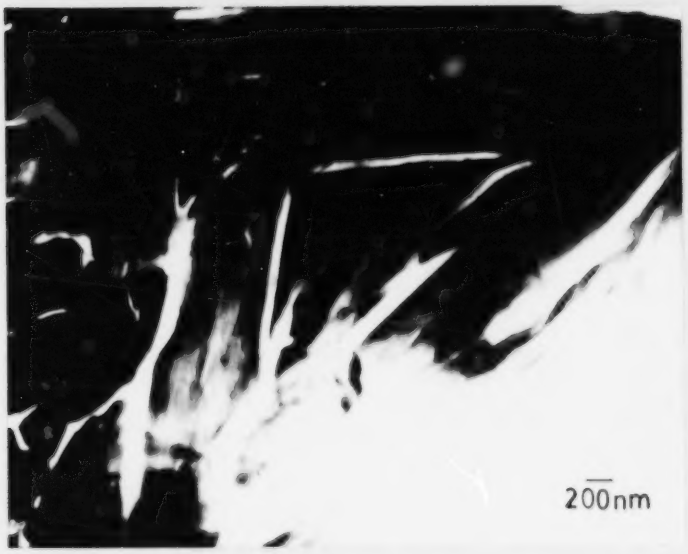

Fig. 4.2.22 TEM micrograph of a 60 day old 2 M Cr(III) paste showing Ca-Cr rods.

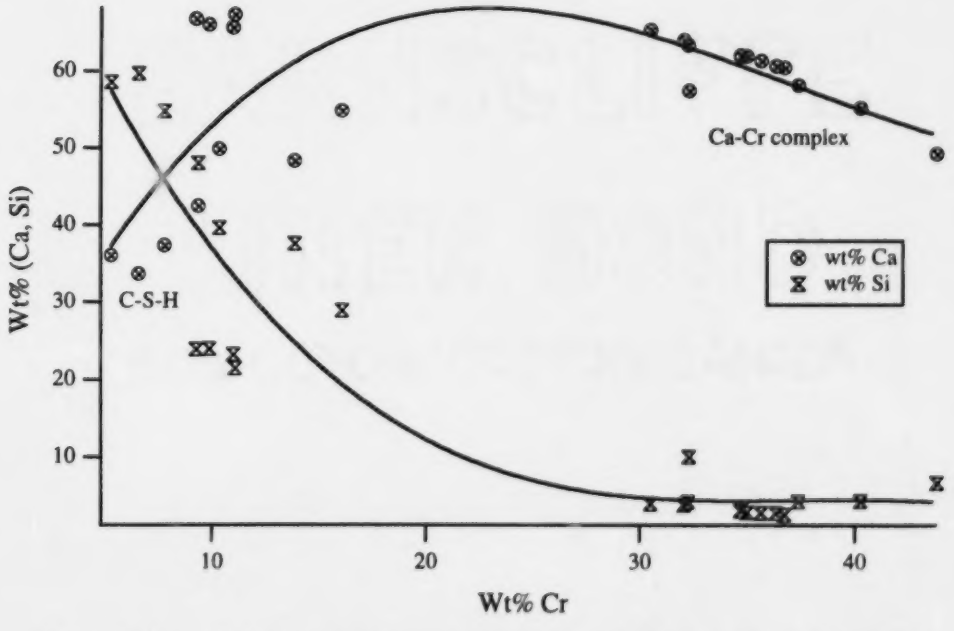

Fig. 4.2.23 Relationship between chromium concentrations and calcium and silicon concentrations in the hydration products of a 60 day old 2 M Cr(III) paste.

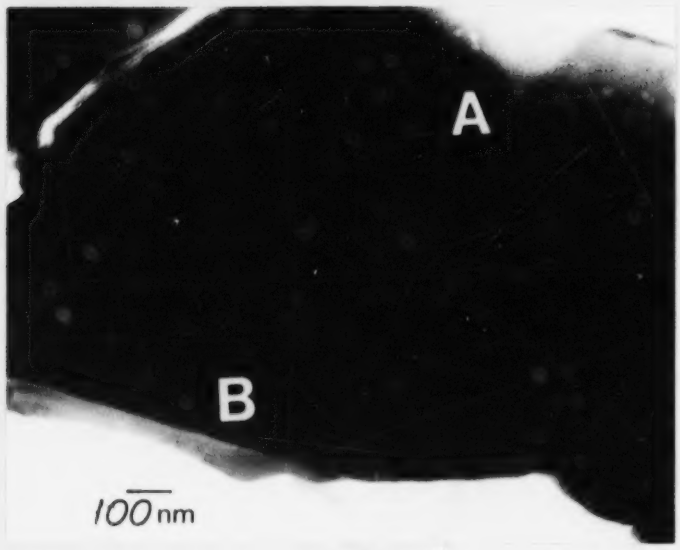

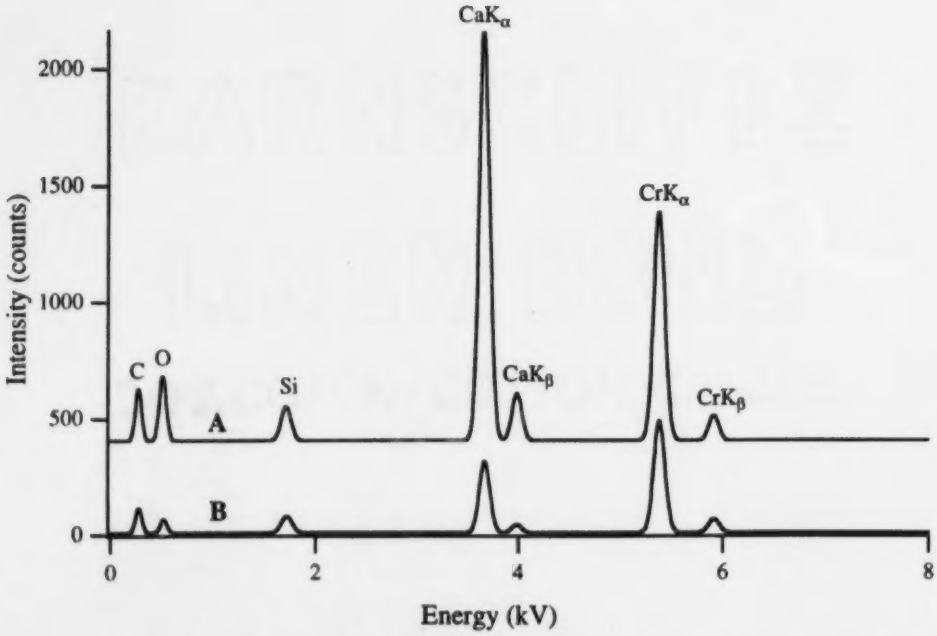

Fig. 4.2.24 TEM micrograph and EDS spectra of a 14 month old 2.75 M Cr(III) paste showing typical regions containing (A) a high Ca/Si ratio and (B) a low Ca/Si ratio.

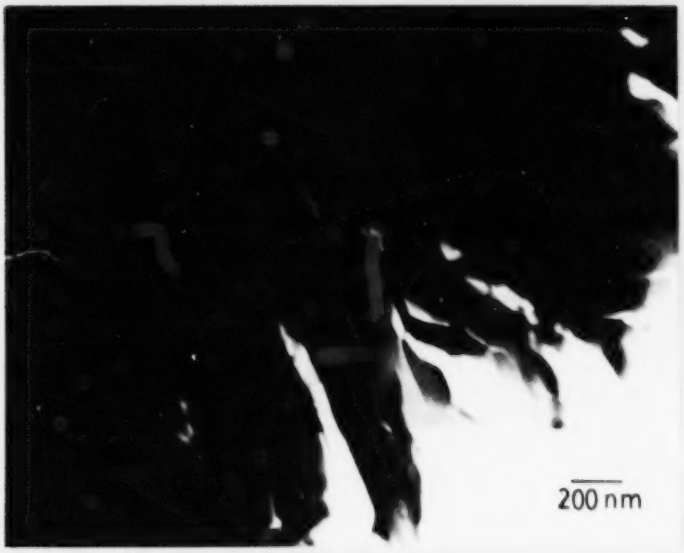

Fig. 4.2.25 TEM micrograph of a 14 month old exposed 2.75 M Cr(III) paste showing the late Ca-Cr rods.

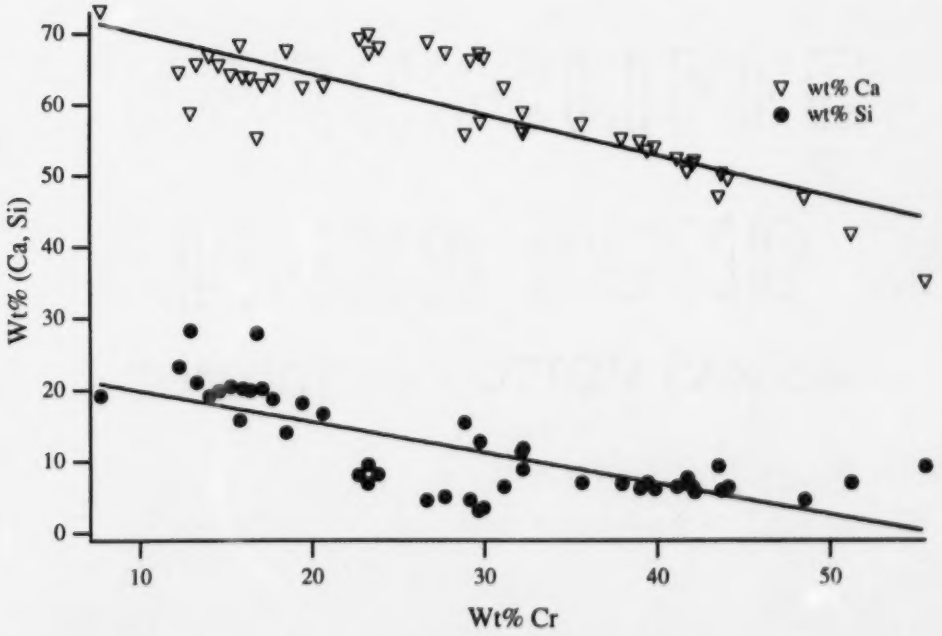

Fig. 4.2.26 Variation of Ca and Si with Cr in a 14 month old exposed 2.75 M Cr(III) paste. Cr containing C-S-H, Cr - free C-S-H and Ca-Cr regions were analyzed.

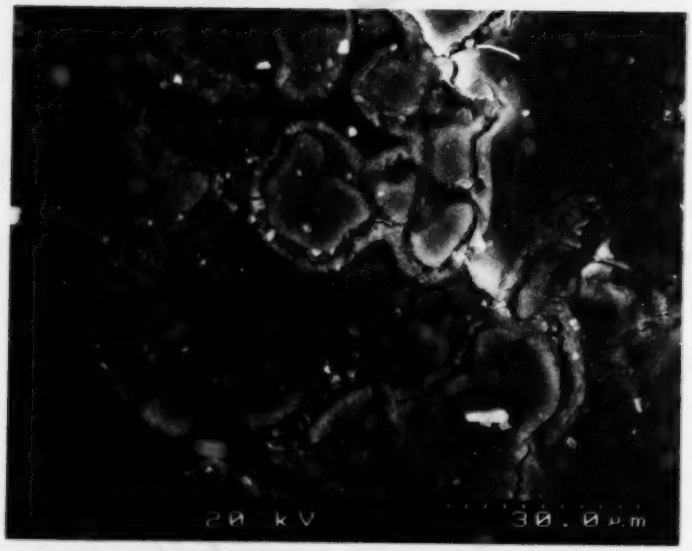

Fig. 4.2.27 Low magnification SEM micrograph of a polished 14 month old 2.75 M Cr(III) paste, showing the spatial distribution of the late Ca - Cr complex (A) and C-S-H (B).

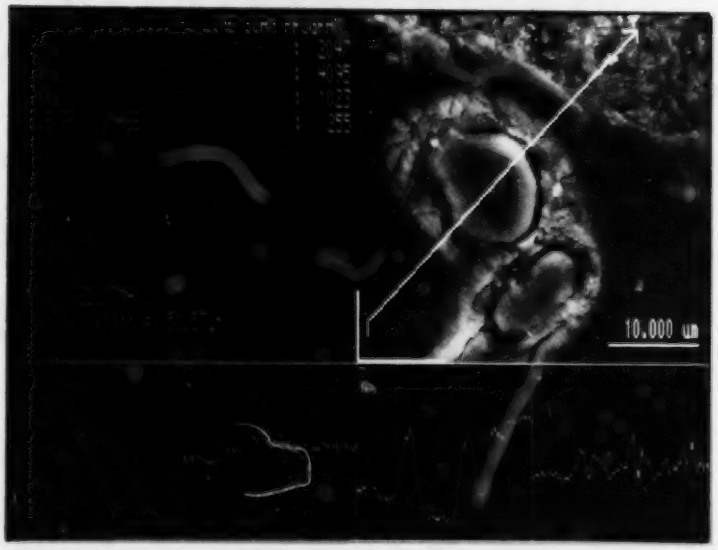

Fig. 4.2.28 X-ray line scan of a polished 14 month old 2.75 M Cr(III) paste showing the relative concentrations of Ca, Cr and Si across several phases.

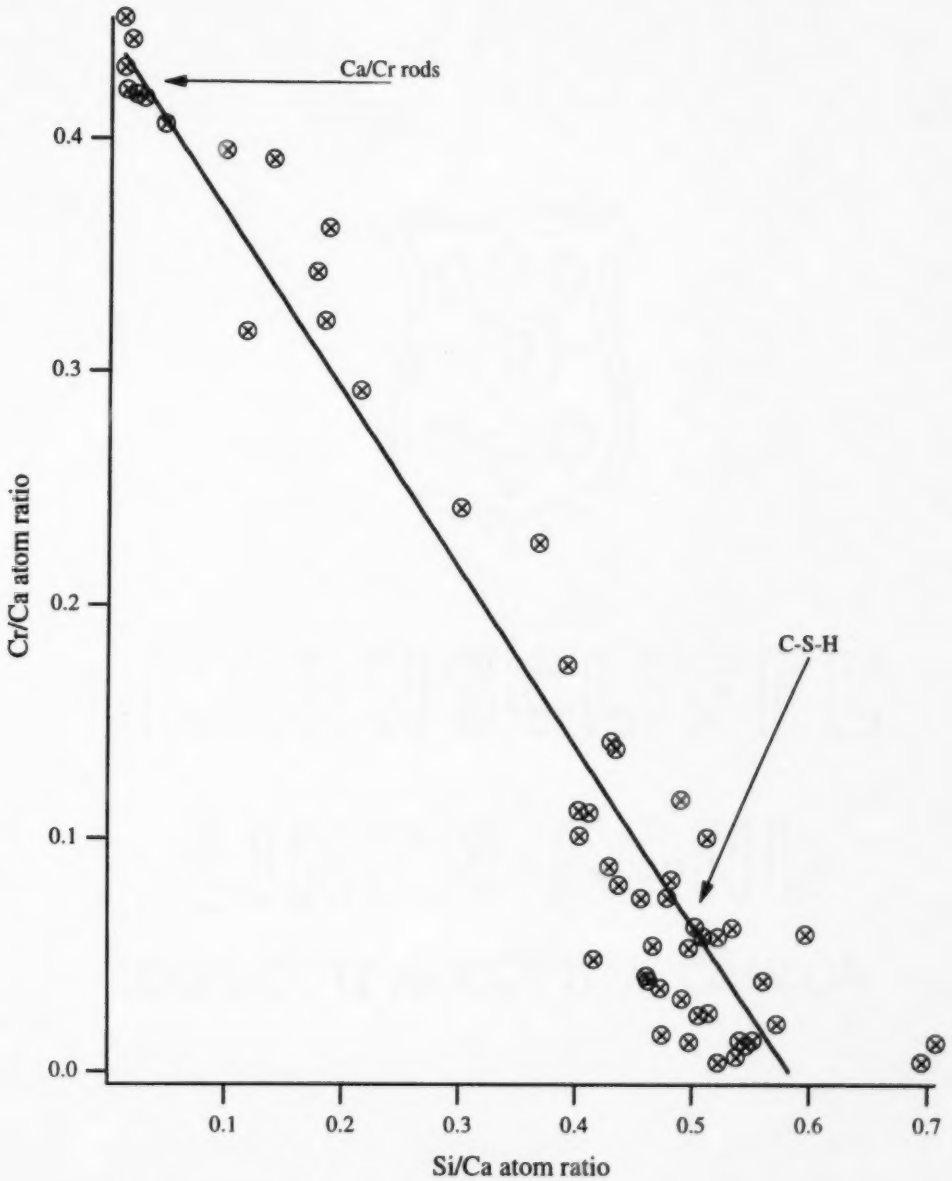

Fig. 4.2.29 SEM/EDS analysis plot of Cr/Ca mole ratio against Si/Ca mole ratios in a typical 14 month old 2.75 M Cr(III) paste. CH was not represented.

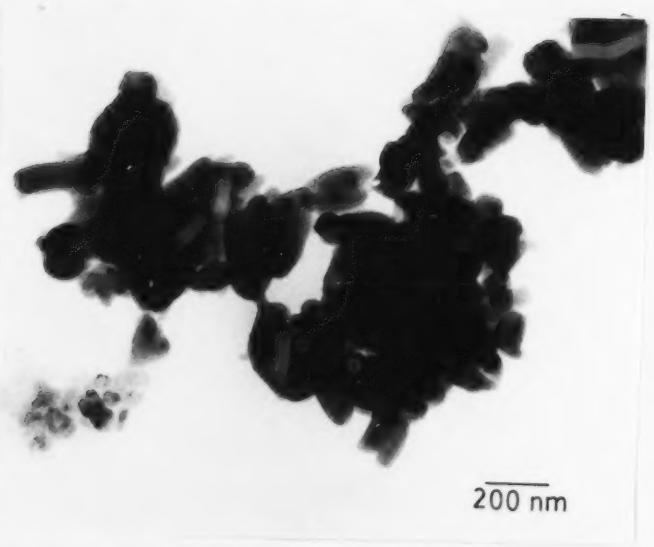

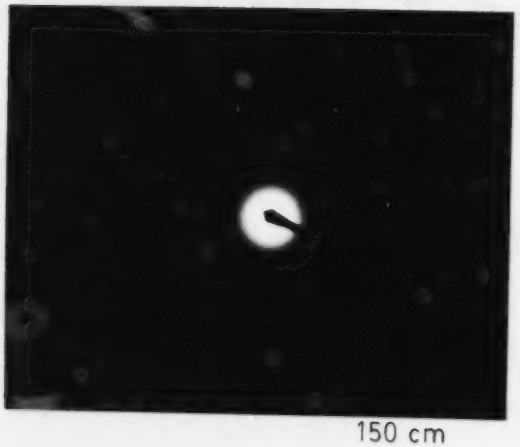

Fig. 4.2.30 TEM micrograph and SAD pattern of early Ca - Cr complex powder examined on a carbon coated grid. (Ca/Cr ratio = 3).

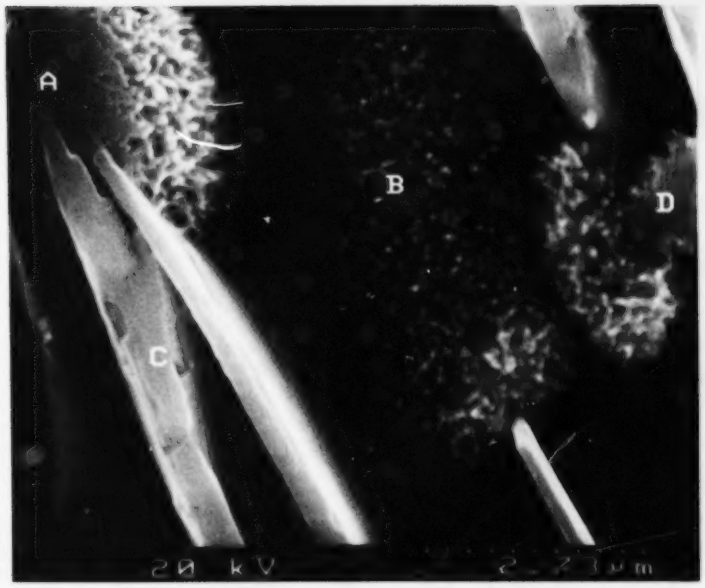

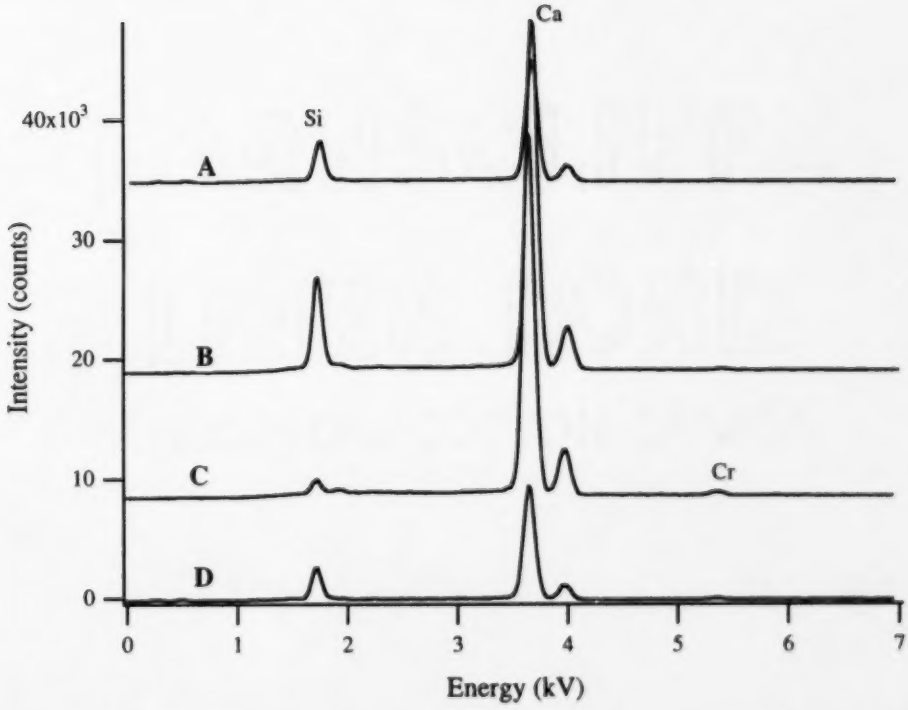

Fig. 4.2.31 SEM micrograph and EDS spectra of a typical 0.1 M Cr(VI) paste hydrated for 24 hours. The analyzed regions are mainly CH and C-S-H.

Fig. 4.2.32 SEM micrograph of 0.1 M
crystals and fibrous C-S-

Fig. 4.2.33 SEM micrograph of 1 M
CH crystals (A) and fibro

icrograph of 0.1 M Cr(VI) paste hydrated for 60 days. Long CH
and fibrous C-S-H dominate the structure.

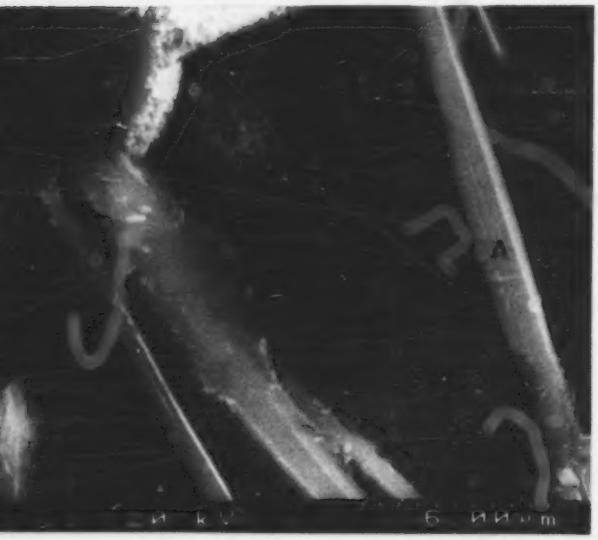

icrograph of 1 M Cr(VI) paste hydrated for 60 days, showing
stals (A) and fibrous C-S-H (B).

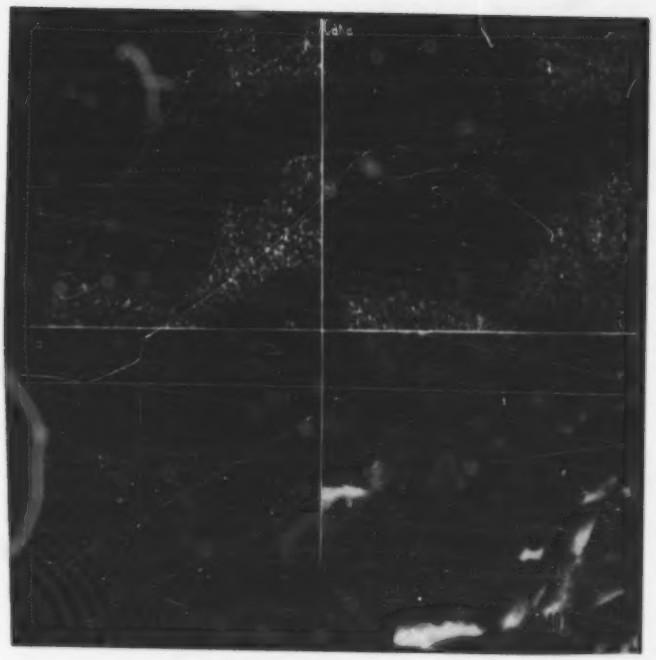

Fig. 4.2.34 X-ray maps of a polished 1 M Cr(VI) paste hydrated for 60 days, showing the distribution of Ca, Si and Cr in the reaction products.

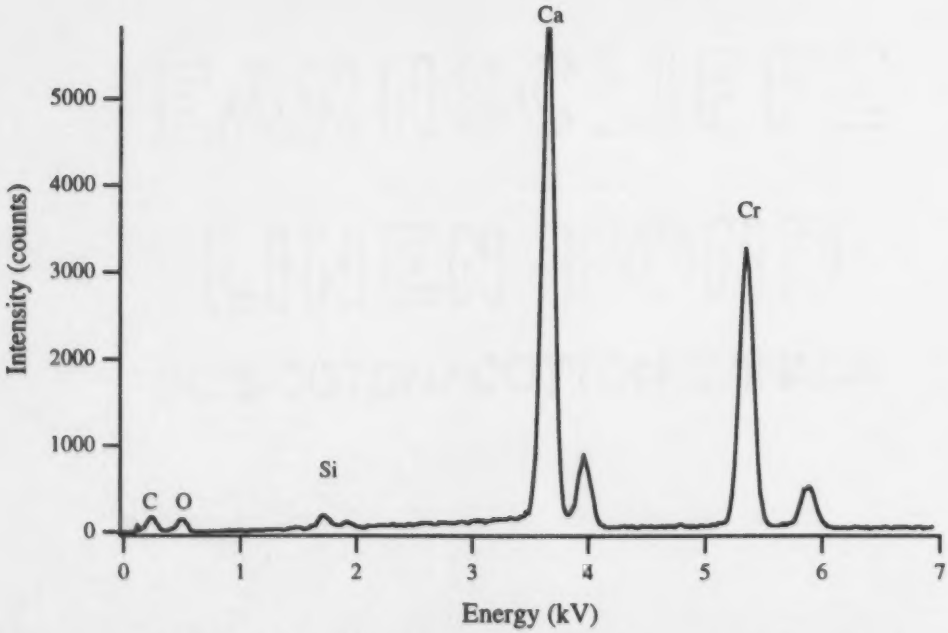

Fig. 4.2.35 SEM micrograph and EDS spectrum of a 5 minute old 2 M Cr(VI) paste. A typical EDS spectrum of the calcium chromate rod is shown.

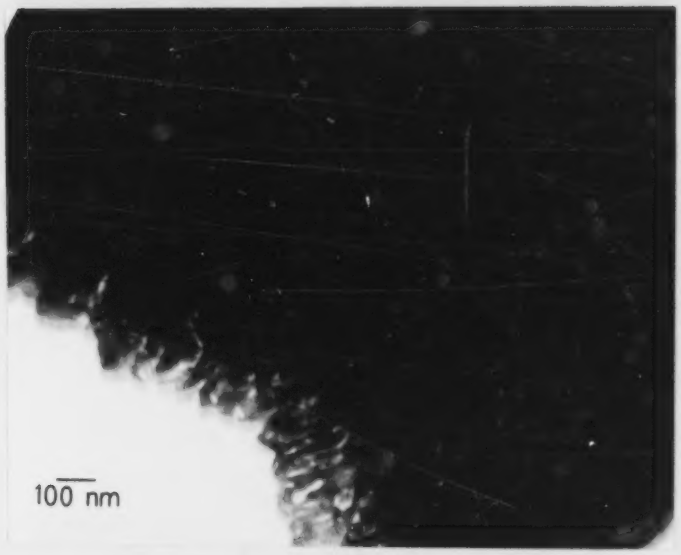

Fig. 4.2.36 TEM micrograph of a typical $CaCrO_4.2H_2O$ rod in a 5 minute old 2 M Cr(VI) paste.

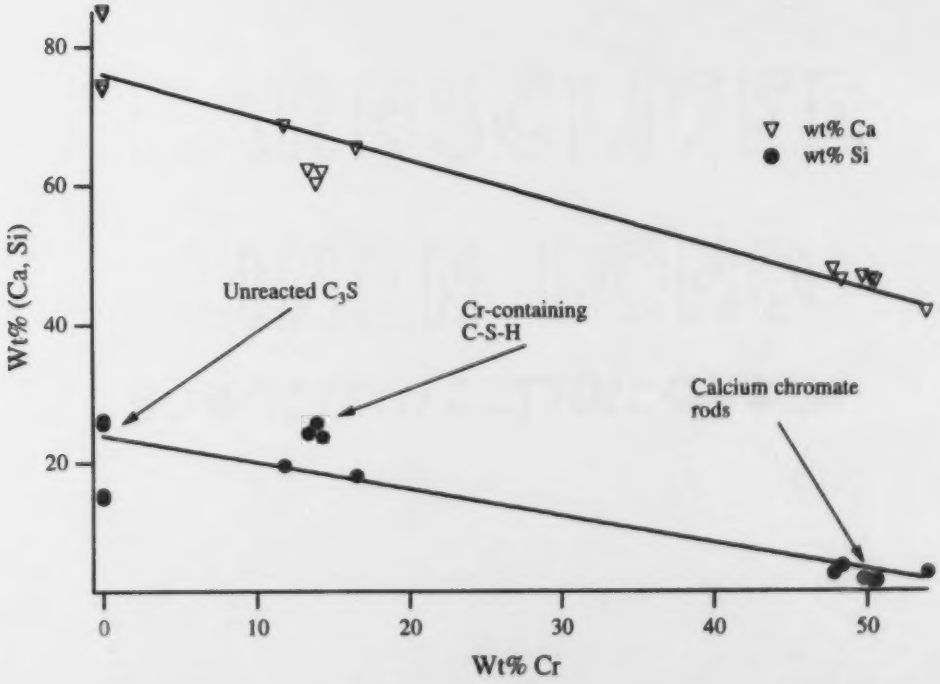

Fig. 4.2.37 TEM/x-ray microanalysis of typical phases in a 5 minute old 2 M Cr(VI) paste, showing the variation of Ca and Si with Cr.

Fig. 4.2.38 SEM micrograph of 2 M Cr(VI) paste hydrated for 24 hours, showing CH and fibrous C-S-H.

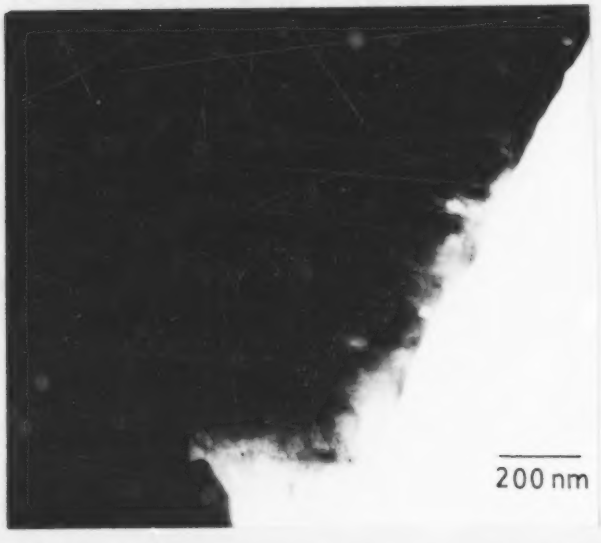

Fig. 4.2.39 TEM micrograph of 2 M Cr(VI) paste hydrated for 24 hours, highlighting the dicalcium chromate trihydrate phase (Ca/Cr ratio ~ 1.38).

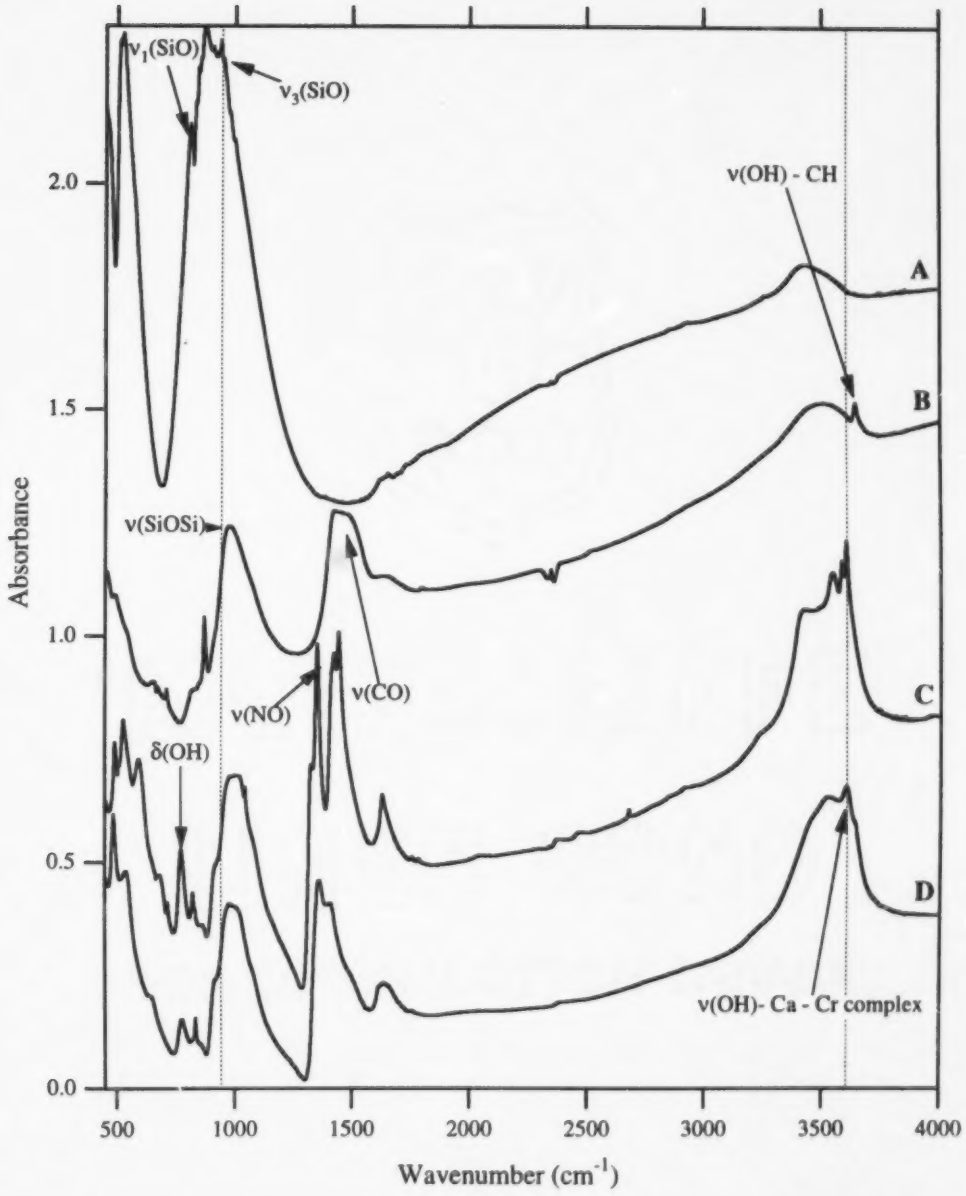

Fig. 4.3.1 FTIR spectra of C_3S and fully hydrated pastes; (A) C_3S, (B) blank, (C) sealed 2.75 M Cr(III) and (D) exposed 2.75 M Cr(III).

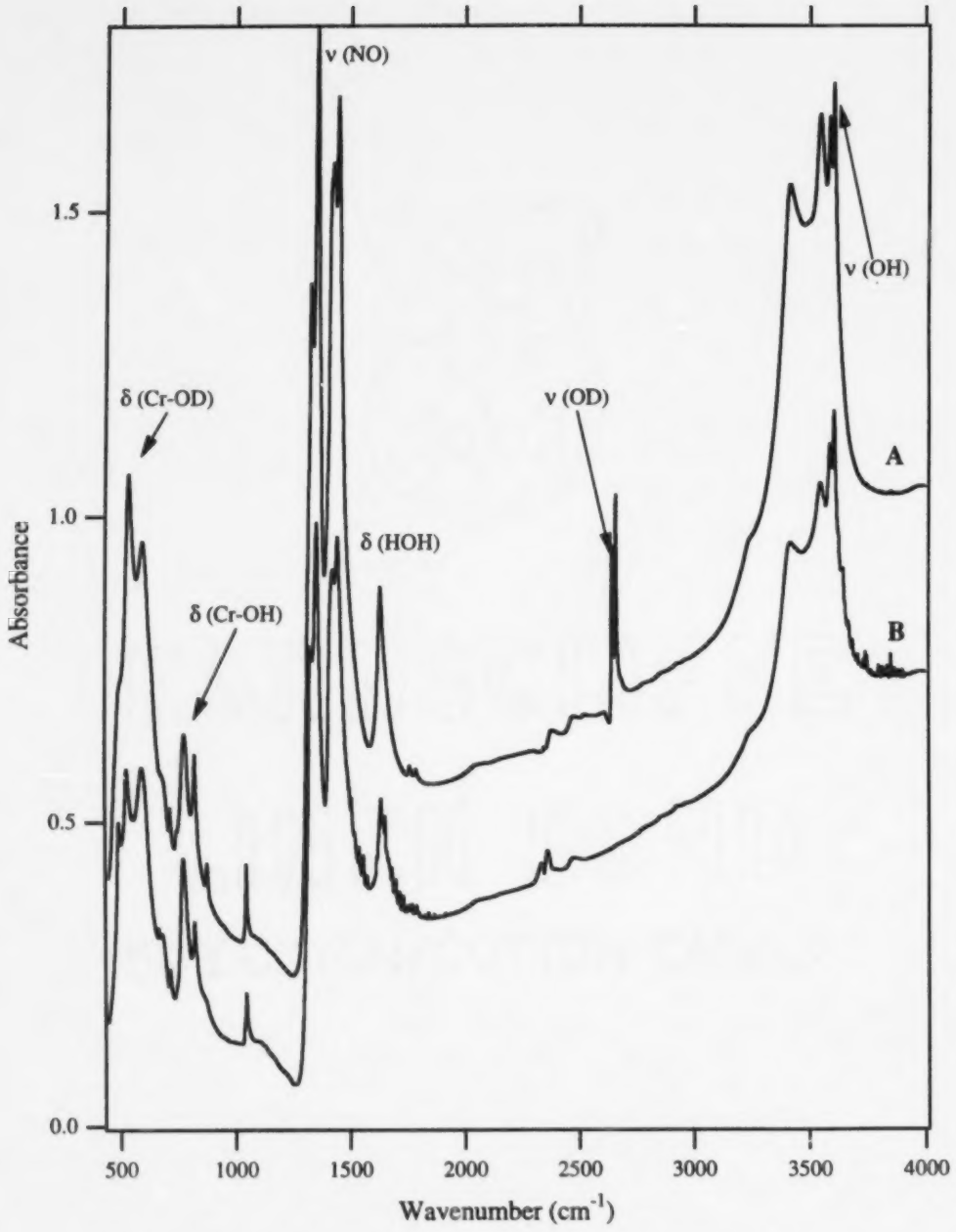

Fig. 4.3.2 FTIR spectra of early calcium chromium complex formed from;
(A) $Ca(OD)_2$ / $Cr(NO_3)_3.9H_2O$ in D_2O
(B) $Ca(OH)_2$ / $Cr(NO_3)_3.9H_2O$ in H_2O.

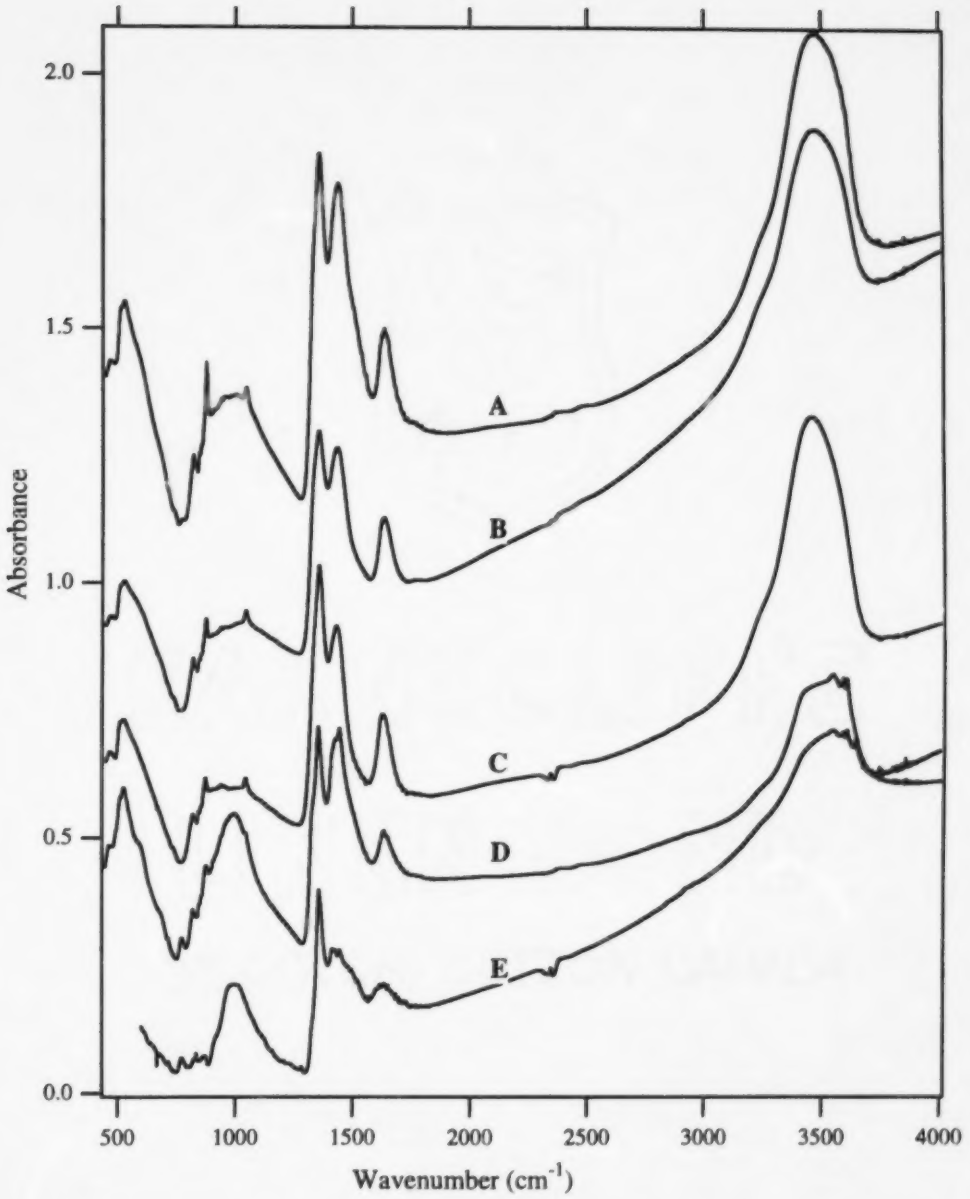

Fig. 4.3.3 FTIR spectra of exposed 2 M Cr(III) pastes hydrated for; (A) 5 mins, (B) 6 hours, (C) 24 hours, (D) 72 hours and (E) 60 days.

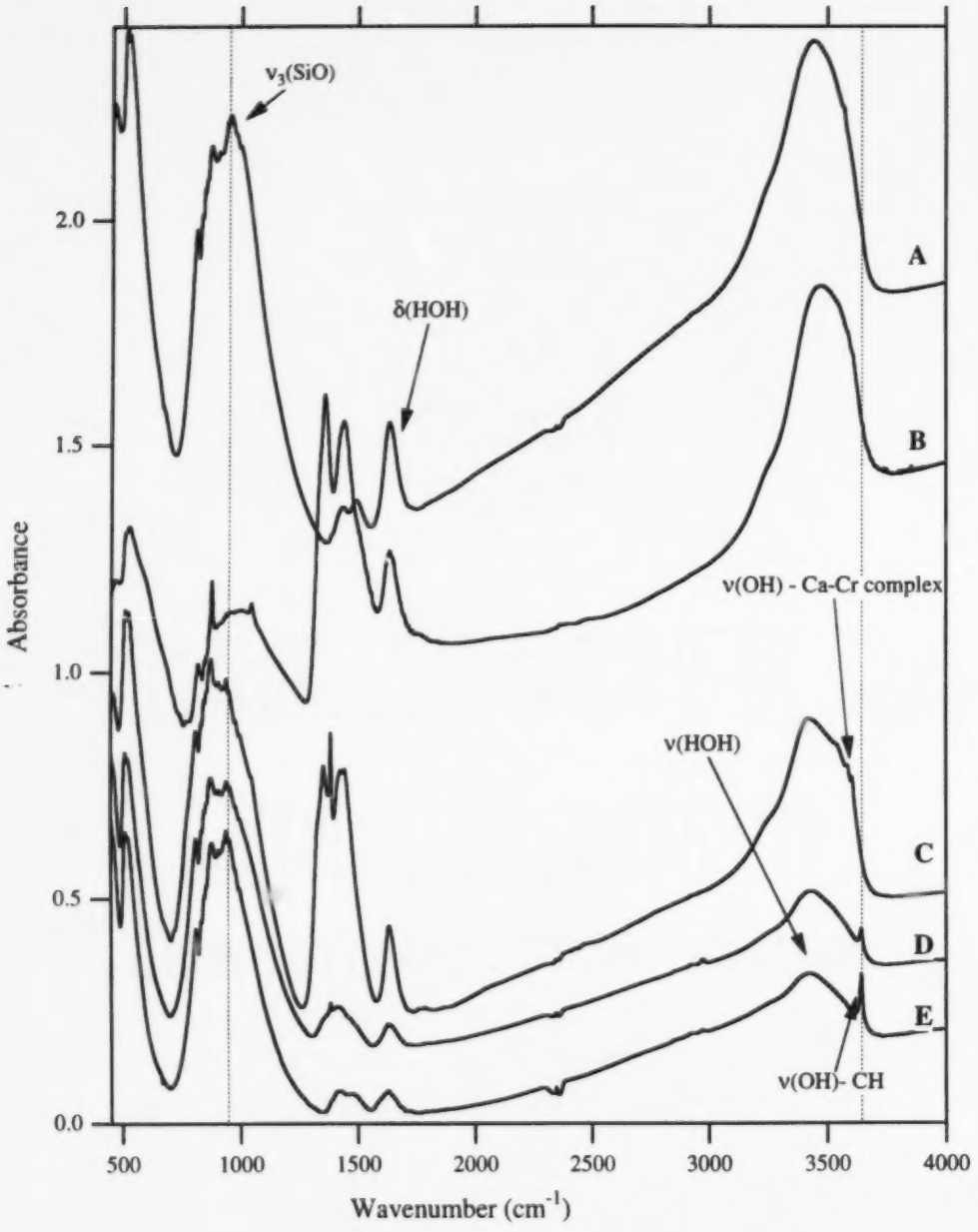

Fig. 4.3.4 FTIR spectra of varying Cr(III) concentrations in C_3S paste hydrated for 24 hours; (A) 1 M Cr(III) chloride, (B) 2 M Cr(III) nitrate, (C) 1 M Cr(III) nitrate, (D) 0.1 M Cr(III) nitrate and (E) blank.

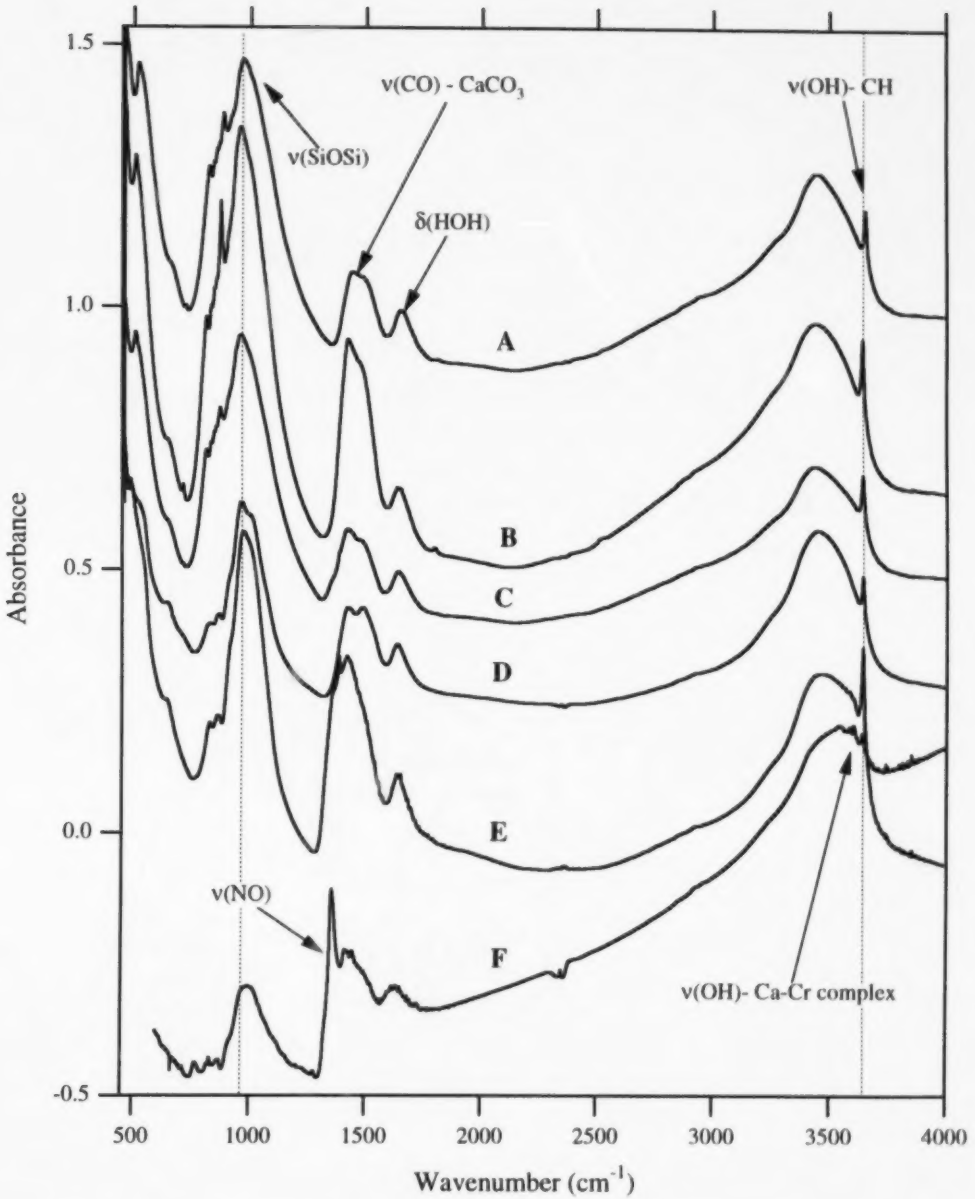

Fig. 4.3.5 FTIR spectra of 60 day old samples; (A) Blank, (B) 0.1 M Cr (III) chloride, (C) 0.1 M Cr (III) nitrate, (D) 1 M Cr (III) chloride, (E) 1 M Cr(III) nitrate and (F) 2 M Cr(III) nitrate.

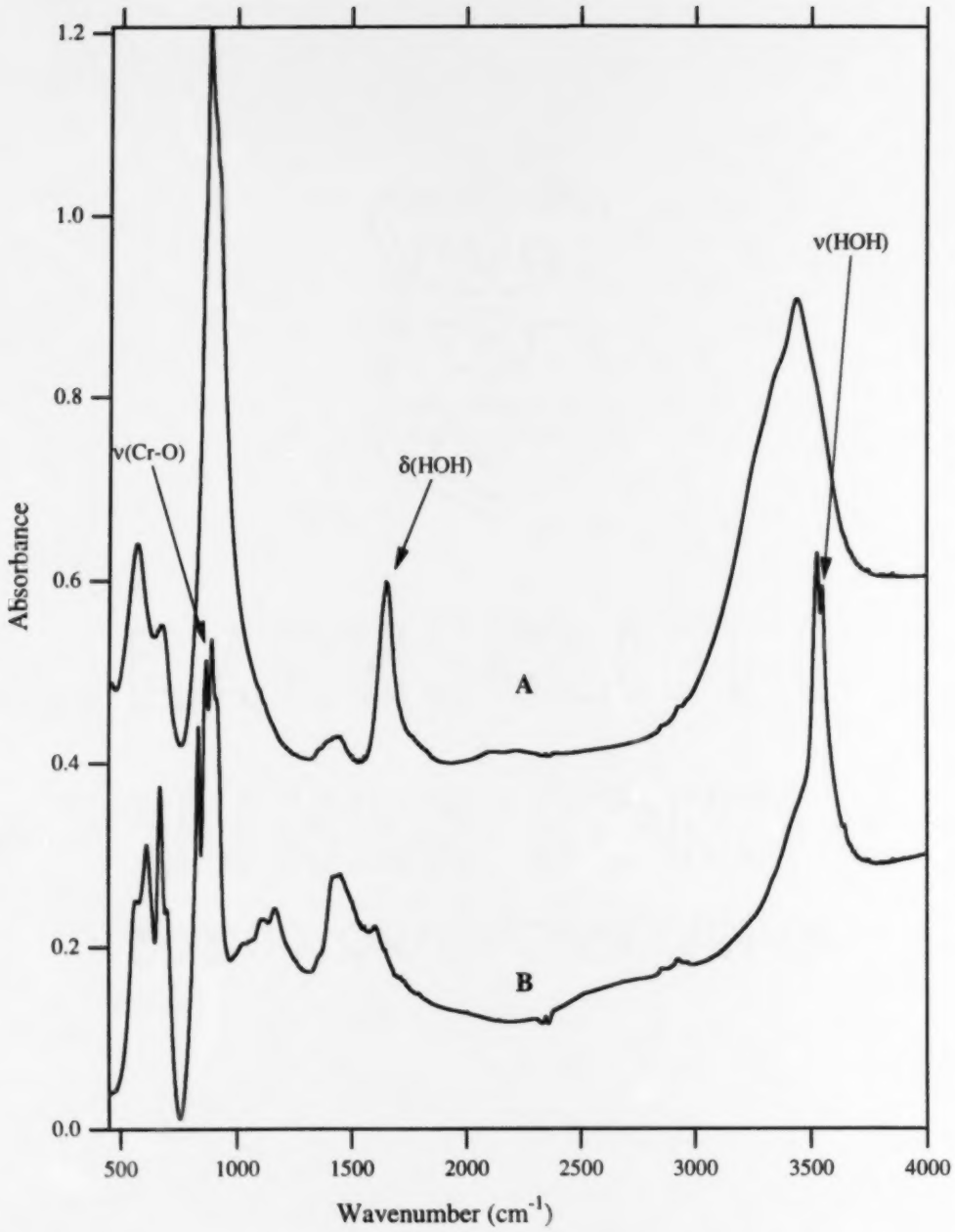

Fig. 4.3.6 FTIR spectra of calcium chromates formed during hydration of Cr(VI) doped C_3S (A) $CaCrO_4.2H_2O$ (B) $Ca_2CrO_5.3H_2O$.

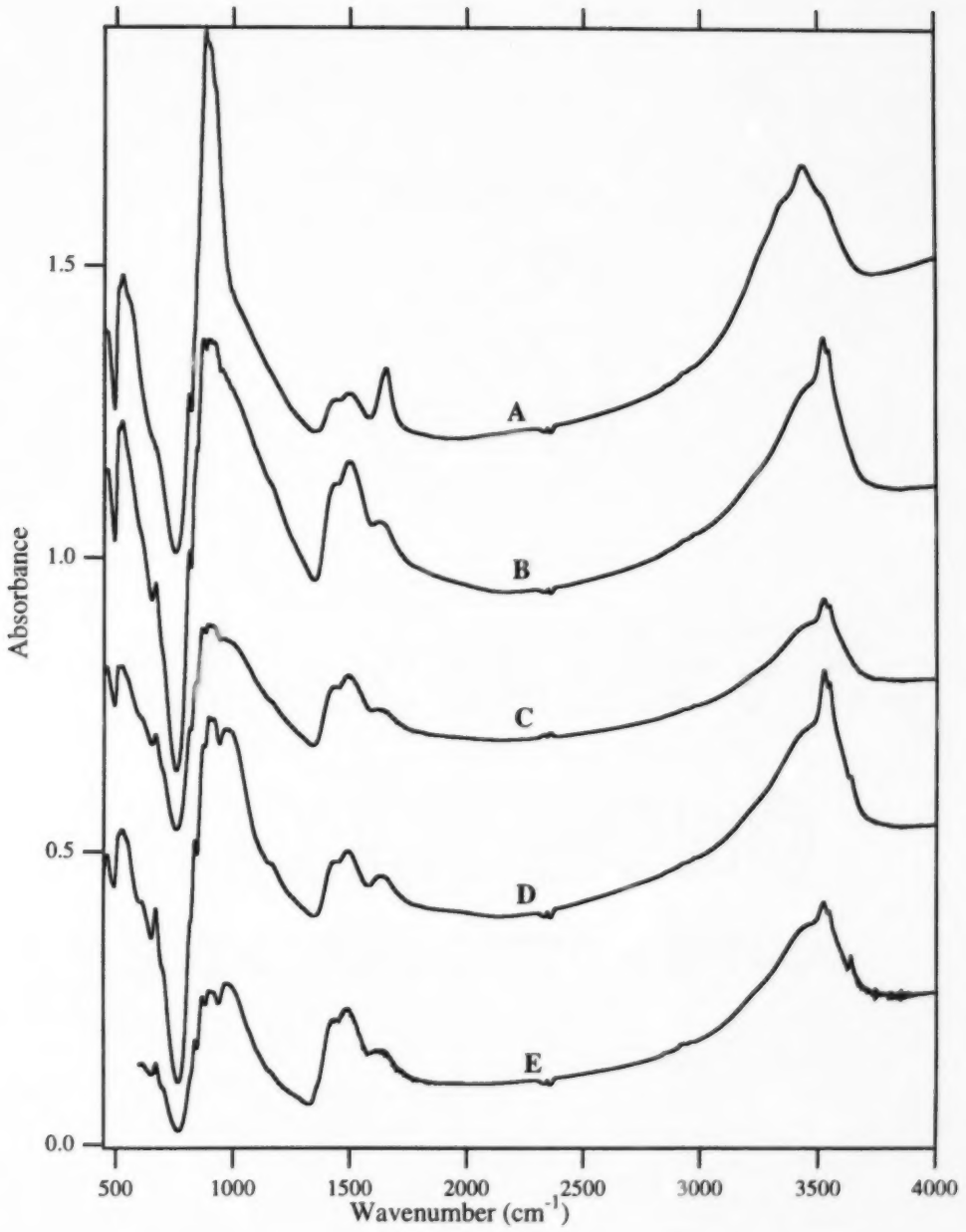

Fig. 4.3.7 FTIR spectra of exposed 2 M Cr(VI) pastes hydrated for; (A) 5 mins, (B) 6 hrs, (C) 24 hrs, (D) 72 hrs and (E) 60 days.

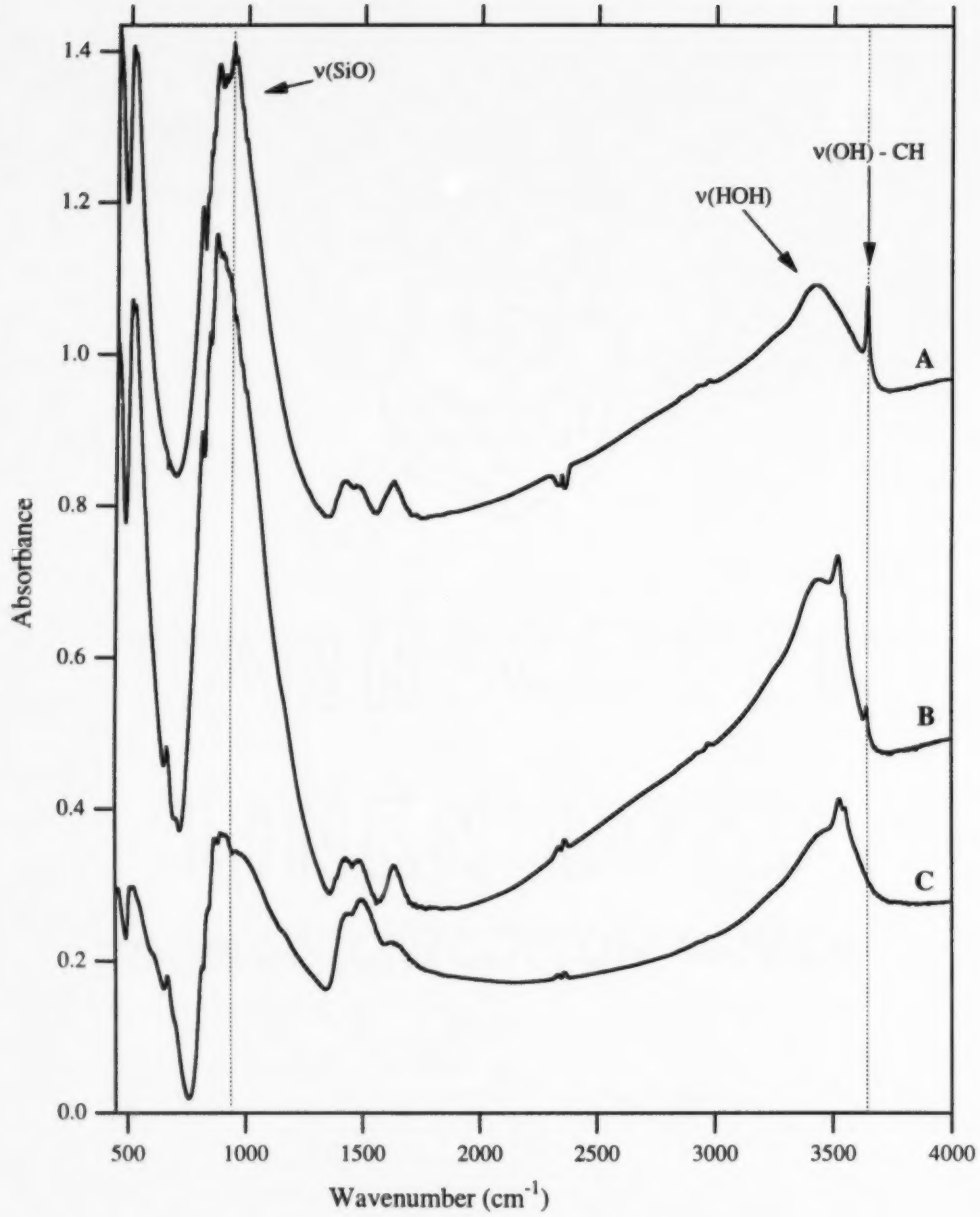

Fig. 4.3.8 FTIR spectra of 24 hour old Cr(VI) pastes;
(A) Blank, (B) 1 M Cr(VI) and (C) 2 M Cr(VI).

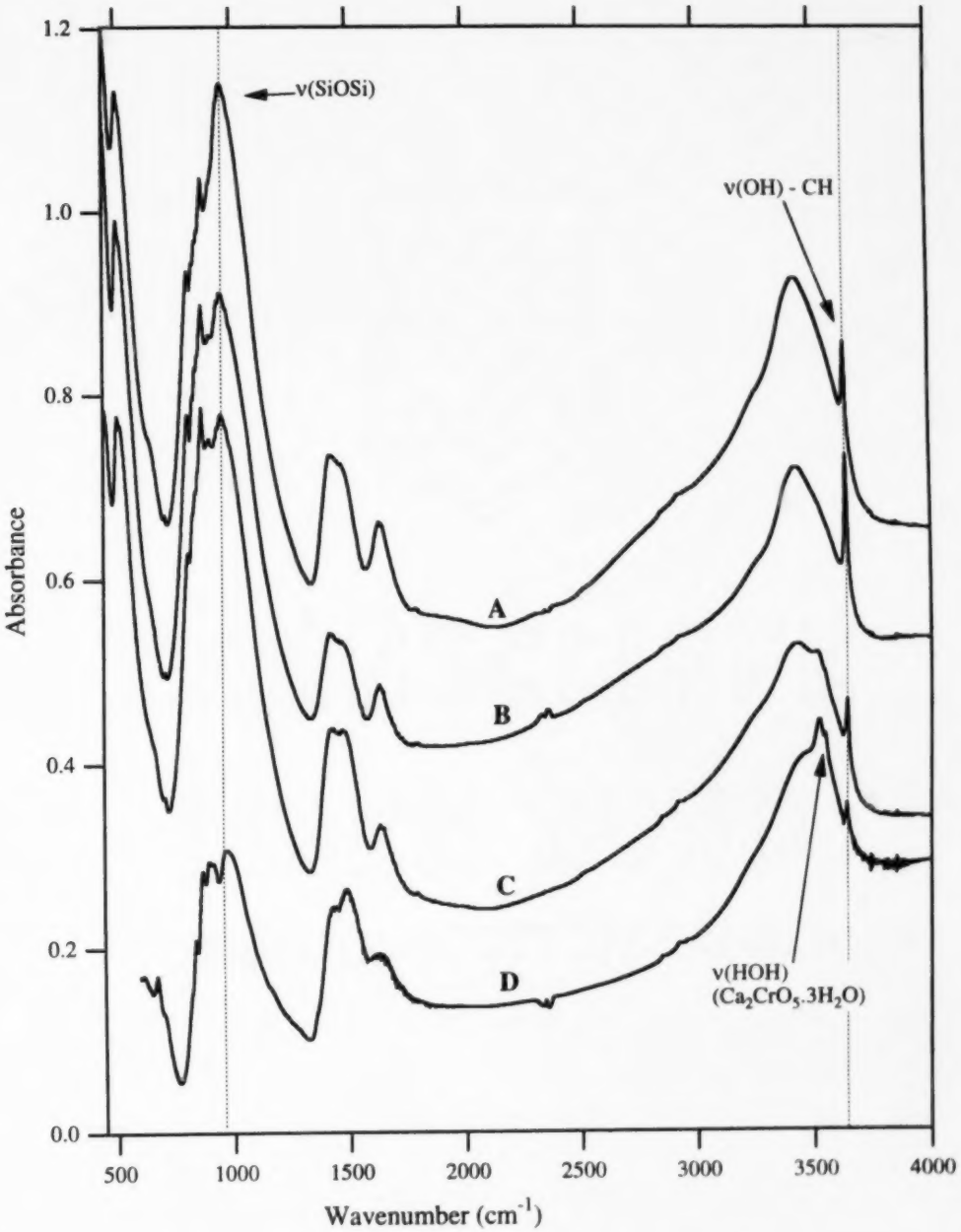

Fig. 4.3.9 FTIR spectra of 60 day old Cr(VI) pastes; (A) blank, (B) 0.1 M Cr(VI), (C) 1 M Cr(VI) and (D) 2 M Cr(VI).

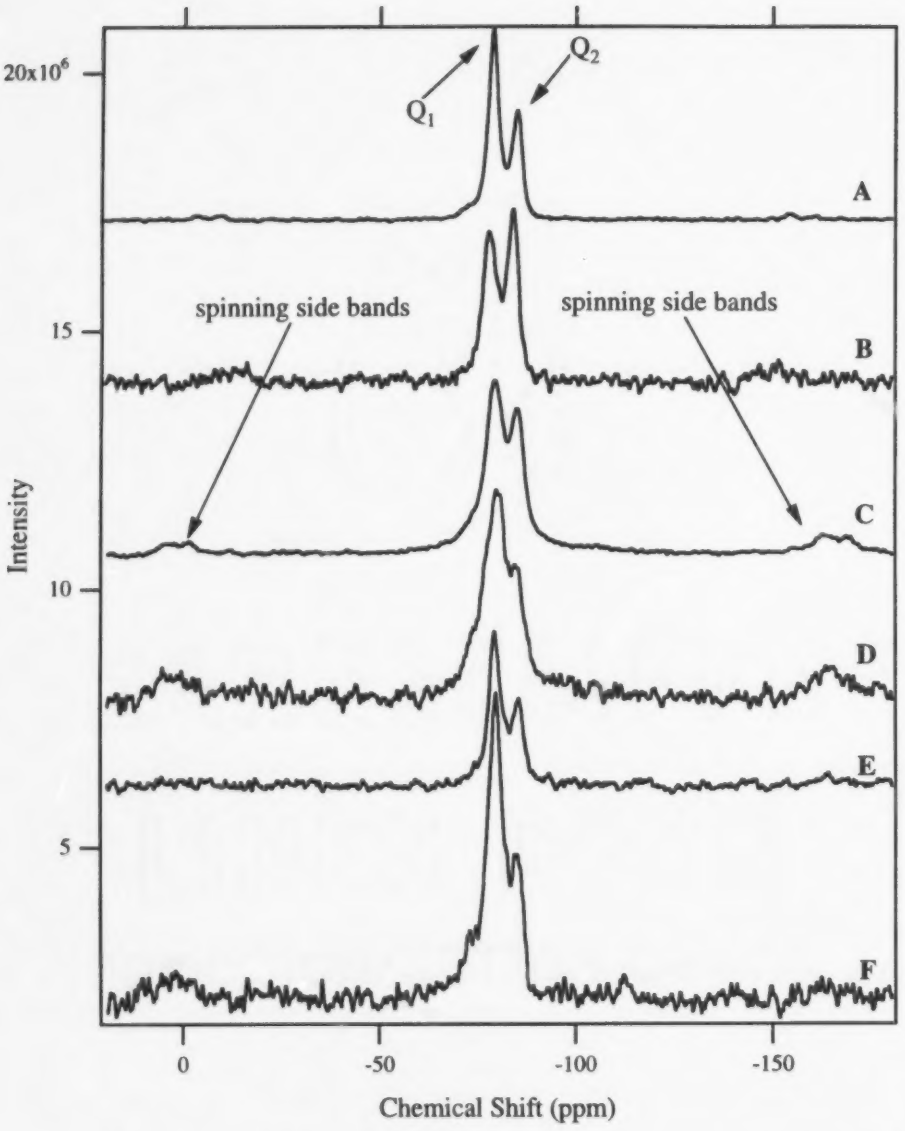

Fig. 4.4.1 ^{29}Si MAS NMR spectra obtained at 59.6 MHz, of partially and fully hydrated chromium doped tricalcium silicate pastes; (A) Blank - 14 months, (B) 2.75 M Cr(III) nitrate - 14 months, (C) 2 M Cr(III) nitrate - 60 days, (D) 2 M Cr(III) nitrate - 72 hours, (E) 2 M Cr(VI) - 60 days and (F) 2 M Cr(VI) - 72 hours.

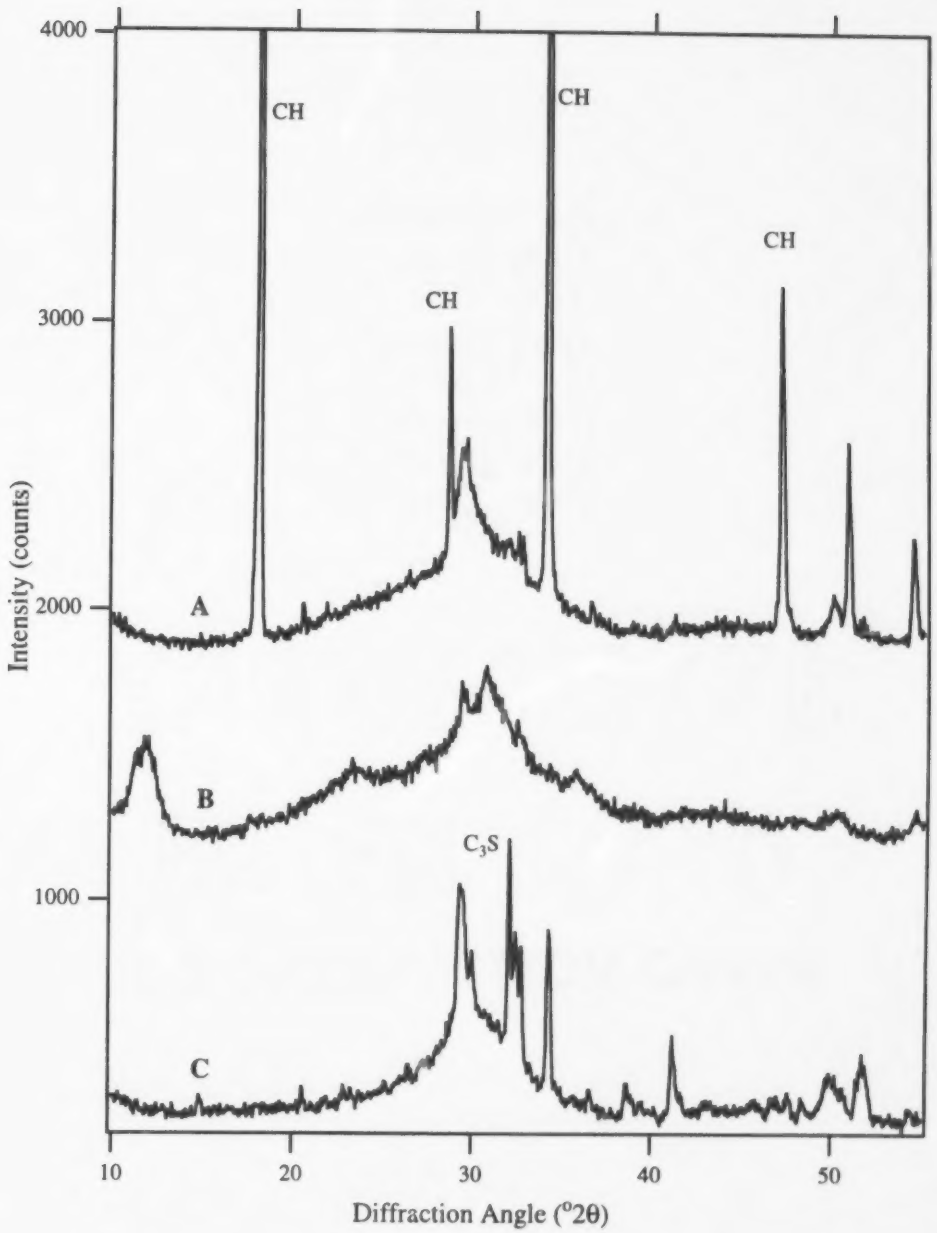

Fig. 4.5.1 XRD patterns of leached pastes; (A) 14 month old blank, (B) 14 month old 2.75 M Cr(III) and (C) 4 month old Cr(VI).

Chapter 5 Proposed Reaction Mechanisms

As previously reported in Chapter 2, two main hypotheses have been advanced to describe the mechanism of chromium containment in Portland cement and C_3S/alite matrices. These are summarized below:

1. Chromium substitutes for Si or Ca (or both) in C-S-H. The stability of the C-S-H network provides the necessary containment framework preventing chromium from leaching into solution (Tashiro et al. [1977], Roy et al. [1991], Mollah et al. [1992], Ivey et al. [1993]).
2. In the hydration of Cr(III) doped C_3S, chromium occurs as chromium hydroxide ($Cr(OH)_3.3H_2O$) which is insoluble in acetic acid leaching solution. In ordinary Portland cement, chromium replaces some or all of the aluminium present in the calcium aluminate hydrate phases of Portland cement pastes. These give the chromium analogue of $Ca_2Al(OH)_7.3H_2O$; $Ca_2Al_2O_5.(6\text{-}8)H_2O$ and $3CaO.Al_2O_3.6H_2O$ (Kindness et al. [1994]).

The tetrahedral nature of the silicate anion in C-S-H makes the first mechanism suspect. The most stable configuration of Cr(III) is in octahedral coordination, which would not be easily accommodated into Si sites. If Cr were to replace Ca, some Cr-O-Si bonds would form. This should give rise to distinct ^{29}Si NMR chemical shifts. Despite the high Cr concentrations used in some of our experiments, only the regular dimeric and polymeric silicate units were observed. Moreover, x-ray microanalysis should reveal high Cr/Si regions with little Ca. This was not observed in either the Cr-doped C_3S pastes polished or thin sections.

The wide variability and inhomogeniety of chromium contents in C-S-H regions might support the fact that insoluble $Cr(OH)_3.3H_2O$ formed and physically mixed with C-S-H on a very fine scale. If this is the case, $Cr(OH)_3.3H_2O$ will form during the early period of hydration within the pores. It should be very easy to isolate this phase since the pore sizes during the early period can be as large as 5 μm in diameter. Also, the hydration reaction would be slowed down since $Cr(OH)_3.3H_2O$ would form preferentially to CH. Because a certain degree of supersaturation of Ca^{2+} and OH^- is required to initiate CH formation, the reaction will be hindered until all the Cr has reacted. It has also been established that at a pH > 10.5, $Cr(OH)_3.3H_2O$ dissolves to form anionic chromium hydroxide (Giovanoli and Stadelmann [1973], Spiccia and Marty [1986]). The pH of hydrating C_3S paste is ~ 12. Continued dissolution of the C_3S will result in a C-S-H of a

higher than average Ca/Si ratio (~ 1.7). In fact, the reverse is the case in our experiments where a decrease in the Ca/Si ratio was observed with increasing chromium concentrations. In addition, no crystalline $Cr(OH)_3.3H_2O$ phase was observed in the XRD patterns and no hydroxyl absorption corresponding to $Cr(OH)_3.3H_2O$ (amorphous or crystalline) was observed in FTIR.

5.1 Containment Mechanism of Cr(III) in C_3S Pastes

The chromium nitrate solution contains $Cr(H_2O)_6^{3+}$, H^+ and NO_3^-. On contact with anhydrous C_3S, Ca^{2+}, O^{2-} and SiO_4^{4-} go into solution. The increasing amount of OH^- formed increases the pH. Because of the weak ligand field exercised by the water molecules in the hexaquo ion, rapid deprotonation of the hexaquo ion is expected to occur with OH^- and SiO_4^{4-} being potential ligand substitutes. Since no hydroxide (calcium or chromium) was found within the first few minutes of reaction from XRD and FTIR data, it is possible that cationic calcium and chromium ions adsorbed on the anionic silicate surface. This would cause precipitation of an unstable active calcium - chromium - silicate - hydrate. A plausible network might be for Ca polyhedra acting as a bridge for silicate tetrahedra and chromium octahedra. It has been established that silanol groups begin to adsorb most polyvalent metal ions (calcium and chromium inclusive), when the pH is raised to within 1 - 2 points below the pH at which the metal hydroxide starts to precipitate (James and Healy [1972], Olsen and O'meila [1973], Schindler et al. [1976]). As more C_3S dissolves, the pH increases which might cause the active calcium - chromium - silicate - hydrate to dissociate into more stable states. It is believed that this initial precipitate dissociates to form stable early C-S-H and the early Ca-Cr complex $[Ca_3Cr(OH)_6(NO_3)_3]_2.(12\text{-}x)H_2O$. As could be seen from the electron micrographs of 1 day old Cr(III) doped pastes (Fig. 4.2.11), the early C-S-H forms a gel-like phase as opposed to the fibrous structure characterizing dimeric C-S-H. The early Ca - Cr complex appears as rods emanating from the gel like phase containing Ca, Si and Cr. Depending on the amount of Cr present in the paste, more $[Ca_3Cr(OH)_6(NO_3)_3]_2.(12\text{-}x)H_2O$ forms as more Ca^{2+} becomes available in the pore solution. At the same time the C-S-H interface grows inwards with Ca^{2+} and, to a lesser extent, Si^{4+} diffusing outwards and H^+ diffusing inwards to form the late polymeric C-S-H. The absence of Cr in the late C-S-H shows that Cr^{3+} does not migrate across the early C-S-H interface. The reaction is accelerated possibly because of the concentration gradient developed between the reactive C_3S grain and the pore space harboring a reactive calcium - chromium - silicate phase. The high Ca content of the Ca - Cr complex necessitates a reduction in the amount of Ca^{2+} available to form C-

S-H with an average Ca/Si ratio ~ 1.7. This will result in the increased formation of highly condensed C-S-H. This is consistent with ^{29}Si NMR studies which show that more Q_2 (polymeric C-S-H) than Q_1 (dimeric C-S-H) formed in a fully hydrated paste. X-ray microanalysis in the TEM also indicates the absence of Cr in the late C-S-H and a wide variability of Ca/Si ratios of Cr - free C-S-H. Many areas with Ca/Si ratio < 0.5 were observed. This is much lower than the lower limit of ~ 0.8 obtained in the blank pastes. The ^{29}Si NMR chemical shift data also indicated the line broadening of the Q_1 units, which reduced with age. This is a further indication that most of the Cr chemically incorporated in the C-S-H at a molecular level during the early stages, gradually precipitated out with age.

It could also be inferred from XRD studies that the presence of a secondary source of moisture affects the reaction mechanism. If the reaction is carried out in an enclosed environment with no secondary source of moisture, as soon as most of the Cr is complexed, the normal hydration reaction continues with the formation of CH and C-S-H. The final product will thus contain $[Ca_3Cr(OH)_6(NO_3)_3]_2.(12\text{-}x)H_2O$, CH, C-S-H (Cr free) and some stable C-S-H containing highly localized Cr. The Cr containing C-S-H forms during the early stages of hydration. On the other hand, if the paste is exposed to a humid atmosphere, the highly reactive components will absorb moisture. This causes $[Ca_3Cr(OH)_6(NO_3)_3]_2.(12\text{-}x)H_2O$ to decompose to give the late Ca - Cr complex (Ca/Cr ratio = 2) and CH (shown in Equation 4.1). The CH formed from this reaction is visible as crystals growing from the supersaturated solution that collects on the paste. This also accounts for the excessive preferred orientation exhibited by the (001) plane in CH diffraction peaks. Total decomposition of the early Ca - Cr complex will occur over time. In both cases, the residual chromium associated with C-S-H should be unaffected.

The formation of the Ca - Cr complexes depends on the concentration of chromium in the hydrating paste. Thus at the lower chromium concentrations of ~ 0.1 M Cr(III), typical of chromium waste streams, small amounts of the Ca - Cr complexes are formed which may not be visible given the detection limits of XRD and FTIR spectroscopy. Some of the Cr will also be chemically incorporated in the C-S-H as discussed above.

5.2 Containment Mechanism of Cr(VI) in C_3S Pastes

Despite the similar nature of the CrO_4 and SiO_4 tetrahedra, Cr(VI) has not been observed to be chemically contained within the C-S-H matrix. As opposed to Cr(III) solutions which contain cationic hexaquo species, a typical Cr(VI) solution contains acidic $HCrO_4^- + H^+$.

As Ca^{2+}, O^{2-} and SiO_4^{4-} go into the Cr(VI) solution, formation of OH^- increases the pH leading to the formation of early C-S-H and calcium chromate. The formation of calcium chromate is represented in equation 5.1 below;

$$Ca^{2+} + 2OH^- + HCrO_4^- + H^+ \rightarrow CaCrO_4.2H_2O \quad (5.1)$$

This phase was observed as long hexagonal rods within 5 minutes of hydration (2 M Cr(VI) paste). C-S-H formed in close proximity to the C_3S grains away from the $CaCrO_4.2H_2O$ rods. As the pH increases and more Ca comes into solution, $CaCrO_4.2H_2O$ becomes unstable and forms $Ca_2CrO_5.3H_2O$ as shown in equation 5.2.

$$CaCrO_4.2H_2O + Ca^{2+} + 2OH^- \rightarrow Ca_2CrO_5.3H_2O \quad (5.2)$$

This phase persisted throughout the hydration period. As soon as all the Cr has been consumed, CH starts to form. Both dimeric and polymeric C-S-H are expected to be forming throughout the course of hydration. From FTIR studies, increased condensation of C-S-H was observed especially in the 2 M Cr(VI) pastes. This can also be attributed to the depletion of Ca available for the formation of CH and C-S-H. The Q_2/Q_1 ratio of ~ 0.5 obtained in the ^{29}Si NMR data of partially hydrated 60 day old 2 M Cr(VI) paste, is greater than the Q_2/Q_1 in fully hydrated blank paste (0.37). Ideally, in hydrating blank pastes, the Q_2/Q_1 ratio reaches a maximum of ~ 0.37 when all C_3S has reacted. This further attests to the increased condensation of the C-S-H units impacted by Cr(VI) ions.

It appeared as if some of the $Ca_2CrO_5.3H_2O$ redissolved in the high alkaline environment of the hydrating paste (pH ~ 12). The decrease obtained from QXRD (Table 4.1) could not be attributed to experimental errors or the loss of water when the reaction was stopped with isopropyl alcohol. The decrease is linear in both the 1 M and 2 M pastes, despite the fact that both experiments were carried out two years apart using different batches of Cr(VI) solutions. The location of the Cr(VI) ions rejected from $Ca_2CrO_5.3H_2O$ is not evident from the experiments carried out. However, some of the CrO_4 units might be located in the tetrahedral SiO_4 sites without creating too much distortion within the C-S-H. This could account for the absence of $Ca_2CrO_5.3H_2O$ in the leached solid which still has some unleached Cr. The same reaction mechanism occurs in the low concentration Cr(VI) pastes, the difference being in the rate of formation of CH and the condensation of C-S-H which increases with Cr(VI) content.

Chapter 6 Conclusions and Recommendations

6.1 Conclusions

The following conclusions can be drawn from the results discussed in Chapters 4 and 5.

- The simulation of ordinary Portland cement with C_3S is justified in view of the fact that Cr(III) is adequately stabilized in C_3S, whereas Cr(VI) is not. The same results have been obtained by several investigators as noted in Chapter 2.

- Two types of Ca - Cr hydroxide complexes were identified in Cr(III) doped C_3S pastes. The early complex has a Ca/Cr mole ratio of 3, and usually starts to form within a few hours, increasing in concentration until most of the Cr has been consumed. If the reacting waste form is exposed continuously to water vapor in a humidifying chamber, this early complex decomposes within a few days to form CH and a late Ca - Cr complex with a Ca/Cr mole ratio of 2. In an environment devoid of moisture, the early Ca - Cr complex is retained at the completion of hydration.

- Small amounts of Cr(III) are inhomogeneously chemically incorporated in the early C-S-H, independent of the hydration environment and to a lesser extent, the concentration of Cr in the reacting mixture. The Cr(III) octahedra are possibly connected to the silicate tetrahedra through Ca - O linkages.

- Increasing Cr concentration increases the condensation of the silicate units. This is manifested in the increased ratio of polymeric C-S-H to dimeric C-S-H. The rate of C_3S reaction is also increased with increasing Cr additions.

- No evidence of Cr(III) replacing Si in tetrahedral sites has been found within the experimental framework studied.

- $Cr(OH)_3.3H_2O$ (crystalline or amorphous) was not observed at any stage of hydration reaction.

- Depending on the concentration of Cr(VI) in the doped paste, soluble $CaCrO_4.2H_2O$ formed within a few minutes of hydration when the Cr/Ca ratio was > 1. Increasing the concentration of Ca^{2+} in the pore solution results in the formation of a more stable and partially soluble $Ca_2CrO_5.3H_2O$ phase, which persisted throughout the period of hydration.

- As opposed to the Ca - Cr complex which increases with age, $Ca_2CrO_5.3H_2O$ was found to decrease slightly with age. Small amounts of the residual Cr^{6+} possibly occupy tetrahedral sites in the C-S-H.

- Condensation of the silicate units increases with increasing Cr(VI) concentration but not as for Cr(III).

- The rate of C_3S consumption increases with increasing Cr(VI) concentration but to a lesser extent than Cr(III).

6.2 Recommendations

To completely characterize the containment of chromium in C_3S or Portland cement matrices, the following are suggested:

- Attempts should be made to grow single crystals of $Ca_2CrO_5.3H_2O$ and the early and late Ca - Cr complexes to facilitate structure determination of these previously uncharacterized phases.

- Direct evidence of chromium coordination in C-S-H should be obtained with extended x-ray absorption fine structure (EXAFS) of the CrL edge and SiK edge. This has been difficult using electron energy extended fine edge structure in the TEM because the oxygen K edge overlaps with the CrL edge. Electron paramagnetic resonance and ^{53}Cr solid state MAS NMR would also yield useful information on the oxidation state of Cr in the waste forms.

- Pore solution analyses and pH determination should be carried out at regular intervals especially during the early periods of hydration. This will aid determination of the pore solution speciation and subsequent development of a thermodynamic model for the hydration reaction.

References

Barnes, J.R., Clague, A.D.H., Clayden, N.J., Dobson, C.M., Hayes, C.J., Groves, G.W. and Rodger, S.A. (1985), *J. Mater. Sci. Lett..*, **4:** 1293.

Beaudoin, J.J. (1987), *Mater. Const.*, **20:** 27.

Bennet, L.H. and Swartzendruber, L.J. in *Metals Handbook*, Ninth Edition **10:** 277 (1986).

Bensted, J. and Varma, S.P. (1971), *Cem. Technol.*, **2:** 73, 100.

Bensted, J. and Varma, S.P. (1972), *Silicates Industriels*, **37:** 315.

Bensted, J. and Varma, S.P. (1973), *Cem. Technol.*, **4:** 112.

Bensted, J. and Varma, S.P. (1974), *Cem. Technol.*, **5:** 256, 378, 440.

Bentur, A. and Berger, R.L. (1979), *J. Am. Ceram. Soc.*, **62:** 117.

Bishop, P.L. (1988), *Hazardous Waste and Hazardous Materials*, **5:** 129.

Bishop, P.L., Ransom, S.B. and Gress, D.L., *Proceedings of the Industrial Waste Conference*, Purdue University, 395 (1983).

Boehm, H.P. (1966), *Advances in Catalysis*, **16:** 179.

Bonen, D., Johnson, T.J. and Sarkar, S.L. (1994), *Cem. Concr. Res.*, **24:** 959.

Briggs, D. and Seah, M.P., *Practical Surface Analysis, 2nd ed.*, Wiley, New York (1990).

Brown, P.W., Galuk, K. and Frohnsdorff, G. (1984), *Cem. Concr. Res.*, **14:** 843.

Butler, L.G., Cartledge, F.K., Eaton, H.C. and Tittlebaum, M.E. in *Proceedings of the Chemistry and Microstructure of Solidified Waste Forms*, ed. R.D Spence, Lewis Publishers, 151 (1993).

Campbell, D.H. and Ahmed, W.U. (1979), *Microstructural Science*, **7:** 369.

Carteledge, F.K., Butler, L.C., Chalsani, D., Eaton, H.C., Frey, F.P., Herrera, E., Tittlebaum, M.E., and Yang, S.L. (1990), *Environ. Sci and Tech.*, **24:** 867.

Carteledge, F.K., *Private Communication.*

Clayden, N.J., Dobson, C.M., Groves, G.W., Hayes, C.J. and Rodger, S.A. (1984), *British Ceramic Society Proceedings,* **35:** 55.

Cocke, D.L. (1990), *J. Hazardous Materials.,* **24:** 221.

Cocke, D.L., McWhinney, H.G., Duffner, D.C., Hornell, B. and Ortego, J.D. (1989), *Hazardous Wastes and Hazardous Materials,* **6:** 84.

Dalgleish, B.J. and Ibe, K. (1981), *Cem. Concr. Res.,* **11:** 729.

Day, R.L. (1982), *Cem. Concr. Res.,* **11:** 341.

Diamond, S., in *Hydraulic Cement Pastes; Their Structure and Properties,* Conference Proceedings, Cement and Concrete Association, 2 (1976).

Double, D.D. (1973), *Mat. Sci. & Eng.*, **12:** 29.

Edge, R. and Taylor, H.F.W (1971), *Acta Cryst.,* **B27:** 594.

Effenberger, H., Kirfel, A., Will, G. and Zobetz, E. (1983), *Neues Jahrb. Mineral. Monatsh.,* 60.

Environmental Protection Agency Federal Register (1986), **51:** 21685.

Environmental Protection Series, *Compedium of Waste Leaching Tests,* Environment Canada, EPS 3/HA/7, 6 (1990).

Etchepare, J. (1970), *Spectrochimica Acta,* **26A:** 2147.

Fierens, P. and Verhaegen, J.P. (1976), *Cem. Concr. Res.,* **6:** 337.

Gadsden, J.A., *Infrared Spectra of Minerals and Related Inorganic Compounds,* Butterworths, 1975.

Gard, J. A., Mohan, K., Taylor, H.F.W. and Cliff, G. (1981), *J. Am. Ceram. Soc.,* **63:** 336.

Gartner, M.E. and Jennings, H.M. (1987), *J. Am. Ceram. Soc.*, **70:** 743.

Ghosh ,S.N and Chatterjee, A.K (1974), *J. Mater. Sci.*, **9:** 1577.

Giovanoli, R. and Stadelmann, W. (1973), *Thermochimica Acta*, **7:** 41.

Glasser, F.P. in *Proceedings of the Chemistry and Microstructure of Solidified Waste Forms*, ed. R.D Spence, Lewis Publishers, 1 (1993).

Golovastikov, N.I., Matveeva, R.G. and Belov, N.V. (1976), *Sov. Phys. Cryst.*, **20:** 441.

Goto, S., Daimon, M., Hosaka, G. and Kondo, R. (1976), *J. Am. Ceram. Soc.*, **59:** 281.

Greenwood, N.N. and Earnshaw, A., Chemistry of the Elements. Pergamon, New York, 1190 (1984).

Grimmer, A.R. and Von Lampe, F. (1986), *Chemical Physics Letters*, **132:** 549.

Groves, G.W . (1987), *Mater. Res. Soc. Symp. Proc.*, **85:** 3.

Grudemo, A., in *The Chemistry of Cement*, ed. H.F.W. Taylor, Academic Press, Part I, 371 (1964).

Gutteridge, W.A. (1984), *British Ceramic Proceedings*, **35:** 11.

Handke, M. (1986), *Applied Spectroscopy*, **40**: 871.

Handke, M. and Jurkiewicz, M.E. (1979), *Ann. Chim. Fr.*, **4:** 145.

Hassan, M.Y and Abdel-Hakeem, N. (1989), *J. Mater. Sci. Lett.*, **8:** 578.

Heimann, R.B. (1986), *Glass Technology*, **27:** 96.

Heimann, R.B., Conrad, D., Florence, L.Z., Neuwirth, M., Ivey, D.G., Mikula, R.J. and Lam, W.W. (1991), *J. Hazardous Mater.*, **31:** 39.

Hjorth, J., Skibsted, J. and Jakobsen, H.J. (1988), *Cem. Concr. Res.*, **18:** 789.

Iler, R.K., *The Chemistry of Silica*. John Wiley, N.Y. 1979.

Ingamells, C.O. and Pitard, F.F., *Applied Geochemical Analysis,* John Wiley, New York, p120 (1986).

Ishida, H., Okada, Y. and Mitsuda, T. (1992), *J. Am. Ceram. Soc.,* **75:** 359.

Ivey, D.G. and Neuwirth, M. (1989), *Cem. Concr. Res.,* **19:** 642.

Ivey, D.G., Mikula, R.J., Lam, W.W., Neuwirth, M., Conrad, D.J. and Heimann, R.B., in *Cement Industry Solutions to Waste Management.* Proc. Can. Port. Cem. Assoc. Symp. Calgary (1992).

Ivey, D.G., Mikula, R.J., Lam, W.W., Neuwirth, M., Conrad, D.J., Heimann, R.B., in *Proceedings of the Chemistry and Microstructure of Solidified Waste Forms,* ed. R.D Spence, Lewis Publishers, 123 (1993).

James, R.O. and Healy, T.W. (1972), *J. Colloid and Interface Sci.,* **40:** 65.

Jawed, I., Skanly, J. and Young, J.F., in *Structure and Performance of Cement,* ed. P. Barnes, Applied Science Publishers, 237 (1983).

Jeffery, J.W. (1952), *Acta Cryst.,* **5:** 26.

Jennings, H.M. (1986), *J. Am. Ceram. Soc.,* **69:** 614.

Jennings, H.M. and Parrot, L.J. (1986), *J. Mater. Sci.,* **21:** 4053.

Jennings, H.M., Dalgleish, B.J. and Pratt ,P.L. (1981), *J. Am. Ceram. Soc.,* **64:** 567.

Joy, D.C., Romrig, A.D. and Goldstein, J.I., *Principles of Analytical Electron Microscopy,* Plenum Press, N.Y (1986) .

Kantro, D.L. (1975), *J. Testing & Evaluation,* **3:** 312.

Keller, R., *Basic Tables in Chemistry,* McGraw Hill, New York (1967).

Kerton, C.P. and Murray, R.J., in *Structure and Performance of Cement.*, ed. Barnes, P. Applied Science Publishers, 205 (1983).

Kindness, A., Macia,s A. and Glasser, F.P. (1994),*Waste Management,* **14:** 3.

Klug, H.P. and Alexander, L.E., *X-ray Diffraction Procedures for Polycrystalline and Amorphous Materials,* John Wiley, New York (1974).

Komarneni, S. and Tsuji, M. (1989), *J. Am. Ceram. Soc.*, **72:** 1668.

Kondo, R., and Daimon, M. (1969), *J. Am. Ceram. Soc.*, **52:** 503.

Kondo, R., Daimon, M., Sakai, E., and Oshiyama, H.J. (1977), *J. Appl. Chem. Biotechnol.*, **27:** 191.

Larsen, E.M., Transitional Elements. W.A Benjamin, New York (1965).

Lawrence Jr., F.W. and De Carvalho, A.A. (1974), *J. Am. Ceram. Soc.*, **57:** 144.

Lazarev, A. N., *Vibrational Spectra and Structure of Silicates,* Consultant Bureau, New York (1972).

Lee, F.C., Banda, H.M. and Glasser, F.P. (1982), *Cem. Concr. Res.*, **12:** 237.

Libeau, F., *Structural Chemistry of Silicates,* Springer - Verlag, Berlin (1985).

Lippmaa, E., Magi, M., Samson, A., Engelharrdt, G. and Grimmer, A.R. (1980), *J. Am. Soc.* **102:** 4889.

Lippmaa, E., Magi, M., Tarmak, M., Wieker, W. and Grimmer, A.R. (1982), *Cem. Concr. Res.*, **12:** 597.

Marchese, B. (1977), *Cem. Concr. Res.*, **7:** 9.

Marchese, B. (1988), *J. Am. Ceram. Soc.* **61:** 349.

Marcott, C., in *Metals Handbook,* Ninth Edition, **10:** 109 (1986).

Matossi, F. (1949), *J. Chem. Phy.*, **17:** 679.

McWhinney, H.G., Cocke, D.L., Balke, K. and Ortego, J.B. (1990), *Cem. Concr. Res.*, **20:** 79.

Means, J.L., Smith, L.A., Nehrig, K.L.W., Brauning, S.E., Gavaskar, A.R., Sass, B.M., Wiles, C.C. and Mashni C.I., *The Application of Solidification/Stabilization to Waste Materials,* Lewis Publishers, Boca Raton (1995).

Menetrier, D., Jawed, I., Sun, T.S. and Skanly, J. (1979), *Cem. Concr. Res.*, **9:** 473.

Midgley, H.G. (1979), *Cem. Concr. Res.*, **9:** 77.

Mohan, K. and Taylor, H.F.W. (1981), *J. Am. Ceram. Soc.*, **64:** 717.

Mollah, M.Y.A., Yung-Nien Tsai, Hess, T.R. and Cocke, D.L. (1992), *J. Hazardous Mater.*, **30:** 273.

Montgomerry, D.M., Sollars, C.J, , and Perry, R. (1988),*Waste Manag. Res.*, **6:** 217.

Moore, A.E. and Taylor, H.F.W. (1968), *Nature*, **218:** 1048.

Moore, A.E. and Taylor, H.F.W. (1970), *Acta Cryst.*, **B26:** 386.

Nakamoto, K., *Infrared and Raman Spectra of Inorganic and Coordination Compounds 4th Edition*, John Wiley (1986).

Nocun-Wczelik, W. (1990), *Journal of Thermal Analysis*, **36:** 2109.

Nyquist, R.A., *Infrared Spectra of Inorganic Compounds (3800 - 45 cm^{-1})*, Academic Press, New York (1971).

Odler, I. and Dorr, H. (1977), *Cem. Concr. Res.*, **9:** 277.

Odler, I. and Dorr, H. (1979), *Cem. Concr. Res.*, **9:** 239.

Okamoto, J.K., Pearson, D.H., Ahn, C.C. and Fultz, B., in *Transmission Electron Energy Loss Spectrometry in Material Science*. EMPMD Monograph Series, TMS Warrendale **2:** 183 (1992).

Olsen, L.L. and O'melia, C.R. (1973), *J. Inorg. Nucl. Chem.*, **35:** 1977.

Omotoso, O.E., Ivey, D.G. and Mikula, R. (1995), *J. Haz. Mater.*, **42:** 87.

Ortego, J.D., Barroeta, Y., Cartledge, F.K. and Akhter, H. (1991), *Environ. Sci. Tech.*, **25:** 1171.

Parry - Jones, G., Al - Tayyib, A.J. and Al - Mana, A.I. (1988), *Cem. Concr. Res.*, **18:** 229.

Parry - Jones, G., Al - Tayyib, A.J. and Al - Mana, A.I. (1989), *Cem. Concr. Res.*, **19:** 228

Poellman, H., St. Auer, Kuzel, H.J. and Wenda, R. (1993), *Cem. Concr. Res.*, **23:** 422.

Poon, C.S., Clark, A.I., Perry, R., Barker, A.P. and Barnes, P. (1986), *Cem. Concr. Res.*, **16:** 161.

Poon, C.S., Clark, A.I., Peters, C.J. and Perry, R. (1985b),*Waste Manag. Res.*, **3:** 127.

Poon, C.S., Peters, C.J. and Perry, R. (1985a),*The Sci. Tot. Environ.*, **41:** 55.

Powder Diffraction File (28-0208), JCPDS International Centre for Diffraction Data, Swarthmore, PA, USA (1989).

Powder Diffraction File (37-1367), JCPDS International Centre for Diffraction Data, Swarthmore, PA, USA (1989).

Powder Diffraction File (41-1451), JCPDS International Centre for Diffraction Data, Swarthmore, PA, USA (1989).

Pressler, E.E., Brunauer, S., Kantro, D.L. and Weise, C.H. (1961), *Anal. Chem.*, **33:** 877.

Rai, D., Sass, B.M. and Moore, D.A. (1987), *Inorganic Chemistry*, **26:** 345.

Ramachandra, V.S (1979), *Cem. Concr. Res.*, **9:** 677.

Rayment, D.L. and Lachowski, E.E. (1984), *Cem. Concr. Res.*, **14:** 43.

Richardson, I.G. and Groves, G.W. (1993), *Cem. Concr. Res.*, **23:** 131.

Rodger, S.A., Groves, G,W., Clayden, N.J. and Dobson, C.M. (1987), *Mat. Res. Soc. Symp. Proc.*, **85:** 13.

Rodger, S.A., Groves, G,W., Clayden, N.J., and Dobson, C.M. (1988), *J. Am. Ceram. Soc*. **71:** 91.

Rodger, S.A., Groves, G.W., Clayden, N.J. and Dobson, C.M. (1988), *J. Am. Ceram. Soc*., **71:** 91.

Rotzinger, F.P., Stunzi, H. and Marty, W. (1986), *Inorganic Chemistry,* **25:** 489.

Roy, A., Eaton, H.C., Cartledge, F.K. and Tittlebaum, M.E. (1991), *Hazardous Wastes and Hazardous Materials,* **8:** 33.

Ryskin, Y.I., in *The Infrar-red Spectra of Minerals,* ed. V.C. Farmer, Mineralogical Society, 137 (1974).

Schindler, P.W., Furst, B., Dick, R. and Wolf, P.U. (1976), *J. Colloid and Interface Sci.,* **55:** 469.

Scrivener, K.L., Patel, H.H., Pratt, P.C. and Parrot, C.J. (1987), *Mat. Res. Soc. Symp. Proc.*, **85:** 67.

Spiccia, L. and Marty, W. (1986), *Inorganic Chemistry,* **25:** 266.

Spiccia, L., Stoeckli-Evans, H., Marty, W. and Giovanoli, R. (1987), *Inorganic Chemistry,* **26:** 474.

Stade, H. and Muller, D. (1987), *Cem. Concr. Res.,* **17:** 553.

Struble, L.J., in *8th ICCC,* **2:** 582 (1986).

Stucke, M.S. and Majumdar, A.J. (1977), *Cem. Concr. Res.,* **7:** 711.

Sujata, K. and Jennings, H.M (1992), *J. Am. Ceram. Soc.,* **75:** 1669.

Tashiro, C., Takahashi, H., Kanaya, M., Hirokida, I. and Yoshida, I. (1977), *Cem. Concr. Res.,* **7:** 288.

Taylor, H.F.W. (1987), *Cem. Concr. Res.,* **17:** 613.

Taylor, H.F.W. and Newbury ,D.E. (1984), *Cem. Concr. Res.,* **14:** 93.

Taylor, H.F.W., Barret, P. and Brown, P.W. (1984), *Mater. Const.,* **17:** 457.

Taylor, H.F.W., *Cement Chemistry,* Academic Press, London (1990).

Thomas, N.L. (1987), *J. Mater. Sci.,* **22:** 3328.

Thomas, N.L. and Double, D.D. (1983), *Cem. Concr. Res.,* **13:** 391.

Thomas, N.L., Sameson, D.A., and Double, D.D. (1981), *Cem. Concr. Res.*, **11:** 143.

Tsuji, M., Komarneni, S. and Malla, P. (1991), *J. Am. Ceram. Soc.*, **74:** 274.

Vempati, R.K., Loeppert, R.H. and Cocke, D.L. (1990),*Solid State Ionics.*, **38:** 53.

Wilberg, K.B., in *Oxidation in Organic Chemistry Part IV.* Academic Press, New York (1965).

Williamson, R.B. (1972), *Prog. Mater. Sci.* **15**: 189

Young, J.F., Tong, H.S. and Berger, R.L. (1977), *J. Am. Ceram. Soc.*, **60:** 193.

Zamorani, E. and Sheik, I. (1989), *Cem. Concr. Res.*, **19:** 259.